

UC Berkeley

UC Berkeley Electronic Theses and Dissertations

Title

Excited States of Molecules with Density Functional Theory and Many Body Perturbation Theory

Permalink

<https://escholarship.org/uc/item/5t65227g>

Author

Hamed, Samia

Publication Date

2020

Peer reviewed|Thesis/dissertation

Excited States of Molecules with Density Functional Theory and Many Body Perturbation
Theory

by

Samia M. Hamed

A dissertation submitted in partial satisfaction of the

requirements for the degree of

Doctor of Philosophy

in

Chemistry

in the

Graduate Division

of the

University of California, Berkeley

Committee in charge:

Professor Jeffrey B. Neaton, Chair
Professor Martin Head-Gordon, Co-chair
Professor Naomi Ginsberg
Professor Michael F. Crommie

Summer 2020

Excited States of Molecules with Density Functional Theory and Many Body Perturbation
Theory

Copyright 2020
by
Samia M. Hamed

Abstract

Excited States of Molecules with Density Functional Theory and Many Body Perturbation Theory

by

Samia M. Hamed

Doctor of Philosophy in Chemistry

University of California, Berkeley

Professor Jeffrey B. Neaton, Chair

Professor Martin Head-Gordon, Co-chair

The accurate prediction of electronic excitation energies in molecules is an area of intense research of significant fundamental interest and is critical for many applications. Today, most excited state calculations use time-dependent density functional theory (TDDFT) in conjunction with an approximate exchange-correlation functional. In this dissertation, I have examined and critically assessed an alternative method for predicting charged and low-lying neutral excitations with similar computational cost: the *ab initio* Bethe-Salpeter equation (BSE) approach. Rigorously based on many-body Green's function theory but incorporating information from density functional theory, the predictive power of the BSE approach remained at the beginning of this work unexplored for the neutral and charged electronic excitations of organic molecules. Here, the results and implications of several systematic benchmarks are laid out in detail.

Contents

Contents	i
List of Figures	iii
List of Tables	vii
1 Electronic excited state calculations in molecules: challenges and opportunities	1
1.1 Case Study 1: Biomimetic light harvesting complexes	3
1.2 Case Study 2: Upconverting dye-functionalized nanoparticles	7
1.3 Summary and Outline	10
2 Electronic structure theory and methods	13
2.1 The Electronic Structure Challenge	13
2.2 Wavefunction Approaches	16
2.3 Density functional and many-body perturbation theory approaches	18
3 Systematic benchmarking of the Bethe-Salpeter equation approach for excitations of organic molecules	24
3.1 Technical Details: the software, the benchmark set, and identification of excitations	26
3.2 evGW eliminates the mean-field starting point present in G0W0 calculations.	26
3.3 OTRSH eliminates the need for evGW calculations	35
4 Assessment of the Bethe-Salpeter equation approach for triplets and triplet instabilities of organic molecules	46
4.1 Introduction	46
4.2 Computational details	48
4.3 Low-lying $\pi \rightarrow \pi^*$ excitations of aromatic hydrocarbons	49
4.4 Results and discussion	50
4.5 Conclusions	56
5 Predicting charged excitations across the oligoacenes	58

5.1	Introduction	58
5.2	Theoretical methods	60
5.3	Ionization potentials and electron affinities	63
5.4	Conclusions	69
6	Outlook	70
	Bibliography	71

List of Figures

1.1	Biomimetic light-harvesting systems	3
1.2	Xanthene core molecules	4
1.3	First major singlet energies calculated in Q-Chem with standard settings for geometry optimizations, and gas-phase TDDFT with a 6-31+g* basis with various xcfs for the xanthene core molecules x = xanthene, fbb = fluorescein backbone, rbb = rhodamine backbone, f = fluorescein, r = rhodamine, jB = Jaffamine B, rB = rhodamine B, and tB = Trungamine B.	5
1.4	A singlet transition involving a significant dipole change kicks off a relaxation pathway comprised of three photophysical processes (blue, red and green $T_{reorg.}$) having different timescales and different viscosity dependencies. See ref. [33].	6
1.5	TDDFT calculations in Q-Chem of the vertical transition energies for the bright S1 transition and the dark S2 transition with the 6-31+g* basis set and the IEF-PCM solvation model. Figure reproduced from SI of ref. [29].	7
1.6	TDDFT calculations in Q-Chem at the PBE0/6-31+g* level including solvation effects from the IEF-PCM of vertical transition energies of the bright S1 transition and the dark S2 transition as functions of phenyl-xanthene rotation angle. The region of the excited state surface that is effectively inaccessible at room temperature (RT) is shaded light gray. For comparison, the ground state energies are plotted in gray, with energies that rapidly increase past a rotation of 10 degrees from an orthogonal geometry. The natural transition orbitals for each of these states are shown, and a comparison of the calculated ground and excited state geometries, which do not change very much at all. Figure reproduced from [29].	8
1.7	Dye functionalized upconverting nanoparticle system Figure reproduced from ref. [30].	9
1.8	TDDFT triplet energies with different xcfs. Vertical excitation energies and natural transition orbitals (NTOs) were calculated in Q-Chem utilizing time-dependent density functional theory (TDDFT), various xcfs, a VTZ basis set, and solvation effects treated with the ptSS and ptLR polarizable continuum models 8,9. Figure reproduced from SI of ref. [30].	10

1.9	a, Time-gated triplet phosphorescence spectrum of IR806 on NaGdF ₄ nanoparticles at 80K (no Yb ₃ or Er ₃ present), overlaid with the NIR portion of the UCNP absorption spectrum (at room temperature). b, Electronic densities of the natural transition orbital (NTO) of the hole and the NTO of the electron for the first excited triplet state of IR806, calculated using TD-DFT with the TDA and the B3LYP functional. c, Spectra from left to right, coloured according to their transitions in d: Er ₃ emission (green and red curves), IR806 absorption (dashed blue curve), IR806 fluorescence (solid, light blue curve), UCNP absorption (dashed purple curve) and IR806 phosphorescence (yellow curve). d, Jablonski diagram of proposed energy transfer (ET) landscape, showing dye ISC to the triplet state T ₁ before transfer to UCNP lanthanides. See ref. [30].	11
3.1	The 28 molecules contained in Thiel's set. H is white, C is light blue, N is dark blue, and O is red.	25
3.2	Convergence with basis set of the first 1B _{1u} excitation in ethene (left panel) and of the first 1B ₂ excitation in pyrrole (right panel) within CCSD (from Ref. [67]), TD-B3LYP and BSE based on B3LYP inputs. The excitation energy for the largest basis set (aug-cc-pVQZ) has been used as the zero for each theoretical approach.	27
3.3	GW-BSE workflow. Approximations explored here are included in gray text. . .	28
3.4	Correlation plots for singlet excitations between BSE with different starting points and the BTE. A linear fit of the data is shown with a dashed line.	30
3.5	Mean signed error (upper panel) and mean absolute error (lower panel) for singlet excitations for different schemes. TDDFT based on B3LYP (from Ref. [42]) is given as a comparison.	31
3.6	Correlation plots for triplet excitations between BSE the different starting points and the BTE. A linear fit of the data is shown with a dashed line.	32
3.7	Mean signed error (upper panel) and mean absolute error (lower panel) for triplet excitations for different schemes. TDDFT based on B3LYP (from Ref. [67]) is given as a comparison.	33
3.8	Dependence of the mean signed error for the singlet excitation energies of the Thiel's set with respect to the content of exact exchange of the underlying xc functional. The xc functional is used for TDDFT (red square symbols) or as the starting point of GW and BSE (blue diamond symbols).	34
3.9	Correlation plot for HOMO-LUMO gap from single-shot GW and from CCSD(T)	36
3.10	Gammas for Thiel's set.	39
3.11	The top and bottom graphs summarize respectively the MAEs and MSDs when compared to best theoretical estimates (BTEs) from high-level quantum chemistry wavefunction based methods, including the multireference CASPT2 technique, and coupled cluster theories. The XCFs are listed in order of increasing HF exact exchange percentage. All methods shown here utilize the aug-cc-pVTZ basis set.	41

3.12	Distributions of errors for lowest lying singlets of Thiel set molecules computed from different G_0W_0 -BSE starting points	42
3.13	Correlation plots for singlets	43
3.14	Triplet MAEs	44
3.15	Basis set dependence of triplet MAEs	45
4.1	Top: Subset of 20 organic molecules from Thiel’s set for which triplets are studied here utilizing the OTRSH functional. Bottom: The general formula for an acene molecule, and the three other aromatic hydrocarbons studied here: azulene, benzo[<i>e</i>]pyrene (BP) and dibenzo[<i>a, c</i>]anthracene (DBAn). H is white, C is light blue, N is dark blue and O is red.	47
4.2	MSD (see text for details) with respect to CCSD(T) [122, 99] of calculated neutral excitations of the acene molecules ($n = 1$ to 6). The calculated 1L_a (blue bars), 1L_b (orange bars), and 3L_a (pink bars) excitations, and $^1L_b - ^1L_a$ (black bars) energy difference are shown for a few representative TDDFT and GW-BSE approaches: TD-OTRSH and TD-CAM-B3LYP in panel a, and G_0W_0 -BSE@BHLYP, G_0W_0 -BSE@OTRSH-PBE and evGW-BSE@PBE0 in panel b.	51
4.3	Low-lying singlet excitations of acenes calculated with TD-OTRSH-PBE and G_0W_0 -BSE@OTRSH-PBE in panels a and b; 1L_a and 1L_b excitation energies, with blue and orange lines respectively, are compared to CCSD(T) references from Refs. [99] and [77] (dashed lines). The corresponding excitations with the TDA at the TDDFT and GW-BSE theories are shown in panels c and d.	52
4.4	First-triplet excitation energies of organic molecules in Thiel’s set (see Figure 4.1) calculated with GW-BSE are benchmarked against reference data [77]. The MSD (read text) corresponding to molecules in Series 1 is shown in blue bars, Series 2 in orange bars, Series 3 in black bars and the total in pink bars. We consider several GW-BSE schemes with the full-BSE and the TDA.	54
4.5	Ratio of the first triplet energy (T) calculated within GW-BSE diagonalizing the full BSE Hamiltonian and using the TDA. Several representative GW-BSE schemes are shown: G_0W_0 -BSE@BHLYP in dashed-blue lines and crosses, G_0W_0 -BSE@OTRSH-PBE in dotted-orange lines and circles and evGW-BSE@PBE0 in black lines and crosses. GW-BSE predicts a negative triplet energy (shown at zero) for hexacene for all GW schemes used in this work.	55
5.1	The general chemical formula for the acenes.	58

- 5.2 Convergence of charged excitations with respect to the basis set size for the oligoacene molecules within GW based on a PBE0 starting point. Calculated IP–EA gap energies (E_g) converge fast with respect to the basis set size, whereas IPs and EAs are extrapolated to the basis set (CBS) limit using a function of the form $f(x) = a + b/(x - x_0)$ (dotted-blue lines). Note that as the molecule size increase, calculations with large basis sets become unfeasible, and hence some points are omitted in the figures2. For convenience, we show the energy difference with respect to the results obtained with the aDZ basis, $\Delta E_{\text{aDZ}} = E - E_{\text{aDZ}}$; In fact, points for different molecules overlap making evident that all quantities converge at similar rates for the different molecules considered here. 63
- 5.3 Charged excitations of oligoacenes calculated within GW and DFT are compared to CCSD(T); our IPs in Table 5.1 and EAs from Refs.[137]. Calculated IP–EA gaps, vertical ionization potentials (IP), electron affinities (EA) and their corresponding difference with respect to the theoretical reference, Δ , are shown in panels a - f. Several GW approaches are considered (see text). For comparison, quantum Monte Carlo (QMC) data from Ref.[139] for anthracene are also shown. 65
- 5.4 Top: Mean absolute deviation (MAD) with respect to the theoretical reference [CCSD(T)] in the calculated IPs (green bars), EAs (orange bars) and IP–EA gaps (blue bars) of the acene family of molecules. Bottom: Mean signed deviation (MSD). Several DFT and GW approximations are considered (see text). 66
- 5.5 Correlation and linear fit between evGW gaps and their corresponding G_0W_0 gaps for the oligoacenes. Results of GW calculations with PBE, PBE0 and BHLYP starting points are used in constructing this plot. All energies are in units of eV. 68

List of Tables

3.1	xc functionals and %HF	40
4.1	Singlet and triplet energetics of representative aromatic hydrocarbons calculated with GW-BSE@BHLYP with the full-BSE (denoted simply BSE above) and the TDA. We consider benzene (Benz), naphthalene (Naph.), anthracene (Anth.), tetracene, (Tetra.), pentacene (Penta.), hexacene (Hexa.), azulene (Azu.), benzo[<i>e</i>]pyrene (BP) and dibenzo[<i>a, c</i>]anthracene (DBAn). MSD and MAD with respect to CCSD(T) are also shown (see text). All energies are in units of eV.	57
5.1	Best theoretical estimates based on CCSD(T) calculations following Ref.[138], for the vertical IP of the acenes. Here, we compare our calculations with those of Ref.[138], determined by a focal point analysis[138] at the CCSD(T) level of theory. All energies are in units of eV.	64

Acknowledgments

No man is an island, and although I am not a man, I am also not an island.

I would like to first thank my family: my mother Marcia Hamed, my father Sammy Hamed, my stepmother Irene Borkenhagen and my brother Adam Hamed. Without your love and support I would not be where I am today. To paraphrase the poet E. E. Cummings (I hope he doesn't mind): Here is the deepest secret nobody knows, here is the root of the root and the sky of the sky of a tree called life: although we are far apart, I carry you with me, I carry your hearts in mine. Anywhere I go, you go too, and whatever is done by me is your doing too. Dad, I am finally Ustatha Samia. I love you, my dear family. Thank you for everything.

Secondly I would like to thank the Neaton Group. In particular, I would like to thank my advisor Jeff Neaton for his unwavering support and optimism, his scientific guidance, and his kindness. Thank you Jeff, it has been an honor and joy to be part of the Neaton group. I would like to thank Tonatiuh Rangel and Fabien Bruneval with whom I spent some very happy years working on much of what is presented in this dissertation. I learned a tremendous amount from both of you, and enjoyed the coffee breaks that fueled our discoveries. I would also like to thank my friends in the Neaton group. In no particular order: Florian Altvater-Brown who fought with me against the dangers of procrastination; Stephanie Mack, with whom I share the incommunicable past; Sahar Sharifzadeh, my first teacher and guide into the lands of DFT and beyond; Mariana Hildebrand whose brief stint in the Neaton group resulted in what I hope will be a lifelong friendship; Michele Kotiuga, my APS roommate with whom I spent many nights staying up too late; Sinead Griffin who has always inspired me, sometimes fed me, and once painted me; Marina Filip who is at once frighteningly intense and lovingly kind; Jonah Haber whose warm spirit in pre-pandemic times could be felt radiating throughout the 4th floor of Birge Hall; and finally Caroline McKeon whose first year coincided with my last: I pass the torch to you.

Thank you also to my classmates in the chemistry department at UC Berkeley who helped make my time there memorable and happy even when we were buried in homework or losing frisbee games: Mark Shapero, Michelle Leuenberger, Walter Ralston, Jean van Buren, Donghyun Lee, Lisa Alexander, Alec White, Noelle Catarineu, Royce Lam, Monatrice Lam, Jon Witte, Jacob Olshansky, Alex Shearer, and Scott Ellis.

Thank you also to the people not in the Neaton group nor at UC Berkeley who in big and small ways have enriched my PhD adventure, believed in me when I did not, and formed the fibers that weave me firmly into the tapestry of life. Thank you Rachel Ward, Nida Vaid Wower, Aisha Ellahi, Lorena de Oñate, Ryan Spangler, Abhi Nellore, Rubin Mendoza, Regiane Nascimento, Jennifer Ling, Victoria Der, Robin Elizabeth, Lisa Landry, Mikey Lin and the Cosio-Herrera family. Thank you to my extended family in Egypt, Nebraska, Missouri, Illinois, and Iowa. I love you.

Thank you to Austen F. Riggs and Claire Riggs who gave me my first experiences in scientific research in their lab when I was an undergraduate student at UT Austin. You never stopped encouraging me or believing in me and your lifelong pursuit of knowledge was truly inspiring. Thank you to my manager Sam Ang who gave me my first industry job in RD at a Swedish structural foam company called Diab. You taught me to ask for a raise, and to never stop shooting for the stars.

Finally, I would like to thank my dog Hank who was there from the beginning of my PhD effort. He often escorted me to and from campus, slept quietly at my feet while I worked, and was a loyal friend over the years. He loved nothing more than going to the physics building with me, where he had friends who he liked to visit. Thank you Hank for your efforts to keep me safe over the years, and for your love and concern when things were hard.

Chapter 1

Electronic excited state calculations in molecules: challenges and opportunities

Optical excitations of electrons in molecules abound in the universe and are central to processes both mundane and extraordinary. For example they determine the color of everyday objects; they control the fluorescence behavior of molecules used as markers in biomedical imaging applications; and they dictate the absorption and transfer of photons by and between chromophores embedded in proteins relevant to photosynthesis. These diverse phenomena (and many others) are united by the same underlying quantum mechanics.

The ability to reliably and quantitatively predict optical excitations from non-empirical calculations is an important goal, and several competing approaches for this purpose are in use today. Apart from wavefunction-based methods, which are computationally intensive and thus often limited to relatively small systems, two main formalisms are present in the literature: time-dependent density functional theory[1, 2, 3] (TDDFT) and *ab initio* many-body perturbation theory within the so-called GW plus Bethe-Salpeter equation (GW-BSE) approach[4, 5, 6]. Both methods are under active development and have been widely used but for different classes of systems: TDDFT primarily for molecules and BSE for solids[7]. In both formalisms, a central challenge is determining judicious approximations to achieve a balance between feasibility and accuracy.

Linear response TDDFT is a computationally efficient and versatile method with a formal $\mathcal{O}(N^4)$ scaling, where N is the number of basis functions or electrons; it enables coupling to environmental models, it can produce excited state potential energy surfaces, and it can treat relativistic effects. Its average excitation energy errors approach 0.2 eV (adequate for certain cases but not all). Furthermore this good general performance is not unqualified and the limitations of TDDFT are well-documented in the literature. [8, 9, 10, 11] Additionally, while the inclusion of asymptotic long-range exact exchange in hybrid functionals can improve the singlet energies, it can also lead to significant underestimations of the triplets resulting in improper state ordering, although so-called triplet instabilities can be partially remedied by

the Tamm Dancoff approximation (TDA)[12].

Recently, GW-BSE has emerged as a method that can be both efficient and accurate for molecules with similar or even reduced errors compared to TDDFT[13, 14]. Relative to standard contemporary TDDFT approaches, the BSE method has many attractive features: through direct calculation of the screened Coulomb interaction within the random phase approximation, the electron-hole interaction has the correct asymptotic behavior independent of the system, be it a bulk solid, a low-dimensional nanostructure or polymer, or a molecule. This feature has resulted in, for instance, a correct description of charge transfer excitations in molecules.[15, 16] Additionally, the description of neutral excitations within the BSE is built upon a foundation of accurate charged excitation energies, corresponding to electron addition or removal, via the GW approximation[17, 18, 19], where G is the one-particle Green's function and W is the screened Coulomb interaction. The GW approach is known to yield far more accurate values of fundamental (or quasiparticle) gap energies for a variety of systems than, e.g., standard DFT where underlying Kohn-Sham eigenvalues have little physical meaning.[20] Only the highest occupied molecular orbital (HOMO) and lowest unoccupied molecular orbital (LUMO) energies can be safely interpreted as the negative of ionization potential (IP) and the negative of electron affinity (EA) in a generalized Kohn-Sham (gKS) scheme (including hybrid functionals)[21, 22, 23]. All the other gKS eigenvalues are not, strictly speaking, observables, although recent work on tuned range-separated hybrids suggests that both quasiparticle gaps and outer valence spectra from a gKS approach can also be in quantitative agreement with photoemission and GW calculations in certain cases. [24, 25, 26] For these reasons, the BSE approach is increasingly being used to predict excitation energies for molecules and is an alternative to TDDFT.

Multiple decades of work have resulted in an increasingly large library of detailed benchmark studies of both TDDFT and BSE [27, 28] on molecules. These studies report on the predictive accuracy of computational methods for low- and high-lying singly and multiply excited states that are local, extended, charge-transfer-like, or Rydberg in nature; and they form the foundation for impactful use in experimental work ranging from astrophysics to the design of new energy technologies. This dissertation reports on the affects of various approximations in the application of both TDDFT and BSE to the electronic excitations of molecular systems. To begin, I review two studies I have been involved with that have resulted in publications[29, 30] in which standard TDDFT has been utilized in systems of significant complexity. In subsequent chapters of this thesis, I present detailed benchmarks motivated by these studies of both TDDFT and GW-BSE methods for excitations in simpler molecules.

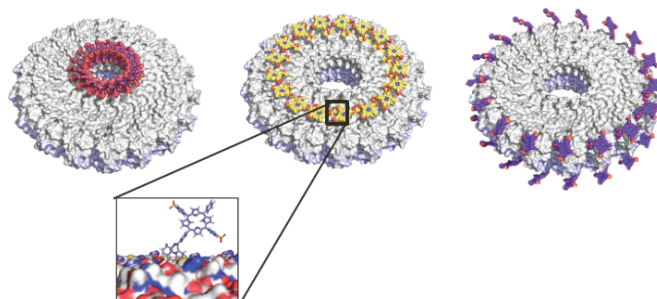


Figure 1.1: Biomimetic light-harvesting systems

1.1 Case Study 1: Biomimetic light harvesting complexes

Figure 1.1 was one of the first images presented to me when I began work towards this dissertation. The gray pinwheels are made of tweaked tobacco mosaic virus (TMV) protein amino acid sequences[31] and used as scaffolds for the attachment of chromophores (molecules that absorb light in the visible range of the electromagnetic spectrum); the resulting nature-mimicking platforms enable precision studies of the first stages of photosynthesis wherein photons of light are captured and transported with awesome efficiency by chromophores embedded in aqueous protein environments.[32] Jointly with experimentalists in the Francis and Ginsberg groups, our studies have been aimed at discovering and understanding experimentally tunable parameters that might guide the design of solar energy devices in the future. As a first step, I undertook a TDDFT benchmarking study of xanthene-derivative chromophores. See figure 1.2. While other chromophore benchmarks[27] exist, none existed for this particular system, and while TDDFT is an exact formalism for excited states, it is approximate in practice as the exact exchange correlation functional is unknown. Therefore, the reliability of TDDFT is limited by the efficacy of existing approximate functionals. The xanthene family of chromophore molecules is interesting experimentally and theoretically as functionalization of xanthene influences excitation energies.

Moving from left to right on the x-axis in figure 1.3, the influence of various functional groups on the lowest singlet excitation energy is apparent. Qualitatively, the trends predicted by the sample of eight different exchange correlation functionals (xcfs) are in good agreement. Xanthene is not conjugated through all three of its hexagons; rather, there is conjugation on the left and on the right but not in the middle, and so just as in the particle-in-a-box problem, electronic confinement leads to higher excitation energies; xanthene has the highest-energy singlet excitation regardless of choice of xcf. The introduction of either oxygen- or nitrogen-based functional groups at R1 and R2 relax the confinement and conjugation extends to

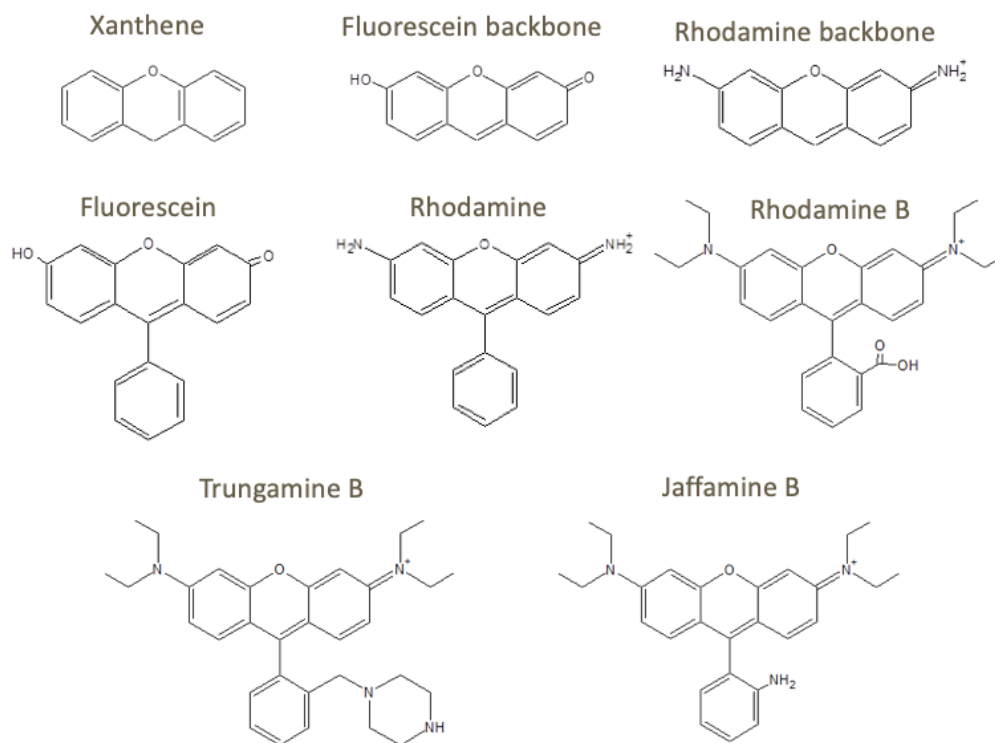


Figure 1.2: Xanthene core molecules

the entire molecule causing the excitation energies to drop. In comparison, the addition of a functional group at position R3 does not affect the excitation energy too much as long as it is simple. When we get to the "B" group - rhodamine B, Jaffamine B, and Trungamine B - we see that there is a drop in excitation energy yet again. These are the trends for the molecules regardless of the choice of xcf; the quantitative story is of course quite different. Which xcf gives the best agreement with experiment for a particular excitation? How important are the details of the solvent and protein environments?

The need for predictive models of energy transfer to distinguish between possible photophysical paths requires accurate descriptions of the excited state manifolds of individual molecules. For example, in the study[33] pictured in figure 1.4 of the effect of solvent viscosity on relaxation times, the Ginsberg group discovered three distinct photophysical processes between absorption and fluorescence for the protein pigment complex (see the blue, red, and green reorganization timescales in figure 1.4). Although calculated and experimental singlet energies were not in strong agreement, TDDFT calculations were able to reveal significant dipole differences between excited and ground electronic states. This helped to support the discovery of a design principle: that reorganization times, which impact energy transfer paths and efficiencies, can be tuned by (1) increasing ground and excited state dipole differences

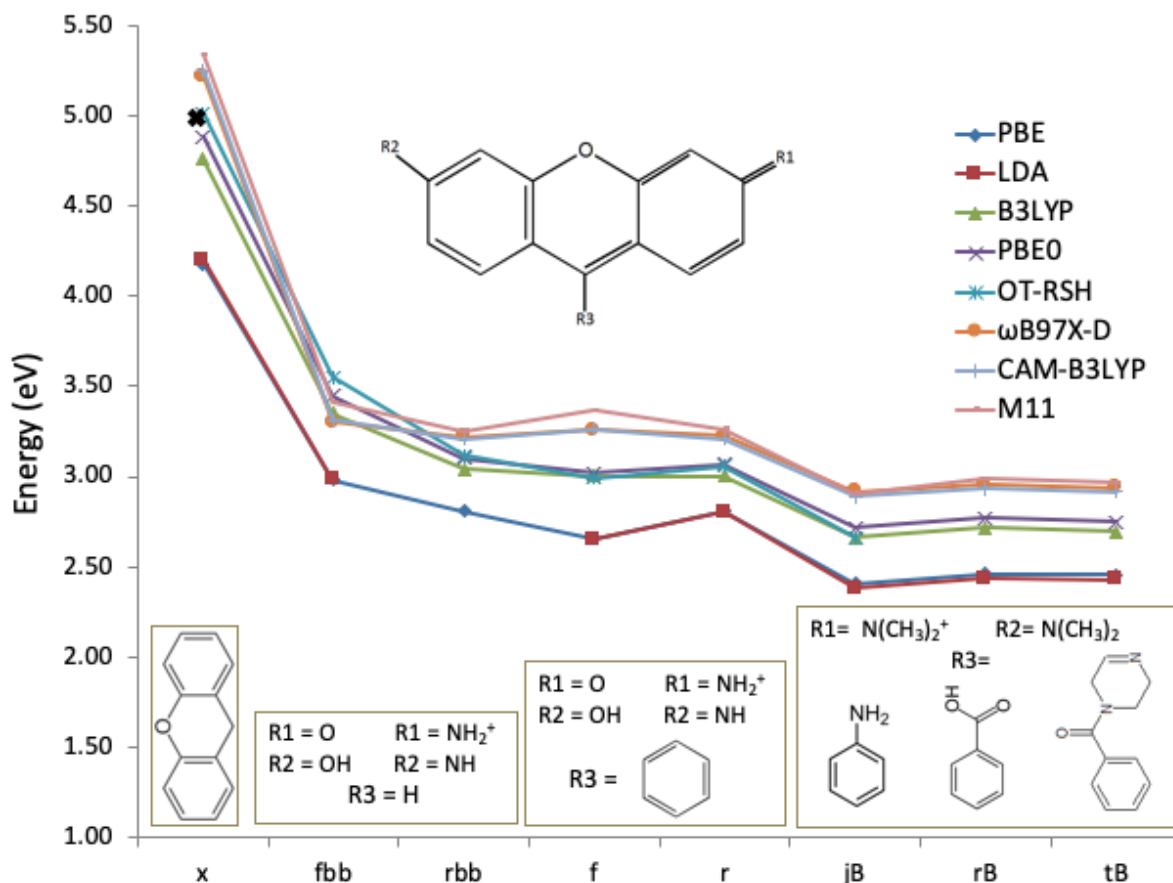


Figure 1.3: First major singlet energies calculated in Q-Chem with standard settings for geometry optimizations, and gas-phase TDDFT with a 6-31+g* basis with various xcfs for the xanthene core molecules x = xanthene, fbb = fluorescein backbone, rbb = rhodamine backbone, f = fluorescein, r = rhodamine, jB = Jaffamine B, rB = rhodamine B, and tB = Trungamine B.

and (2) engineering the aqueous protein environment to adjust viscosity by changing the attachment position of the chromophore to make it either more or less protein-embedded.

Another line of inquiry involved examining chromophore-protein interactions through linker engineering to tune photoinduced dynamics in the TMV light-harvesting platform.[29] A comparison of TDDFT results with different xcfs to the experimental excitation energy as represented by the red dotted line in figure 1.5, illustrates the strong xcf-induced variations in predicted singlet values. In figure 1.6 we see that DFT calculations on the ground and excited state geometries displayed minor intramolecular structural rearrangement, and showed

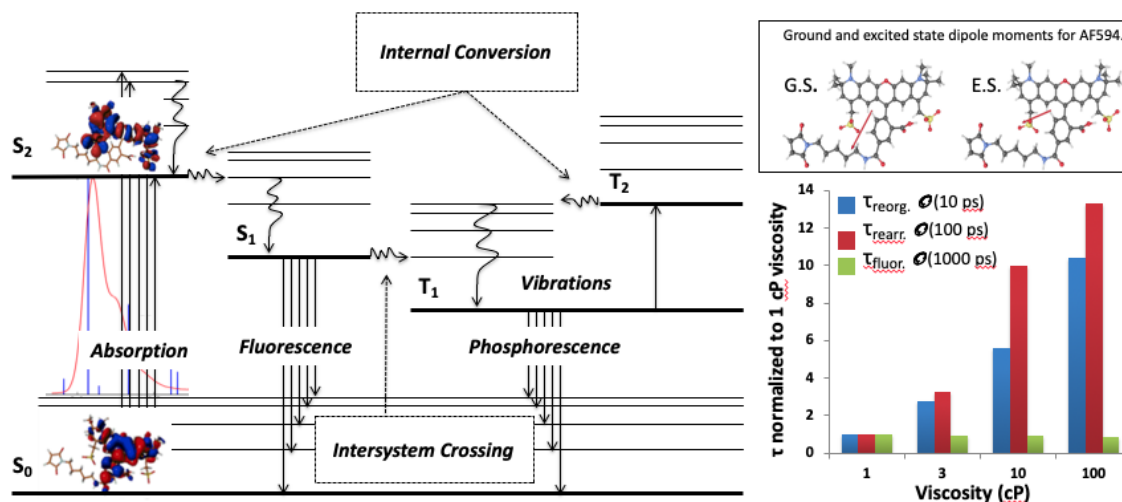


Figure 1.4: A singlet transition involving a significant dipole change kicks off a relaxation pathway comprised of three photophysical processes (blue, red and green $T_{\text{reorg.}}$) having different timescales and different viscosity dependencies. See ref. [33].

that although an excited state crossing exists around a phenyl-xanthene rotation angle of 55 degrees, this configuration was predicted to be inaccessible at room temperature. This eliminated the possibility of photoinduced dynamics involving such a crossing. While the degree of qualitative insight into these complex systems is remarkable, the quantitative disagreement between our calculations and measurements is notable, motivating the benchmark studies in later chapters of this thesis.

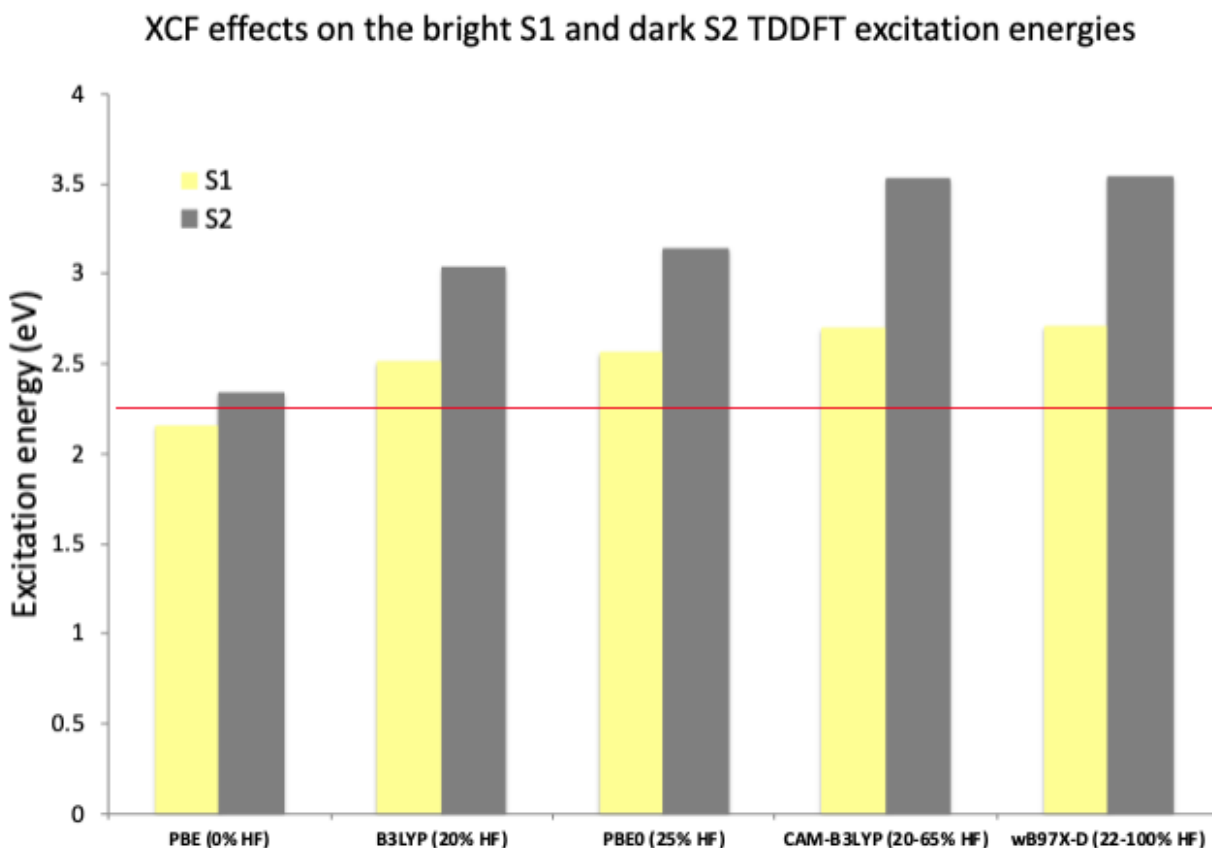


Figure 1.5: TDDFT calculations in Q-Chem of the vertical transition energies for the bright S1 transition and the dark S2 transition with the 6-31+g* basis set and the IEF-PCM solvation model. Figure reproduced from SI of ref. [29].

1.2 Case Study 2: Upconverting dye-functionalized nanoparticles

In an experimental collaboration I undertook with researchers at the Molecular Foundry,[30] mechanisms that enable organic light-harvesting chromophore antennas (this time cyanine dyes) to significantly enhance performance in lanthanide-doped upconverting nanoparticles (UCNPs - see figure 1.7) have been discovered and leveraged to design a system with a whopping 33,000-fold increase in brightness and a 100-fold increase in efficiency compared to non-dye-functionalized UCNPs. This study presented another opportunity to apply predictive methods for excited state energies. Because the best hypothesis for the mechanism involved an intersystem crossing and energy transfer from a triplet state on the chromophore

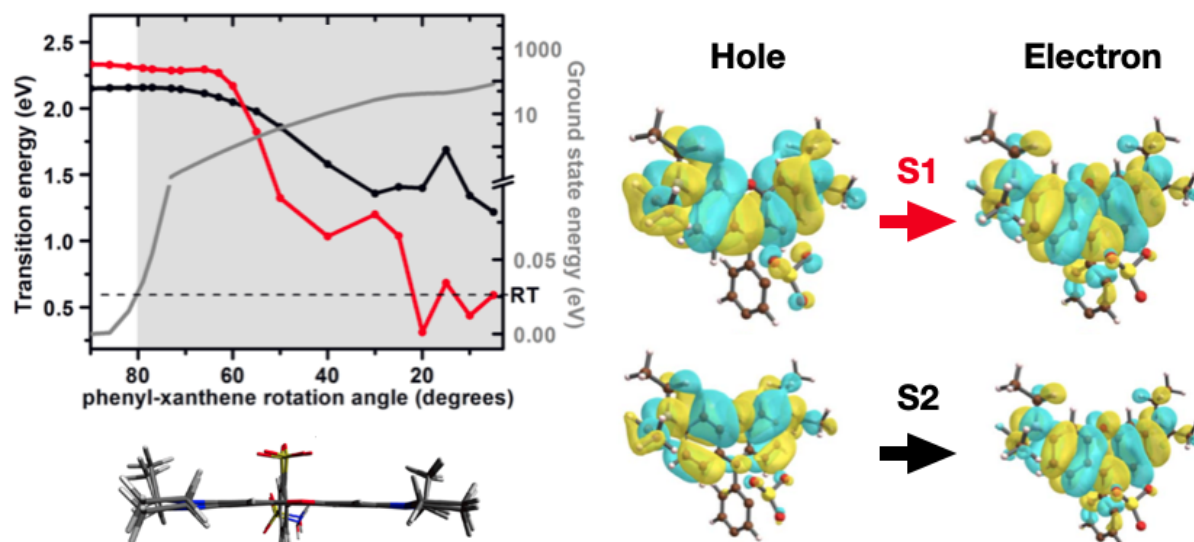


Figure 1.6: TDDFT calculations in Q-Chem at the PBE0/6-31+g* level including solvation effects from the IEF-PCM of vertical transition energies of the bright S1 transition and the dark S2 transition as functions of phenyl-xanthene rotation angle. The region of the excited state surface that is effectively inaccessible at room temperature (RT) is shaded light gray. For comparison, the ground state energies are plotted in gray, with energies that rapidly increase past a rotation of 10 degrees from an orthogonal geometry. The natural transition orbitals for each of these states are shown, and a comparison of the calculated ground and excited state geometries, which do not change very much at all. Figure reproduced from [29].

to the nanoparticle, more information about whether or not the involved excitations were charge-transfer-like or delocalized, and calculated trends in singlet and triplet energies were needed. While singlet excitation energies can be obtained experimentally, the orbital character is harder, and the triplet measurement is prohibitively challenging.

Our TDDFT calculations revealed that the lowest lying bright singlet and first triplet transitions are both dominated by p-p* HOMO to LUMO transitions (see figure 1.9b). It is worth noting that the molecule belongs to the cyanine family of dyes whose singlet excitations have been challenging[34, 35] to capture with theory. DFT geometry optimization at the B3LYP/VTZ level of theory, performed with two possible initial geometries, yielded two molecular configurations which are pictured in figure 1.8 and were of nearly identical energy. The total SCF ground state energy difference at the B3LYP level was 0.08 eV, with the second pictured molecule in figure 1.8 having the lower energy. The effect of the choice of the exchange correlation functional (XCF) was explored and, with the Tamm Dancoff approximation (TDA), yielded triplet energies between 0.9 and 1.2 eV. The effect of the

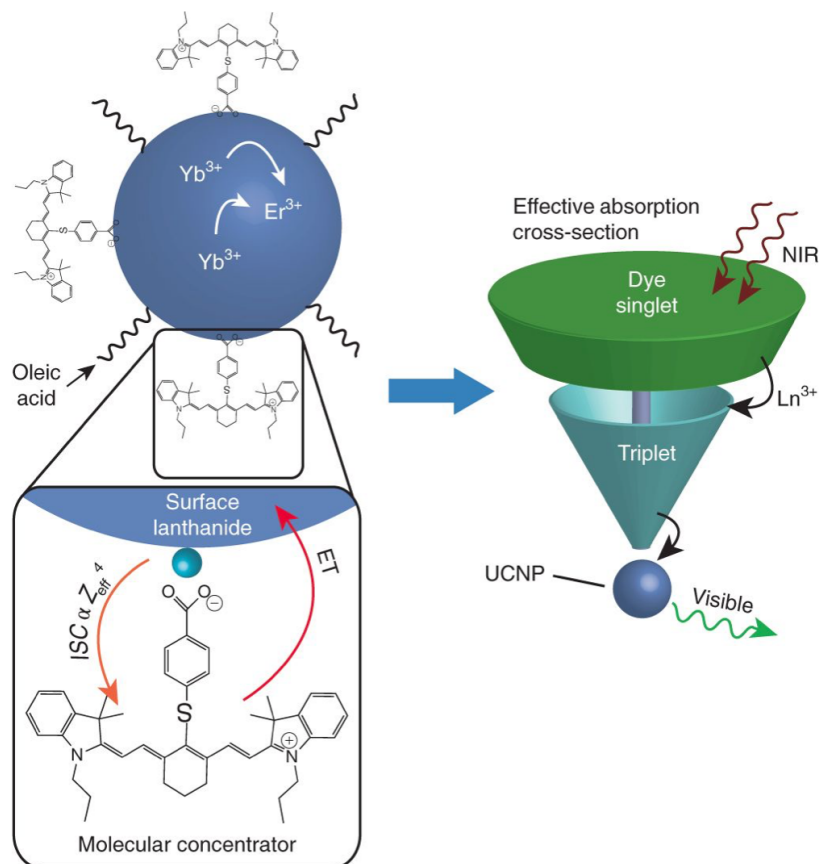


Figure 1.7: Dye functionalized upconverting nanoparticle system Figure reproduced from ref. [30].

TDA was significant in some cases, and its energies are likely more accurate[36]. It was intriguing to observe here that the TDA seemed to diminish the difference between the xcfs.

Finally, in figure 1.9 we see the proposed mechanism supported by theory, involving dye intersystem crossing (ISC) to the triplet state before transfer to the UCNP lanthanides. The TDDFT triplet electron and hole densities (pictured in figure 1.9b) were delocalized and (not-pictured) very similar to those of the singlet. In this study, our TDDFT calculations were able to confirm the presence of a delocalized triplet near-to but lower than the experimentally observed singlet state, supporting the mechanism of dye ISC from the singlet to the triplet before transfer to the UCNP lanthanides.

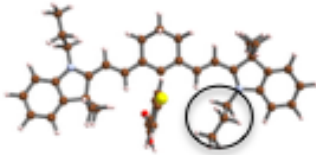
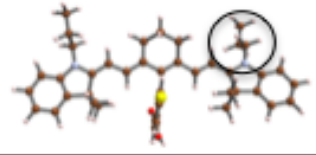
Optimized DFT Geometry	XCF	TDA (eV)	no TDA (eV)
	PBE0	1.0	0.8
	B3LYP	1.0	0.9
	BHLYP	1.0	0.6
	wB97X-D	1.0	0.3
	CAM-B3LYP	0.9	0.4
	B3LYP	1.0	0.9
	BHLYP	1.2	0.8

Figure 1.8: TDDFT triplet energies with different xcfs. Vertical excitation energies and natural transition orbitals (NTOs) were calculated in Q-Chem utilizing time-dependent density functional theory (TDDFT), various xcfs, a VTZ basis set, and solvation effects treated with the ptSS and ptLR polarizable continuum models^{8,9}. Figure reproduced from SI of ref. [30].

1.3 Summary and Outline

As can be seen through the applications above, the efficient and popular TDDFT method for the calculation of excited states in complex molecules in complex environments has many limitations. In both of the presented case studies, determining a photophysical pathway after initial chromophore excitation requires quantitative determination of the low-lying manifold of excited states. While our TDDFT calculations contributed insight and support to experimentally driven hypotheses, they could not predict the behavior a priori. In the case of the up-converting nanoparticle, our calculations could not quantitatively match the singlet and triplet energies involved in the proposed mechanism unless a different starting geometry was used for each (and a transition between these geometries was found to be energetically forbidden). In the case of the chromophores attached to the TMV scaffolds, the singlet energies were highly dependent on the xcfs, and the best agreement with experiment came from PBE - a result known to sometimes occur because of cancellation of errors.

Inspired by these limitations, in what follows in this dissertation, the relatively new-to-molecules GW-BSE approach from many-body perturbation theory is systematically bench-

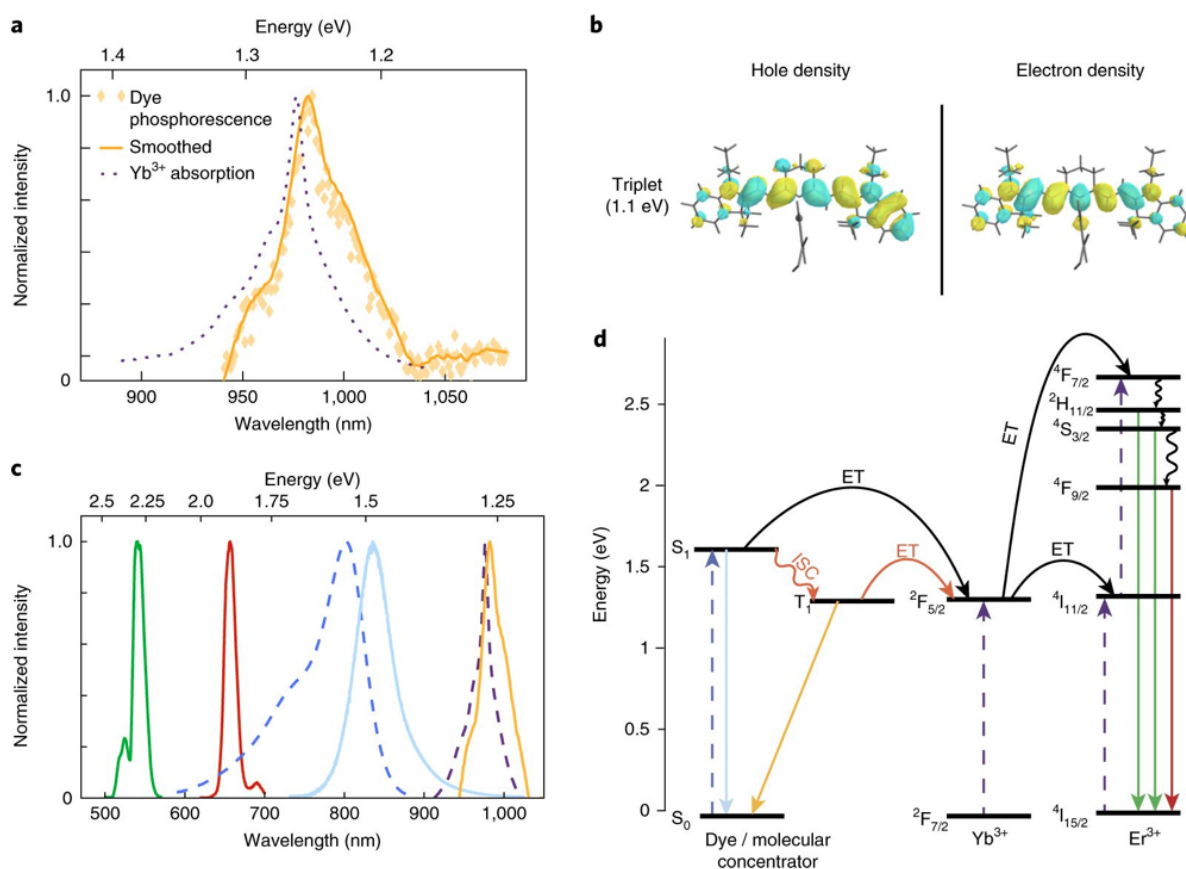


Figure 1.9: a, Time-gated triplet phosphorescence spectrum of IR806 on NaGdF₄ nanoparticles at 80K (no Yb³⁺ or Er³⁺ present), overlaid with the NIR portion of the UCNP absorption spectrum (at room temperature). b, Electronic densities of the natural transition orbital (NTO) of the hole and the NTO of the electron for the first excited triplet state of IR806, calculated using TD-DFT with the TDA and the B3LYP functional. c, Spectra from left to right, coloured according to their transitions in d: Er³⁺ emission (green and red curves), IR806 absorption (dashed blue curve), IR806 fluorescence (solid, light blue curve), UCNP absorption (dashed purple curve) and IR806 phosphorescence (yellow curve). d, Jablonski diagram of proposed energy transfer (ET) landscape, showing dye ISC to the triplet state T₁ before transfer to UCNP lanthanides. See ref. [30].

marked and compared to TDDFT. After a brief review of theory in chapter 2, GW-BSE in various formulations is applied in chapter 3 to the low-lying optical excitations of organic molecules and compared to higher-level wavefunction-based calculations. In chapter 4 the analysis is extended to triplet instabilities in such systems, and in chapter 5 to charged

excitations across the oligoacenes. In chapter 6, an outlook is given on future directions.

Chapter 2

Electronic structure theory and methods

In this dissertation I evaluate the performance of density functional theory and many body perturbation theory as methods for understanding and predicting the neutral and charged excited states of molecules. I have compared results with these approaches to those obtained from the computationally expensive but more accurate wavefunction-based approaches. Here I will briefly review the theory behind these methods. Note that all equations herein make use of Hartree atomic units unless stated otherwise ($m_e = \hbar = e = 4\pi\epsilon_0 = 1$).

2.1 The Electronic Structure Challenge

The electronic structure challenge in general is essentially one of describing the behavior of many interacting electrons in fields of relatively larger nuclei. It is a quantum many-body problem that is too complex to be solved exactly for anything but the simplest of systems, and so we must make and mix various approximations in order to compute quantities of interest.

The Schrödinger Equation

The time-independent non-relativistic Schrödinger equation at the heart of the electronic structure challenge can be written simply as an eigenvalue problem

$$\hat{H} |\Psi_i\rangle = E_i |\Psi_i\rangle, \quad (2.1)$$

where $|\Psi_i\rangle$ is an eigenfunction of the Hamiltonian operator \hat{H} , and E_i is the corresponding energy eigenvalue of the state characterized by $|\Psi_i\rangle$. The index i labels the solutions to the Schrödinger equation $E_i = \langle \Psi_i | \hat{H} | \Psi_i \rangle$ and runs from $i=0$ to infinity such that $E_0 \leq E_1 \leq E_2 \leq \dots E_i \leq \dots$. The many-particle Hamiltonian \hat{H} can be written as a sum of terms

representing the kinetic and potential energies of the electrons and nuclei that comprise the molecular system:

$$\begin{aligned} \hat{H} = & - \sum_{i=1}^n \frac{1}{2} \nabla_i^2 - \sum_{A=1}^M \frac{1}{2m_A} \nabla_A^2 + \\ & \sum_{i=1}^n \sum_{j>i}^n \frac{1}{|\mathbf{r}_i - \mathbf{r}_j|} - \sum_{i=1}^n \sum_{A=1}^M \frac{Z_A}{|\mathbf{r}_i - \mathbf{R}_A|} + \sum_{A=1}^M \sum_{B>A}^M \frac{Z_A Z_B}{|\mathbf{R}_A - \mathbf{R}_B|}, \end{aligned} \quad (2.2)$$

where the first and second terms correspond respectively to the kinetic energies of the electrons and nuclei, while the remaining three terms describe the potential energies associated with (1) repulsion between electrons, (2) attraction between electrons and nuclei, and (3) repulsion between nuclei. The indices i and j label the n electrons, while A and B label the M nuclei. m = mass, \mathbf{r} and \mathbf{R} label three dimensional position coordinates, and Z represents the nuclear charge, i.e. the atomic number of the nucleus.

Since \hat{H} and $|\Psi_i\rangle$ depend on nuclear and electronic coordinates, solving the Schrödinger equation means solving a partial differential equation in $3n+3M$ dimensions. Our computers and algorithms cannot yet perform this task exactly, and so for now we must utilize approximations.

The Born-Oppenheimer Approximation

Relative to nuclei, electrons are light. They are three orders of magnitude less massive than atomic nuclei, and so the first approximation typically made is to treat the nuclei as static. By clamping the nuclei, \hat{H} can be reduced from five terms to just three, and the dimensionality of the problem from $3n+3M$ to just $3n$. The second term in equation 2.2 (kinetic energy of nuclei) vanishes, the fifth term (potential energy of nuclear repulsion) becomes an additive constant; and although the electronic Hamiltonian in equation 2.3 retains a parametric dependence on the nuclear coordinates, it only depends explicitly on the electronic ones. The total electronic energy of the ground state, $E_{tot,0}$ is now given by equation 2.5, which takes its first term from equation 2.4 ($i=0$). More explicitly, we have

$$\hat{H}_e = - \sum_{i=1}^n \frac{1}{2} \nabla_i^2 + \sum_{i=1}^n \sum_{j>i}^n \frac{1}{|\mathbf{r}_i - \mathbf{r}_j|} - \sum_{i=1}^n \sum_{A=1}^M \frac{Z_A}{|\mathbf{r}_i - \mathbf{R}_A|}, \quad (2.3)$$

and

$$\hat{H}_e |\Psi_{e,i}\rangle = E_{e,i} |\Psi_{e,i}\rangle, \quad (2.4)$$

with

$$E_{tot,0} = E_{e,0} + \sum_{A=1}^M \sum_{B>A}^M \frac{Z_A Z_B}{|\mathbf{R}_A - \mathbf{R}_B|}. \quad (2.5)$$

But equation 2.4 still involves solving a $3n$ -dimensional partial differential equation, and since n is not typically a very small number, the problem is still too difficult to be solved exactly.

Hartree-Fock Theory

Hartree-Fock theory is an important reference for most efforts to solve electronic structure problems and serves as a starting point for more accurate methods. It is where we begin to make some progress; of course we do so by invoking more approximations. In addition to the Born-Oppenheimer approximation and the neglect of relativistic effects in the Hamiltonian, two more approximations are made in the Hartree-Fock method: (1) the single Slater determinant wavefunction ansatz and (2) the neglect of correlation via a mean-field approximation. While finite basis sets are utilized in every computational electronic structure method used in practice, the single determinant ansatz is unique to Hartree-Fock; on the other hand, mean-field approximations appear everywhere in physics, chemistry, and probability theory.

To begin, let's consider what a first attempt to approximate an n -electron wavefunction might comprise. If we simply write it as a product of n single-particle wavefunctions, the result is an uncorrelated or independent-electron wavefunction called the Hartree product:

$$|\Psi_{e,i}(\mathbf{x}_1, \mathbf{x}_2, \dots, \mathbf{x}_n)\rangle \approx |\Phi_H(\mathbf{x}_1, \mathbf{x}_2, \dots, \mathbf{x}_n)\rangle = \prod_{i=1}^n |\phi_i(\mathbf{x}_i)\rangle, \quad (2.6)$$

where \mathbf{x}_n are general coordinates involving both space (\mathbf{r}) and spin degrees of freedom, and ϕ_i represent single-particle wavefunctions. But the Hartree product wavefunction fails to incorporate the antisymmetry of the wavefunction and so is not a suitable ansatz. Electrons are identical particles of half integer-spin that follow Fermi-Dirac statistics; one of the consequences of this is that their wavefunctions must be antisymmetric with respect to exchange of the spatial and spin coordinates of any two electrons. That is, applying a permutation operator (that switches the coordinates of two electrons) to $|\Psi_{e,i}\rangle$ should return $-|\Psi_{e,i}\rangle$. In equation 2.7 we see that the Hartree product does not return the required result:

$$\hat{P}_{12} |\Phi_H(\mathbf{x}_1, \mathbf{x}_2)\rangle = \hat{P}_{12} (|\phi_1(\mathbf{x}_1)\rangle |\phi_2(\mathbf{x}_2)\rangle) = |\phi_1(\mathbf{x}_2)\rangle |\phi_2(\mathbf{x}_1)\rangle \neq -|\phi_1(\mathbf{x}_1)\rangle |\phi_2(\mathbf{x}_2)\rangle. \quad (2.7)$$

In equations 2.8 and 2.9 below, we see that a so-called Slater determinant wavefunction (for 2 electrons for simplicity) successfully incorporates the fermionic nature of electrons. It is in fact the simplest antisymmetric n -electron wavefunction that we can write down, and so is the simplest valid approximation of $|\Psi_{e,i}\rangle$:

$$\Phi_S(\mathbf{x}_1, \mathbf{x}_2) = \frac{1}{\sqrt{2}} \begin{vmatrix} |\phi_1(\mathbf{x}_1)\rangle & |\phi_2(\mathbf{x}_1)\rangle \\ |\phi_1(\mathbf{x}_2)\rangle & |\phi_2(\mathbf{x}_2)\rangle \end{vmatrix} = \frac{1}{\sqrt{2}} [|\phi_1(\mathbf{x}_1)\rangle |\phi_2(\mathbf{x}_2)\rangle - |\phi_2(\mathbf{x}_1)\rangle |\phi_1(\mathbf{x}_2)\rangle] \quad (2.8)$$

and

$$\hat{P}_{12} |\Phi_S(\mathbf{x}_1, \mathbf{x}_2)\rangle = -|\Phi_S(\mathbf{x}_1, \mathbf{x}_2)\rangle. \quad (2.9)$$

Taking a Slater determinant wavefunction and using the variational principle to find the spin orbitals ϕ_i that minimize the electronic energy E_e^{HF} subject to the constraint that the orbitals remain orthonormal is known as the Hartree-Fock approximation. The variational principle guarantees that the Hartree-Fock energy for a given atomic system is an upper limit to the true energy of the system, i.e.,

$$E_e^{HF} = \min_{\Phi_S} \left\{ \langle \Phi_S | \hat{H}_e | \Phi_S \rangle \right\}. \quad (2.10)$$

The variational conditions on the one-electron spin orbitals give rise to the Fock operator f and its eigenvalue equation, namely

$$f(i) = -\frac{1}{2}\nabla_i^2 - \sum_{A=1}^M \frac{Z_A}{r_{iA}} + v^{HF}(i) \quad (2.11)$$

with

$$f(i)\phi(\mathbf{x}_i) = \varepsilon\phi(\mathbf{x}_i). \quad (2.12)$$

The Fock operator is an effective one-electron Hamiltonian operator that treats the electron-electron interactions in an average way, and because its eigenvalue equation is non-linear, it is solved iteratively utilizing a self-consistent-field (SCF) procedure. The SCF procedure involves the following steps: (1) make an initial guess at the spin orbitals, (2) from these, calculate the average electric field v^{HF} for each electron, (3) solve the eigenvalue problem of equation 2.12 for a new set of spin orbitals, and (4) plug the spin orbitals from the third step into the first step. The steps are repeated until self-consistency is reached, i.e. until both the electric fields v^{HF} and the spin orbitals stop changing.

Although the Hartree-Fock method recovers $> 99\%$ of the electronic energy, it turns out that due to the mean-field approximation, we miss out on something essential called correlation energy. Correlation energy is comprised of particular dynamic and static interactions between individual electrons, and it is a necessary ingredient for most electronic structure studies of interest. There are two broad categories of approximations that attempt to capture the correlation energy: approaches based on wavefunctions, and those based on density functionals.

2.2 Wavefunction Approaches

Wavefunction approaches generally attempt to capture in some way the instantaneous electron-electron interactions missed by the Hartree-Fock method. I will briefly review two of these approaches here.

Møller-Plesset Perturbation Theory

In 1934 a "Note on an Approximation Treatment for Many-Electron Systems" appeared in the literature describing the development of a perturbation theory for "a system of n electrons in which the Hartree-Fock solution appears as the zero-order approximation." [37] Whereas Hartree Fock ignores electron correlation entirely, the new method (today called "second-order Møller-Plesset perturbation theory", or MP2 for short) treated the instantaneous interactions between electrons *perturbatively*, with the central assumption being that these interactions are small enough to do so.

The second-order correction to the electronic energy of the MP2 method which can be derived from the application of Rayleigh-Schrödinger perturbation theory to the Hartree-Fock single determinant wavefunction is given by the following expression

$$E^{(2)} = -\frac{1}{4} \sum_{ij}^{\text{occ}} \sum_{ab}^{\text{virt}} \frac{|\langle ij||ab \rangle|^2}{\epsilon_a + \epsilon_b - \epsilon_i - \epsilon_j}. \quad (2.13)$$

The indices i and j are for the occupied orbitals; a and b represent unoccupied or "virtual" orbitals; ϵ_i is the energy eigenvalue corresponding to the Fock operator of equation 2.12; and the symbol $\langle ij||ab \rangle$ represents the following antisymmetrized two-electron integral:

$$\begin{aligned} \langle ij||ab \rangle &= \langle ij|ab \rangle - \langle ij|ba \rangle \\ &= \int d\mathbf{x}_1 d\mathbf{x}_2 \phi_i^*(\mathbf{x}_1) \phi_j^*(\mathbf{x}_2) r_{12}^{-1} \left(1 - \hat{P}_{12}\right) \phi_a(\mathbf{x}_1) \phi_b(\mathbf{x}_2). \end{aligned} \quad (2.14)$$

Although MP2 is the most commonly used perturbation theory in quantum chemistry today, it was not always so. The method was mostly ignored at first, in part because it is not a variational method and thus was seen as unreliable, but also because a few early tests of the theory were not motivating in their results. Developments in the field have been such that by now, MP2 is a method known to be fairly reliable and cheap.[38]

MP2 is the most basic post-Hartree-Fock wavefunction-based approach to electron correlation, but it is not a cure-all, particularly for systems where correlation is not perturbatively small.

Coupled-Cluster Theory

Coupled-cluster theory is one of the most accurate electronic structure approaches available today, and is often used as a theoretical benchmark for other methods. In short, it is a method built by applying an exponential excitation operator to the Hartree-Fock wavefunction resulting in multi-electron wavefunctions that account for electron correlation, as in

$$|\Phi_{\text{CC}}\rangle = e^{\hat{T}} |\Phi_{\text{HF}}\rangle. \quad (2.15)$$

In the above equation, the cluster operator \hat{T} is equal to $\hat{T}_1 + \hat{T}_2 + \hat{T}_3 + \dots$ where \hat{T}_1 is a single excitations operator, \hat{T}_2 is a double excitations operator, etc. Utilizing the second quantization formalism, the expression for an n-fold cluster operator can be written as

$$T_n = \frac{1}{(n!)^2} \sum_{i_1, i_2, \dots, i_n} \sum_{a_1, a_2, \dots, a_n} t_{a_1, a_2, \dots, a_n}^{i_1, i_2, \dots, i_n} \hat{a}^{a_1} \hat{a}^{a_2} \dots \hat{a}^{a_n} \hat{a}_{i_1} \dots \hat{a}_{i_2} \hat{a}_{i_n}, \quad (2.16)$$

where t are unknown excitation amplitudes that must be solved for; i is an index for an occupied electronic orbital and a is for an unoccupied orbital; \hat{a}^a is a creation operator and \hat{a}_i is a destruction operator.

It is possible to improve coupled-cluster results systematically by incorporating higher-order excitations to get closer to the exact electronic energy, but it quickly becomes prohibitively costly to do so. Full inclusion of excitations up to the triple and quadruple levels (CCSDT and CCSDQ) is not feasible for most systems; so the triples and quadruples are often treated perturbatively as in CCSD(T) and CCSDT(Q). Currently, due to cost, going beyond quadruples is almost never done.

2.3 Density functional and many-body perturbation theory approaches

Ground-state DFT

In density functional theory (DFT), instead of computing the total energy as an expectation value of the Hamiltonian, which involves knowledge of the $3N$ coordinate electronic wavefunction, the energy can be expressed as a function of the density $\rho(\mathbf{x})$, a quantity dependent on only three spatial coordinates. This was formally proven by Hohenberg and Kohn in 1964[39] through two important theorems: (1) there exists a one-to-one mapping between the ground-state electron density and the energy of a many-electron system for non-degenerate ground states, and so the ground-state energy is a functional of $\rho(\mathbf{x})$; and (2) there exists a variation principle such that $E[\rho(\mathbf{x})]$ is minimal when $\rho(\mathbf{x})$ is the true ground-state density. So in principle the complicated determination of the many-electron wavefunction can be skipped, and the Hamiltonian and corresponding ground state energy can be found through minimization of $E[\rho(\mathbf{x})]$.

For molecules, a DFT computation is similar to Hartree-Fock in terms of computational cost; but because DFT does not neglect electron correlation, it is far more accurate. For these reasons, DFT (that of Hohenberg, Kohn, and Sham[39, 40]) has become the most widely used method in computational chemistry today. The main challenge lies in the fact that the exact functional $E[\rho(\mathbf{x})]$ is unknown and so approximations are required. The question of designing and/or utilizing the best functional for a given situation is particularly important for the study of excited states, and discussions regarding this are central to the work contained within this dissertation.

Over 100 Kohn-Sham DFT (KS-DFT) exchange-correlation functionals (xcfs) exist today, and they can be conveniently categorized with a structure called "Jacob's Ladder" proposed by John Perdew in 2001[41]. On Jacob's Ladder, the first rung is comprised of the local spin-density approximation (LSDA or LDA for short) which is exact for the uniform electron gas and only depends on the electron density. But the electron density in molecules is never uniform; so this is not a good approximation to use in general. Going up the ladder to the next rung, we find the generalized gradient approximation (GGA) functionals (like PBE[42]) better account for the real situation in molecules by including the gradient $\nabla\rho(\mathbf{x})$ of the density. To improve the situation further, we ascend the ladder again and find meta-GGAs which go beyond GGAs by including either the Laplacian of the density $\nabla^2\rho(\mathbf{x})$ or the kinetic energy density for n electrons of spin σ ,

$$\tau_\sigma = \sum_i^{n_\sigma} |\nabla\psi_{i,\sigma}|^2, \quad (2.17)$$

where ψ is a Kohn-Sham orbital.

On the fourth rung are the hybrids which include among their ranks "arguably the most popular density functional of our time"[43], B3LYP[44, 45]. Hybrids come in two flavors, global and range-separated. Global hybrids add a constant fraction of Hartree-Fock exchange (also called exact exchange) to any of the DFT functionals on lower rungs. The B3LYP functional is given as follows

$$E_{xc}^{\text{B3LYP}} = c_x E_x^{\text{HF}} + (1 - c_x - a_x) E_x^{\text{Slater}} + a_x E_x^{\text{B88}} + (1 - a_c) E_c^{\text{VWN1RPA}} + a_c E_c^{\text{LYP}}, \quad (2.18)$$

where the subscript c stands for correlation, the subscript x for exchange, and the superscripts are types of exchange or correlation; and more specifically for B3LYP, $c_x = 0.20$, $a_x = 0.72$, and $a_c = 0.81$. PBE0[46, 47], another popular global hybrid which I have utilized frequently in the work presented herein, has a similar but simpler form:

$$E_{xc}^{\text{PBE0}} = 0.25 E_x^{\text{HF}} + 0.75 E_x^{\text{PBE}} + E_c^{\text{PBE}} \quad (2.19)$$

In contrast to global hybrids which apply the same amount of HF exchange for every electron-electron spacing, range-separated hybrids ramp up from a short-range fraction containing less HF exchange to a long-range portion containing more HF exchange; the short and long ranges are usually connected with the error function.

In the optimally-tuned range separated hybrid (OTRSH) scheme[48, 49], the partitioning of the Coulomb potential introduces three parameters and is implemented as

$$\frac{1}{r_{12}} = \frac{\alpha + \beta \operatorname{erf}(\gamma r_{12})}{r_{12}} + \frac{1 - (\alpha + \beta \operatorname{erf}(\gamma r_{12}))}{r_{12}}, \quad (2.20)$$

where the first term is treated explicitly and the second term is replaced with a semi-local functional, such as one of several GGAs. In OTRSH, γ is tuned such that the ionization

potential theorem[50, 51, 52, 53, 54] is satisfied, α is usually fixed to 0.2, and $\alpha + \beta$ is set to unity, enforcing that the exchange potential goes to zero at infinity. Two examples of OTRSH functionals are that of Baer-Neuhauser-Lifshitz (BNL)[55, 56] and the Perdew-Burke-Ernzerhof (PBE)-based OTRSHs[24, 25, 57]. We will return to OTRSH specifically later in this thesis.

The Realm of Excited States

Whereas DFT is a ground state theory, this dissertation is about the calculation of excited states which involve the interaction of many-electron systems with time-dependent fields. TDDFT and many-body perturbation theory (GW-BSE) are formalisms allowing for such computations and so I will introduce them briefly here.

TDDFT

In 1984 TDDFT was born when Runge and Gross extended the Hohenberg-Kohn theorems of DFT to the time-dependent domain by demonstrating that the expectation value of any physical time-dependent observable of a many-electron system is a unique functional of the time-dependent electron density (and of the initial state).[1] A decade after that, Casida[3] published the linear-response formalism of TDDFT allowing for the efficient and effective application of TDDFT to molecular systems.

In this formalism, excitation energies are obtained by finding poles in the response of the ground state density to a time-varying applied electric field. In practice, this requires solution of a non-Hermitian eigenvalue problem of the form

$$\begin{pmatrix} A & B \\ -B & -A \end{pmatrix} \begin{pmatrix} X_s \\ Y_s \end{pmatrix} = \Omega_s \begin{pmatrix} X_s \\ Y_s \end{pmatrix}, \quad (2.21)$$

where the Ω_s are neutral excitations and (X_s, Y_s) are the eigenvectors. The complex conjugation has been dropped because the wavefunctions are assumed to be real-valued. The upper block A accounts for resonant transitions from occupied to unoccupied orbitals, whereas the lower block $-A$ accounts for the antiresonant transitions, and the two types of transitions are coupled through the blocks B and $-B$. The neglect of the coupling B blocks leads to the Tamm-Dancoff approximation.[58] Details regarding A and B and how they differ from GW-BSE are given in the following section.

GW-BSE

In the GW-BSE approach excitations are computed via a Green's function formalism in a multiple step process. First, the so-called GW self-energy, where G is the one-particle Green's function and W the fully frequency-dependent screened Coulomb interaction, is constructed from a generalized Kohn-Sham eigensystem generated from an initial DFT calculation, the so-called DFT "starting point"; then the BSE, an effective two-particle equation, is solved,

typically in a static approximation for W . In this static limit, the BSE is analogous to TDDFT's Casida equations, but is built upon GW-corrected one-particle energies.

In the single shot G_0W_0 approach the one-electron self-energy reduces to

$$\Sigma(1, 2) = iG(1, 2)W(1^+, 2), \quad (2.22)$$

where the composite index 1 is short for position, time, and spin (r_1, t_1, σ_1) (and 1^+ indicates the limit as time goes to t_1). As mentioned, G is the one-particle Green's function and W is the screened Coulomb interaction. This is the first and lowest order term in an expansion of the self-energy in the screened Coulomb interaction W . The GW self-energy produces quasiparticle energies which are, by definition, the binding energies of electrons or holes in a system. These energies approximate the observables measured by photoemission (for occupied states) and inverse-photoemission (for unoccupied states). In practice, the GW quasiparticle energies show good agreement with experiment, albeit with a notable starting point dependence.[16, 59, 60, 61, 62, 63, 64, 65].

The BSE is a Dyson-like equation for the so-called two-particle correlation function L . The full equation reads as

$$\begin{aligned} L(1, 2; 1', 2') = & L_0(1, 2; 1', 2') + \int d3d4d5d6 L_0(1, 4; 1', 3) \\ & \times \frac{\delta M(3, 4)}{\delta G(6, 5)} L(6, 2; 5, 2'), \end{aligned} \quad (2.23)$$

where the non-interacting correlation function L_0 is expressed as

$$L_0(1, 2; 1', 2') = G(1, 2')G(2, 1'), \quad (2.24)$$

and M is the sum of the Hartree potential and the self-energy

$$M(3, 4) = v_H(3)\delta(3, 4) + \Sigma(3, 4). \quad (2.25)$$

When the indices are contracted, L and L_0 yield the usual interacting and non-interacting polarizabilities

$$\chi(1, 2) = -iL(1, 2; 1^+, 2^+) \quad (2.26)$$

and

$$\chi_0(1, 2) = -iL_0(1, 2; 1^+, 2^+). \quad (2.27)$$

When expressed in this form, the BSE in Eq. 2.19 and the central equations of TD-DFT in the linear response formalism

$$\chi(1, 2) = \chi_0(1, 2) + \int d3d4 \chi_0(1, 3) \frac{\delta v_{KS}(3)}{\delta \rho(4)} \chi(4, 2) \quad (2.28)$$

can be seen to be linked in an intuitive fashion.

In practice, the BSE is generally solved using the screened Hartree-Fock approximation to Σ , a choice that can alternatively be viewed as a *GW* approximation to Σ in the static limit. Hence, the BSE kernel simplifies to the following frequency independent expression:

$$\begin{aligned} \frac{\delta M(\mathbf{r}_3, \mathbf{r}_4)}{\delta G(\mathbf{r}_6, \mathbf{r}_5)} = & -iv(\mathbf{r}_3 - \mathbf{r}_5) \delta(\mathbf{r}_3 - \mathbf{r}_4) \delta(\mathbf{r}_5 - \mathbf{r}_6) \\ & + iW(\mathbf{r}_3, \mathbf{r}_4, \omega = 0) \delta(\mathbf{r}_3 - \mathbf{r}_5) \delta(\mathbf{r}_4 - \mathbf{r}_6), \end{aligned} \quad (2.29)$$

where v is the bare Coulomb interaction in the previous equation. Within this static assumption, the BSE can be recast into a matrix form in a transition space spanned by the orbital products $\phi_i(r)\phi_j(r)$ where pairs of states i and j are either occupied/unoccupied or unoccupied/occupied. Thus the BSE results in an eigenvalue problem with the same block form as the TDDFT equations in equation 2.21 above, and the only difference between TDDFT and the BSE lies in the specific expression of the matrix elements in A and B . In the BSE, if i and j are occupied states and a and b are unoccupied states, these elements read as, for spin-restricted calculations,

$$\begin{aligned} A_{ia}^{jb} = & \left(\epsilon_a^{\text{QP}} - \epsilon_i^{\text{QP}} \right) \delta_{ij} \delta_{ab} - \alpha^{S/T} (ia|jb) + W_{ij}^{ab}(\omega = 0) \\ B_{ia}^{jb} = & -\alpha^{S/T} (ia|bj) + W_{ib}^{aj}(\omega = 0), \end{aligned} \quad (2.30)$$

where $(ia|jb)$ are Coulomb integrals in Mulliken notation. The coefficient $\alpha^{S/T}$ is set to 2 in the case of a singlet final state or to 0 in the case of a triplet final state. W is the screened Coulomb interaction.

The eigenvalue problem posed by the BSE is numerically cumbersome: the matrix size grows as the square of the number of atoms (2 times the number of occupied states times the number of unoccupied states). Furthermore, it is a non-symmetric eigenvalue problem. However it is well known from TDDFT that this problem can be reduced to a symmetric eigenvalue problem whose size is cut in half.[58] After some algebra, the problem can be recast as $CZ_s = \Omega_s^2 Z_s$, where $C = (A - B)^{1/2}(A + B)(A - B)^{1/2}$ is a symmetric matrix that is half the size of the initial problem in Eq. 2.25. The above expression assumes the matrix $(A - B)$ to be positive definite. From the knowledge of an eigenvector Z_s , one can build both X_s and Y_s as

$$X_s = \frac{1}{2} [(A - B)^{1/2} + \Omega_s(A - B)^{-1/2}] Z_s \quad (2.31)$$

and

$$Y_s = \frac{1}{2} [(A - B)^{1/2} - \Omega_s(A - B)^{-1/2}] Z_s. \quad (2.32)$$

Here the calculation of the square root of matrix $(A - B)$ requires another diagonalization. Note that within semi-local approximations of TDDFT, $(A - B)$ is a diagonal matrix and its square root is readily obtained. However recent work[66] has proven that Cholesky

decompositions can be a workaround to avoid this second diagonalization. A TDDFT calculation would proceed along essentially identical lines except that the eigenvalues entering in A would be gKS eigenvalues instead of quasiparticle energies from a GW approximation with the W term replaced by the xc kernel f_{xc} (with a different index ordering).

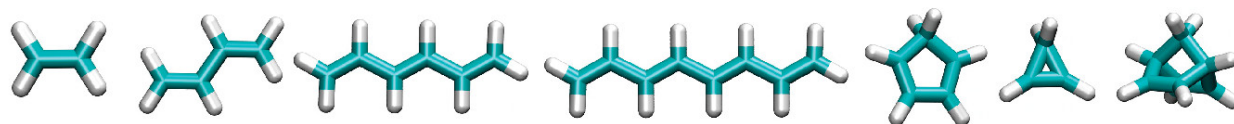
Chapter 3

Systematic benchmarking of the Bethe-Salpeter equation approach for excitations of organic molecules

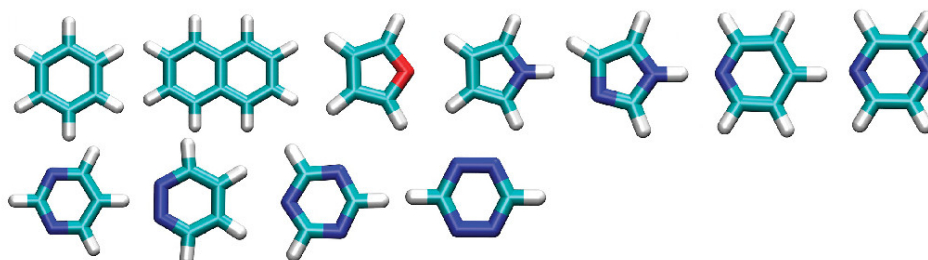
When we first undertook the work presented in this chapter published in Ref [13], the predictive power of the GW-BSE approach had already been demonstrated for the optical gaps and spectra of solid-state systems, but no systematic benchmarks for neutral electronic excitations of organic molecules yet existed. Here, we present the results of an initial study and its follow-up, in which we have evaluated the performance of various approximations within the GW-BSE approach for the calculation of gas-phase singlet and triplet excitations on the 28 small molecules of Thiel’s widely used TDDFT benchmark set [Schreiber et al., J. Chem. Phys. 128, 134110 (2008)]. This benchmark set (hereafter referred to as “Thiel’s set”) includes 103 singlet and 63 triplet excitations, computed with multiple coupled-cluster and multireference methods.[67] Following prior studies with TDDFT, we have benchmarked to theoretical values rather than experimental data. Thus, the compared calculations employ the same basis sets and identical atomic positions; vibrations and temperature effects are neglected, and there is no solvent or other environmental conditions to mitigate. With this work, we have provided a general assessment as well as guidelines and rationale for the successful application of the GW-BSE method to the excited states of molecular systems.

In our initial study[13] we demonstrated that when used in combination with a single-shot G0W0 method, BSE produces results that are strongly dependent on the mean-field (DFT) starting point employed in the perturbative approach, and furthermore that this starting point dependence is mainly introduced through the quasiparticle energies obtained at the intermediate GW step. With a judicious choice of starting mean-field, *or* by using the eigenvalue self-consistent evGW approach at the intermediate step instead of G0W0, singlet excitation energies obtained from BSE are in excellent quantitative agreement with higher-level wavefunction methods. The quality of the triplet excitations was less satisfactory. In chapter 4 we show that excellent GW-BSE results for molecular triplets can be obtained by utilizing an OTRSH functional starting point in combination with the TDA; in our follow-up

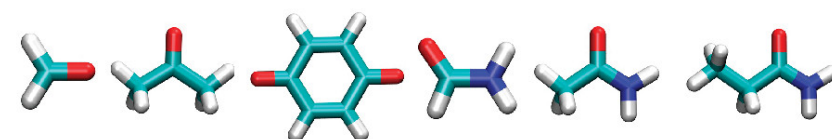
Unsaturated Aliphatic Hydrocarbons



Aromatic Hydrocarbons and Heterocycles



Aldehydes, Ketones and Amides



Nucleobases

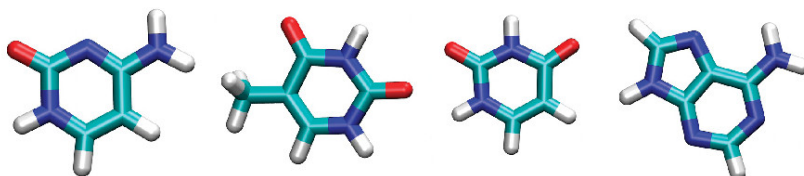


Figure 3.1: The 28 molecules contained in Thiel's set. H is white, C is light blue, N is dark blue, and O is red.

study, which utilized a larger basis set to confirm the results of the initial study, we finally demonstrated that the OTRSH starting point in combination with G0W0 is a balanced and economical approach for both singlet and triplet excitations on organic molecules.

The BSE formalism was already reviewed in Chapter 2. This chapter is organized as follows. In section 3.1, we present practical details regarding the software used, the benchmark molecule set, and identification of excitations. Section 3.2 comprises our first study on these molecules with the GW-BSE technique, and section 3.3 comprises the results of a follow-up study that utilized a larger basis set than the first one and includes OTRSH as a DFT starting point. The main conclusion of each study is stated in the title of each section.

3.1 Technical Details: the software, the benchmark set, and identification of excitations

Our calculations were performed with the molgw code[68, 69] which is an implementation of GW and BSE many-body perturbation theory with Gaussian basis functions that aims first and foremost for accuracy and ease of development. molgw relies on an external library, libint,[70] to evaluate the Coulomb integrals. The xc energies, potentials, and kernels for different starting gKS DFT mean-fields are obtained from the libxc library.[71] molgw solves the random-phase approximation equation for the spectral representation of W and thus computes the GW self-energy analytically from a given xc starting point. For more information about this code see ref. [69].

Thiel’s set contains 28 organic molecules that consist of just four different elements (C, N, O, and H) with the largest molecule being naphthalene $C_{10}H_8$ (see figure 3.1). The geometries of the molecules in Thiel’s set were relaxed within MP2; coordinates for all molecules can be found in the supplementary material of ref. [67]. The set comprises tabulated reference excitation energies for 103 singlet and 63 triplet final states. The reference excitations have been obtained from several flavors of coupled-cluster theory, namely, CC2, CCSD, and CC3[72] and from complete-active-space second-order perturbation theory (CASPT2).[73] These have been used in conjunction with some human intuition about the usual discrepancy between these methods and reality to construct what Thiel and coworkers refer to as “best theoretical estimates” (BTEs for short). Indeed, BTE values can lie outside the range of the calculated values. Note that, consistent with the Thiel group’s subsequent TDDFT study,[67] we disregarded the tabulated double excitation of tetrazine ($C_2N_4H_2$) which so far are not captured by TDDFT or BSE approaches. This explains why we refer to 103 tabulated values instead of the 104 that appear in the original work.

Using reference output of Gaussian09[74] for TD-B3LYP, we have unambiguously identified the nature of all the excitations of Thiel’s set. The identification is based on parity symmetry, reflections through mirror planes, oscillator strength magnitudes, energy separation, and, if necessary, the coefficients of the excitation on the product basis.

3.2 evGW eliminates the mean-field starting point present in G0W0 calculations.

Technical aspects: Basis set, xcfs, and BTEs

Our original calculations used the so-called TZVP basis set of Ahlrichs and coworkers.[75] This relatively limited basis was used so that the highly demanding calculations required to build the BTEs were feasible. For the sake of comparison we have employed the same basis set in our calculations in this work. The TZVP basis contains three series of valence basis functions, but only one series of polarization functions (d orbitals for C, N, and O,

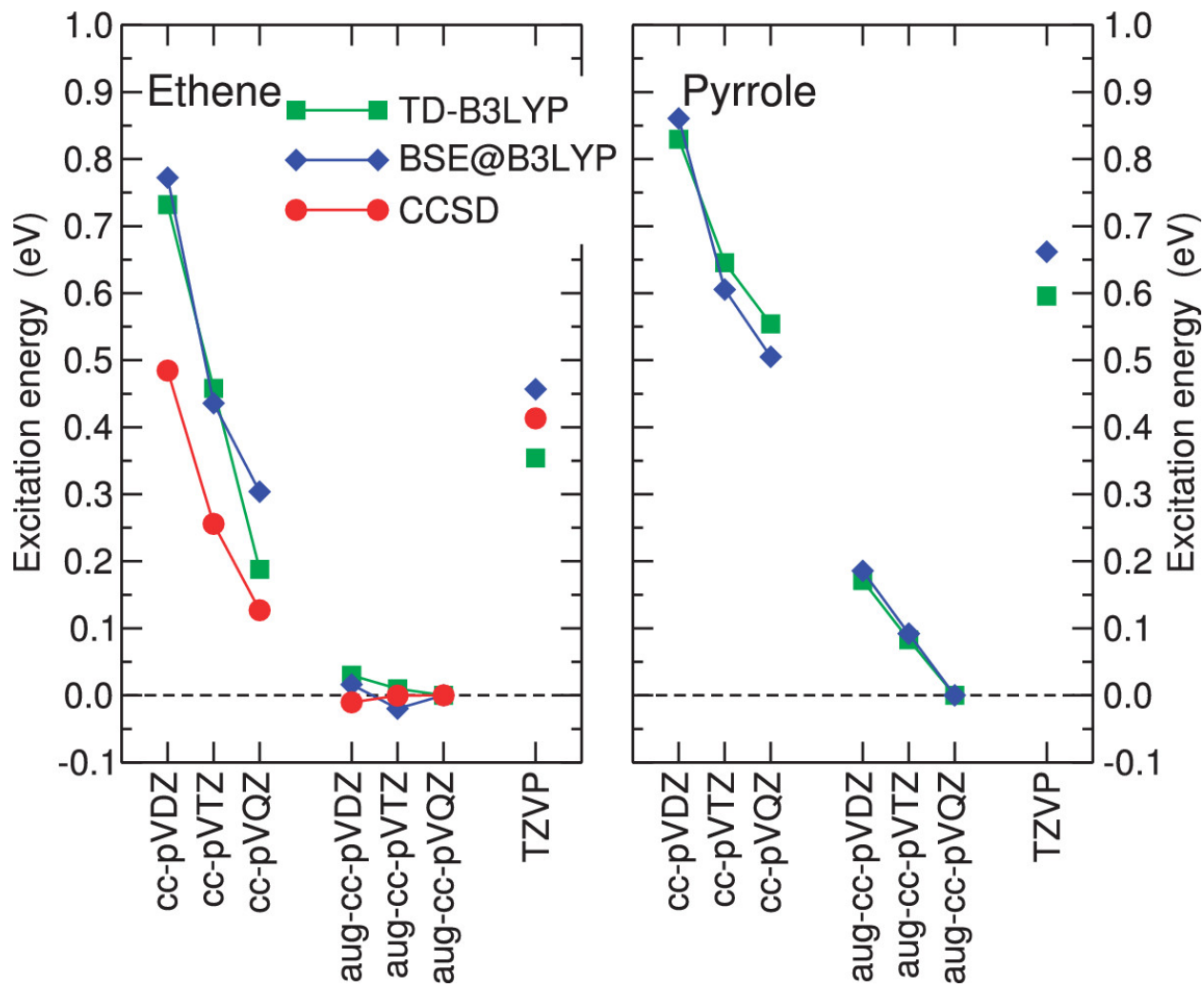


Figure 3.2: Convergence with basis set of the first 1B1u excitation in ethene (left panel) and of the first 1B2 excitation in pyrrole (right panel) within CCSD (from Ref. [67]), TD-B3LYP and BSE based on B3LYP inputs. The excitation energy for the largest basis set (aug-cc-pVQZ) has been used as the zero for each theoretical approach.

and p orbitals for H); it contains no diffuse functions. This basis set yields unconverged results as exemplified in Fig. 3.2 for the first excitation in ethene C_2H_4 , which is one of the smallest molecules of the set, and for the first bright excitation in pyrrole C_4NH_5 , which is a representative medium-sized molecule in the set. Although all methods considered here (coupled-cluster, TDDFT, and BSE) are unconverged for the TZVP basis set compared to, for example, the Dunning aug-cc-VQZ basis set[76], it is demonstrated in Fig. 3.2 that the convergence rate is similar for the different approaches, justifying our drawing conclusions

from a smaller basis. The deviation of the TZVP value from the converged value ranges from 0.35 to 0.50 eV across the different theoretical methods. Because the deviation of these methods with the TZVP basis is within 0.15 eV, we expect our calculations to trend meaningfully. The calculated mean errors with respect to the BTEs that we provide in the following should be interpreted with an uncertainty of 0.15 eV. The Thiel group has also shown that the conclusions drawn from the smaller TZVP basis remain valid with the larger aug-cc-pVTZ basis set that includes diffuse functions.[27, 77]

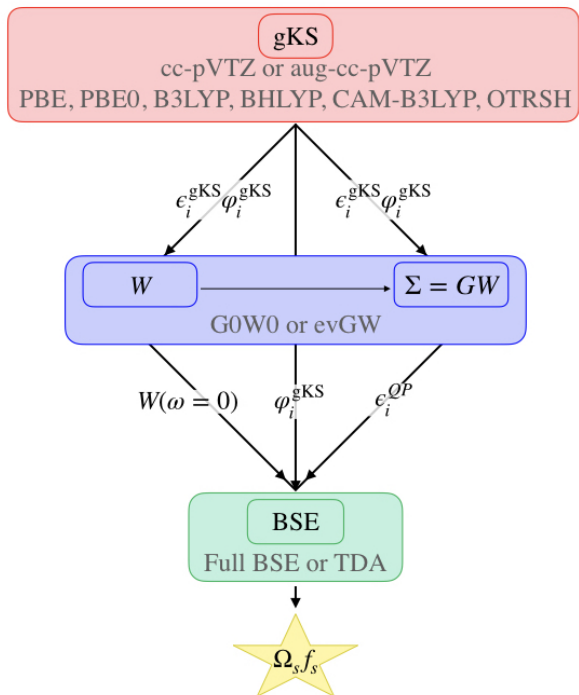


Figure 3.3: GW-BSE workflow. Approximations explored here are included in gray text.

As shown in Fig. 3.3, the BSE excitation energies rely on eigenenergies and wavefunctions from a prior self-consistent gKS DFT calculation. As mentioned, a strong dependence of the GW quasiparticle energies on the DFT starting point has previously been discussed in the literature[16, 61, 63, 78, 79, 80]; thus, it is not surprising that BSE excitation energies, which are built upon GW quasiparticle energies, will also exhibit such a dependence. Although the influence of the DFT starting point was mentioned in earlier works[81] a systematic quantitative study had not yet been performed. We assessed the BSE by its deviation from reference BTEs of Thiel’s set for both singlet and triplet excitations. The BSE is solved using GW quasiparticle energies that have been obtained from different xc approximations to the gKS DFT starting point. We selected 4 different xc approximations that are reasonably representative of the popular choices for molecules. PBE[42] is a pure semi-local functional

with no exact exchange. B3LYP[45] is a hybrid functional containing 20% exact exchange, whose 3 parameters have been adjusted to yield good thermodynamic data, and, to this day, is one of the most widely used functionals in the quantum chemistry community. BHLYP[82] is another hybrid functional due to Becke but contains a significantly larger content of exact exchange, 50%. This functional was identified as one of the best starting points for GW in a previous study.[63] Tuned CAM-B3LYP[83] labeled tCAM-B3LYP in the following, is a range-separated hybrid that has the correct full long-range exchange $\alpha + \beta = 1$. It is constructed to yield accurate results in TDDFT. Our BSE results will be labeled BSE@PBE, BSE@B3LYP, BSE@BHLYP, and BSE@tCAM-B3LYP, respectively. I should reiterate that even though it is not explicitly stated in the short-hand notation, an intermediate single-shot G0W0 calculation is always performed.

Singlet excitations

Figure 3.4 illustrates the correlation between our computed BSE singlet excitation energies and the reference BTEs evaluated by Thiel’s group.[67] Perfect agreement would be the case if all points were to lie along the diagonal line. BSE@PBE consistently yields singlet excitation energies that are too low: almost all data points are below the diagonal. BSE@B3LYP is much improved but still somewhat underestimates the excitation energies for this set. BSE@BHLYP and BSE@tCAM-BL3YP, however, are in excellent agreement, with narrow scattering around the diagonal. The data in Fig. 3.4 remarkably follow the fit by a straight line, whose slope is very close to unity. This means that for a given starting point, the error is quite constant irrespective to the excitation energy.

Thus, whereas semi-local functionals like PBE are less suitable as a starting point for this set of small organic molecules, hybrid functionals do much better, and it appears that a larger content of exact exchange improves the agreement with respect to the best theoretical estimates.

In Fig. 3.5, we report the mean signed error (MSE) and mean absolute error (MAE) with respect to BTEs for the different approaches considered in this study and cite the TD-B3LYP error[77] as a reference. We select TD-B3LYP because it performs best for Thiel’s set among all TDDFT xc functionals.[27] In fact, for the type of excitations considered in Thiel’s set—no charge transfer or Rydberg excitations—TD-B3LYP performs so admirably that we could not expect BSE to outperform it. As previously noticed, the results reported in Fig. 3.5 show a strong dependence of the BSE excitation error on the starting point. More precisely, BSE@PBE underestimates all the excitation energies by almost 1 eV. BSE@B3LYP also yields excitation energies that are too low. However, with a BHLYP or tCAM-BL3YP starting point, the BSE results can indeed challenge the best TDDFT excitation energies, yielding results with a MAE of around 0.25 eV.

In conclusion, for singlet excitations, G0W0-BSE with a properly chosen starting point can be a predictive tool for simple neutral excitations of small organic molecules. We will return to the starting point dependence further in the discussion section.

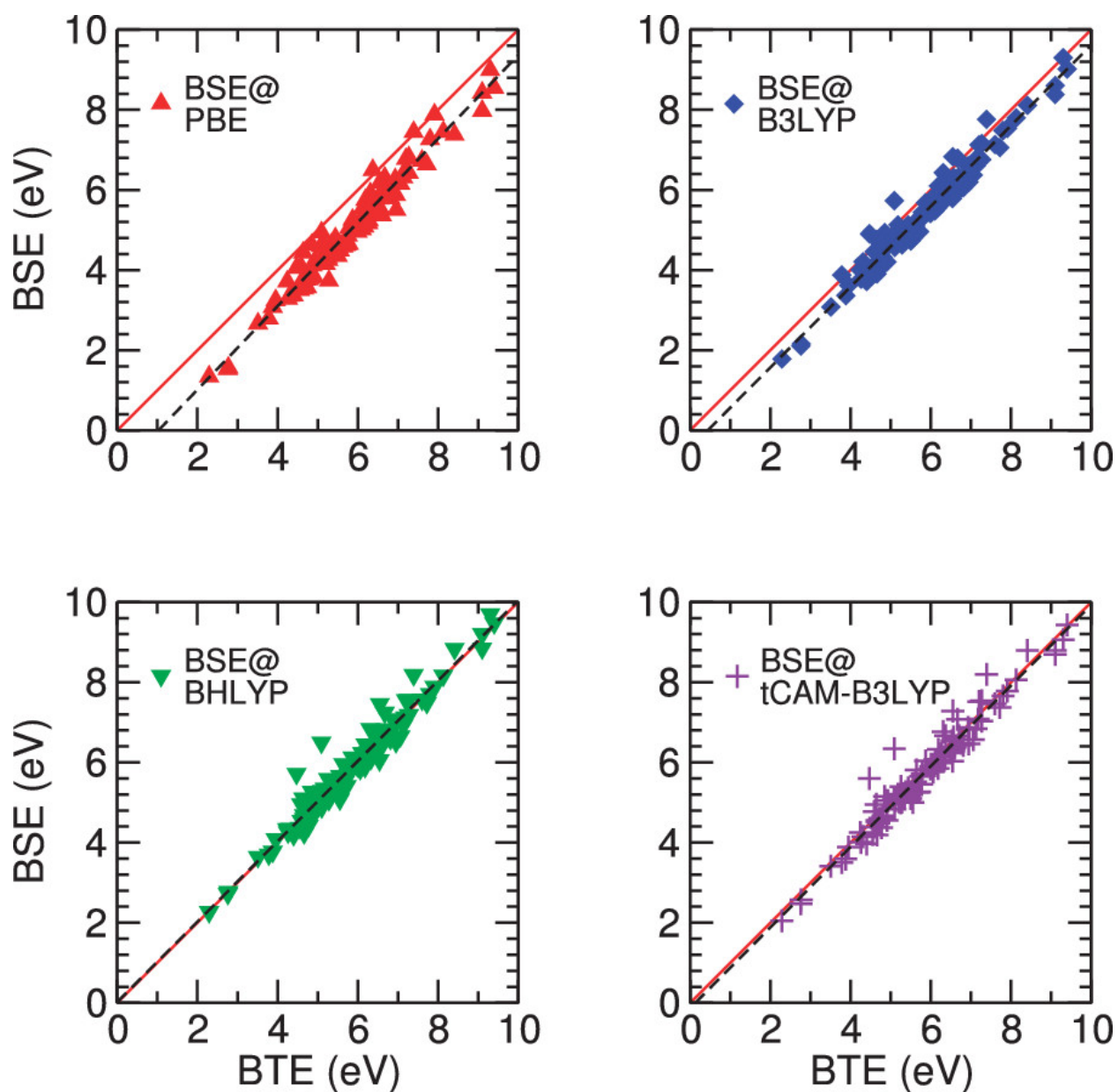


Figure 3.4: Correlation plots for singlet excitations between BSE with different starting points and the BTE. A linear fit of the data is shown with a dashed line.

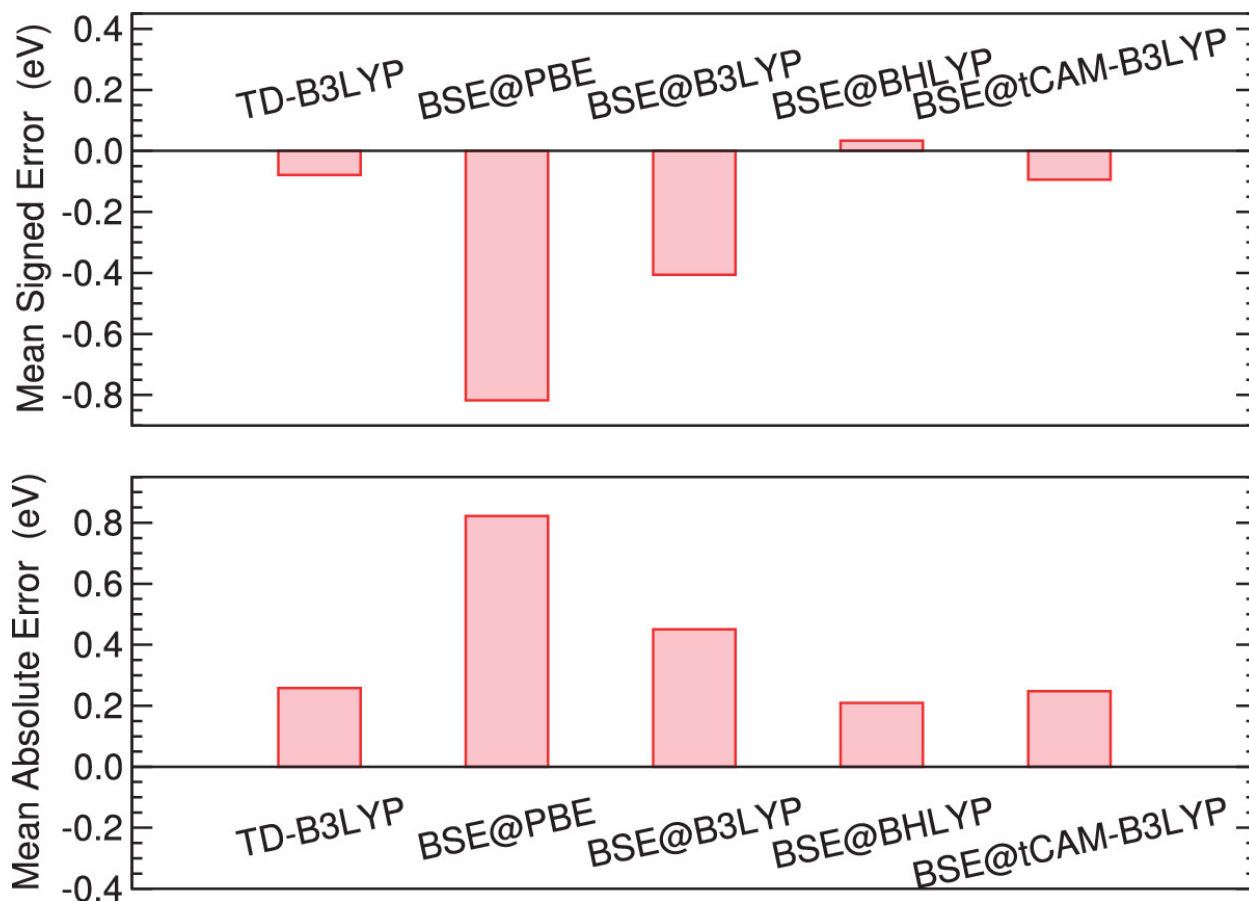


Figure 3.5: Mean signed error (upper panel) and mean absolute error (lower panel) for singlet excitations for different schemes. TDDFT based on B3LYP (from Ref. 42) is given as a comparison.

Triplet excitations

Thiel's set also contains 63 triplet excitation energies. It is well documented that TDDFT can have trouble with triplet excitations[27]: no xc functional of TDDFT has been able to predict triplet energies of the molecules in Thiel's set at the level obtained for singlets. Our BSE calculations in this initial work showed a trend very analogous to TDDFT for triplets. From the correlation plots shown in Fig. 3.6, we see that all BSE triplet excitations are too low, regardless of the initial gKS starting point. (The data used in Fig. 3.6 can be found in the supplementary material of our paper, Ref. [84].) Once again, the excitation energies are well fitted by a straight line, but with a slope that departs from unity. The slope ranging from 0.88 for PBE to 0.97 for tCAM-B3LYP indicates that the error is not perfectly constant across the excitation energies: the larger excitation energies have a greater

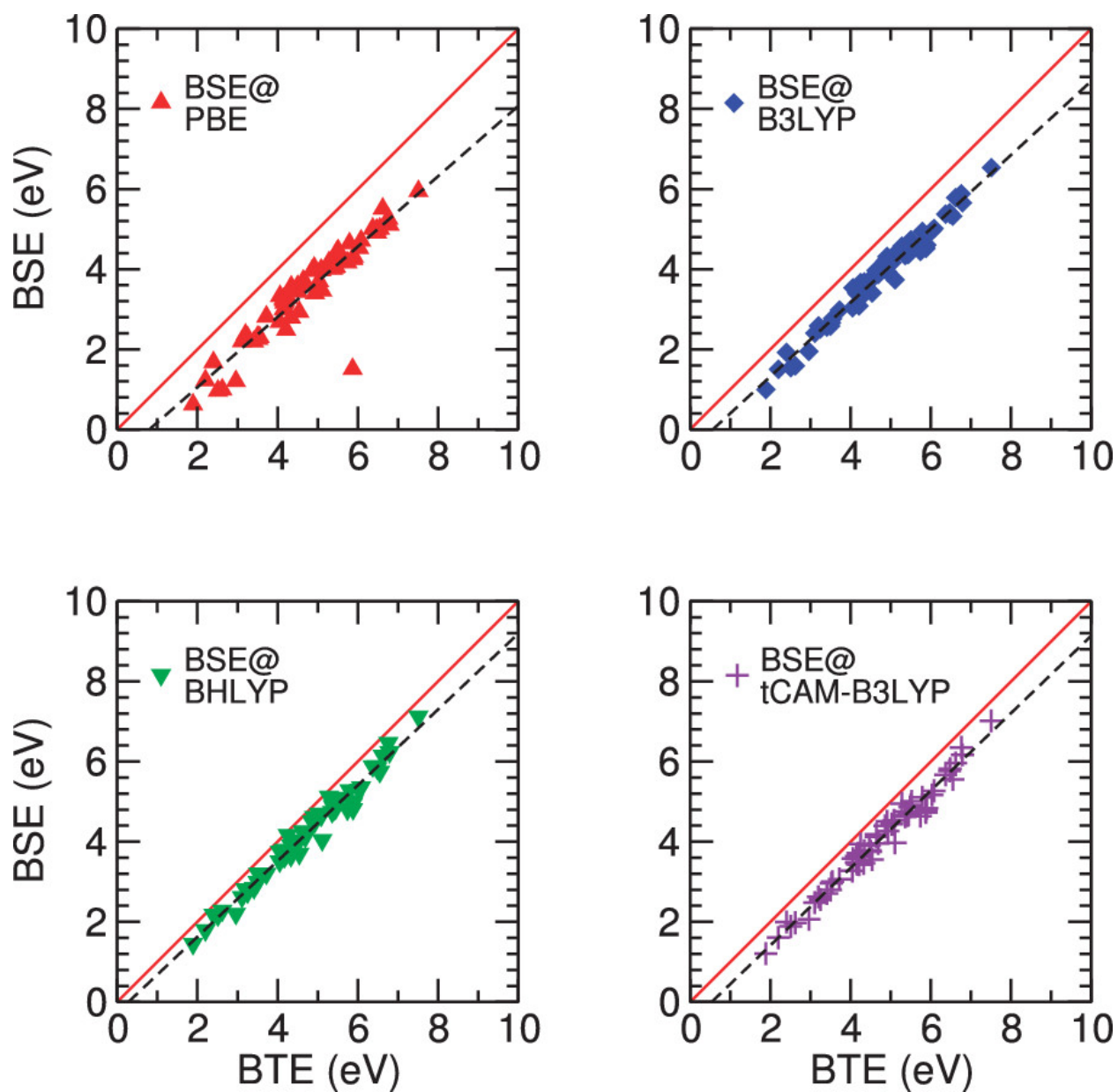


Figure 3.6: Correlation plots for triplet excitations between BSE the different starting points and the BTE. A linear fit of the data is shown with a dashed line.

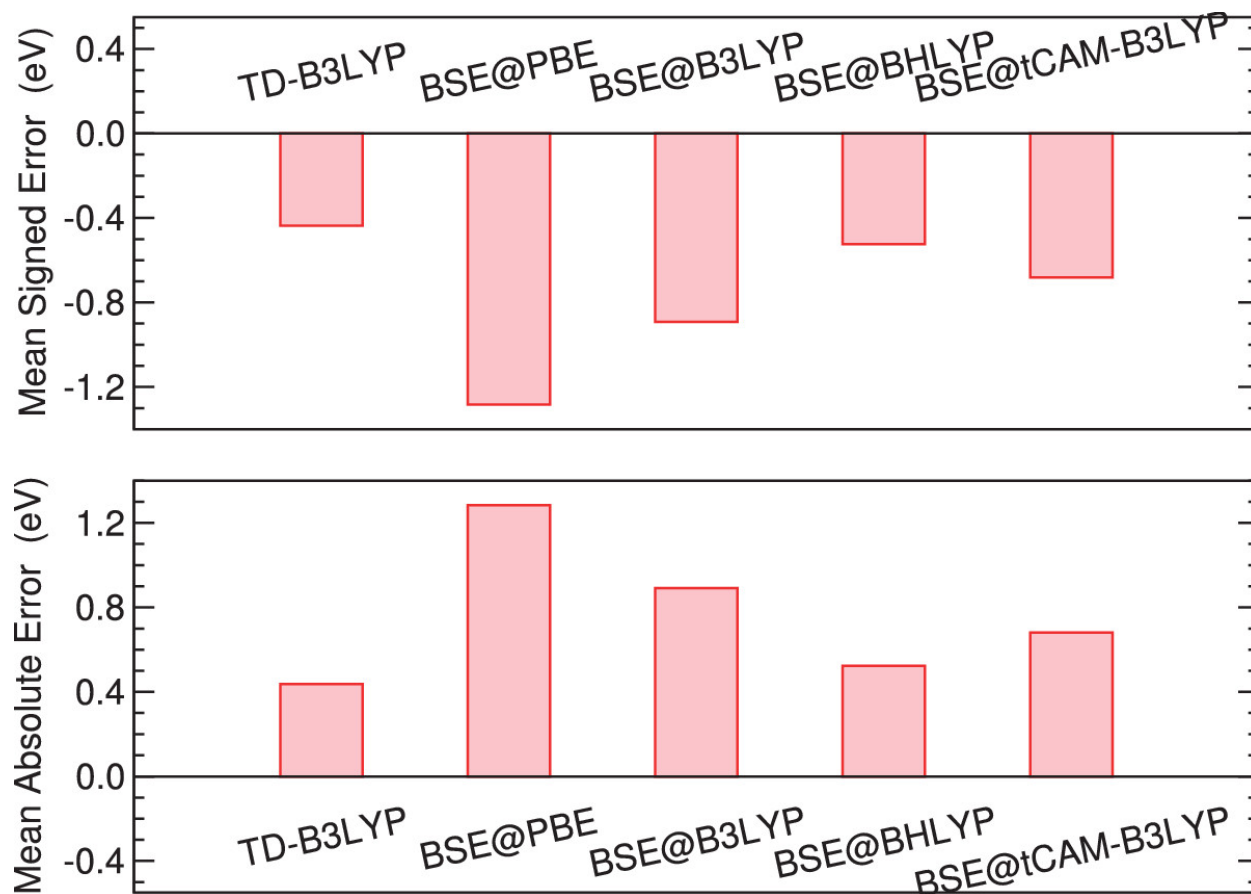


Figure 3.7: Mean signed error (upper panel) and mean absolute error (lower panel) for triplet excitations for different schemes. TDDFT based on B3LYP (from Ref. [67]) is given as a comparison.

error. As expected, BSE@PBE produces the poorest triplet excitation energies of all. Hybrid functionals with some exact exchange (BHLYP and tCAM-BL3YP) improve results relative to the BTE, but the quality of the calculated triplet excitation energies is poorer than for singlets.

The errors shown in Fig. 3.7 confirm that with the best starting point (BHLYP), our BSE calculations match TD-B3LYP in quality but do not do better for Thiel's set. For both TD-B3LYP and BSE@BHLYP, the error is systematic, with an underestimation of the triplet energies by 0.4 eV.

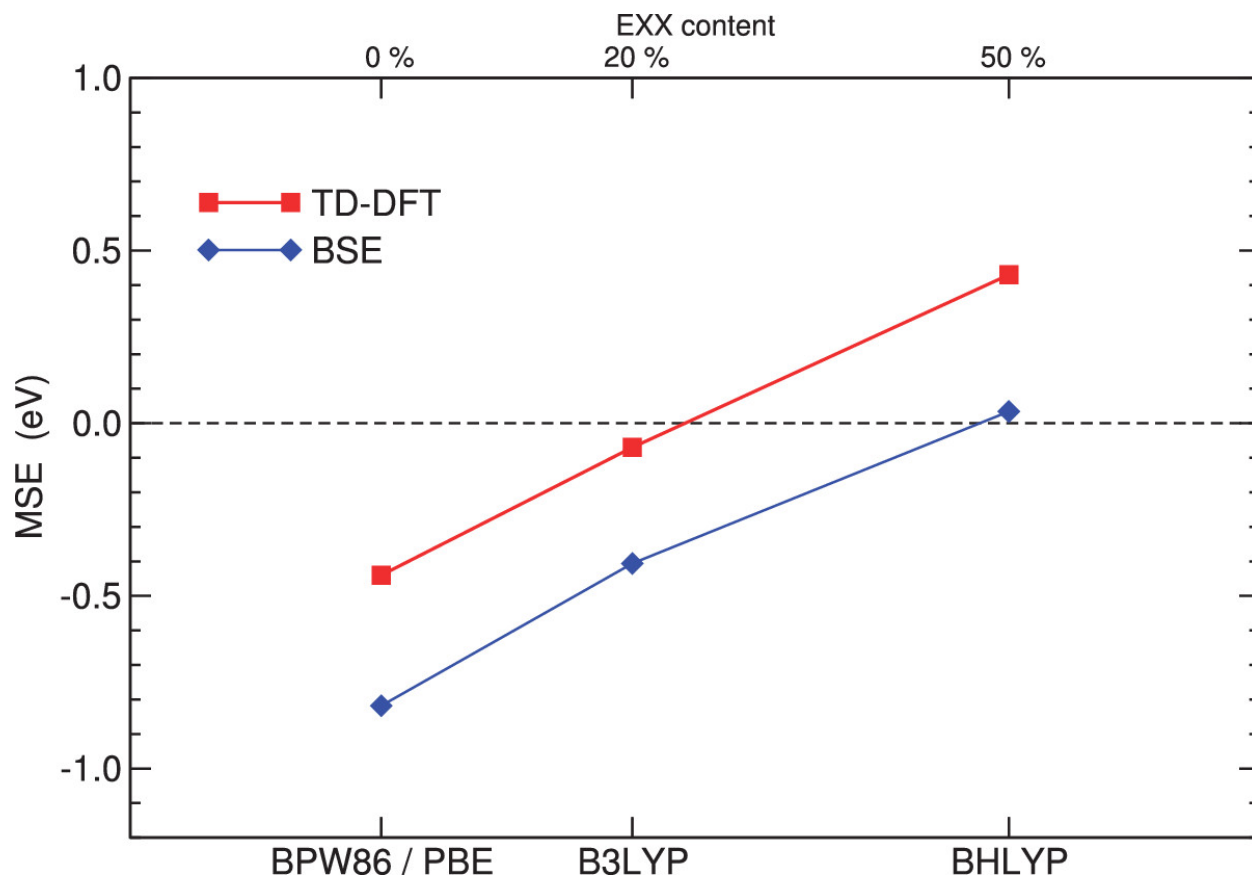


Figure 3.8: Dependence of the mean signed error for the singlet excitation energies of the Thiel’s set with respect to the content of exact exchange of the underlying xc functional. The xc functional is used for TDDFT (red square symbols) or as the starting point of GW and BSE (blue diamond symbols).

Discussion

A strong dependence on the starting point

As shown above, the quality of the BSE excitation energies is strongly affected by the gKS starting point. Here, we discuss the sensitivity of the final BSE result to starting point, relative to TDDFT.

In Fig. 3.8, we represent the mean signed error for Thiel’s set as a function of the amount of exact exchange in the xc functional. The TDDFT results are from Ref. [67], whereas the BSE results are those reported above. Both approaches show a noticeable dependence on the exact exchange content, and in the end, they are nearly equally sensitive to the xc functional.

Interestingly, the primary difference between the TDDFT and BSE schemes lies in the amount of exact exchange that minimizes the error. TDDFT performs best with 20%-25%

exact exchange as in B3LYP or PBE0.[27] On the contrary, for BSE, the best starting points contain much more exact exchange (around 50%). These two very different optima can be rationalized when decomposing the origin of the errors in each of the two schemes as we discuss in what follows.

Analysis of the origin of errors

As summarized in Fig. 3.3, the BSE energies are obtained from a series of three calculations: a self-consistent gKS DFT calculation, a single-shot GW calculation of the quasiparticle energies, and finally an evaluation of the BSE. It is interesting to identify which step introduces the noticeable starting point dependence we highlighted above. Or, another way of posing the same question would be the following: which among (a) GW quasiparticle energies and (b) the BSE solution are most sensitive to gKS input?

To address this question, we need “best theoretical estimates” for the quasiparticle energies too. Although it is not possible to easily access all quasiparticle energies, the HOMO and LUMO energies can be obtained via total energy differences with the so-called SCF procedure. To obtain accurate results, we applied the +SCF procedure within CCSD(T), the well-known and standard coupled-cluster method including single and double excitations with triples introduced perturbatively.⁴³ All of our coupled-cluster calculations are done with the Gaussian09 code[74]. We employ the same TZVP basis set used by Thiel and by us so far in this study. Again, although the diffuse-orbital-less TZVP basis set is, strictly speaking, inadequate for the LUMOs for many of these molecules, we use it for consistency with the rest of the calculations performed in this work. The +SCF procedure requires three separate total-energy calculations for evaluation of the HOMO-LUMO gap: one for the neutral molecule and additional calculations for the cation and anion. Note that the underlying Hartree-Fock self-consistent field calculations have been carefully checked against molgw, since the cation and anion cases can be challenging and quite often converge to local minima.

The comparison between GW HOMO-LUMO gaps and CCSD(T) gaps is summarized in Fig. 3.8, and the data are tabulated in the supplementary material of Ref. [84]. The results are in line with a previous study of the ionization potentials of small molecules[63]: GW on PBE largely underestimates the HOMO-LUMO gap, whereas hybrid functionals with a large fraction of exact exchange do a much better job. Even GW on Hartree-Fock (GW@HF) does well for the gaps, as highlighted in Ref.[16]. It is worth noting that the trends for the HOMO-LUMO gaps are the same as those for singlet excitations.

3.3 OTRSH eliminates the need for evGW calculations

Although the *ab initio* GW-BSE approach has emerged as a leading method for predicting neutral excitations in both solids and molecules, its predictive power is contingent upon

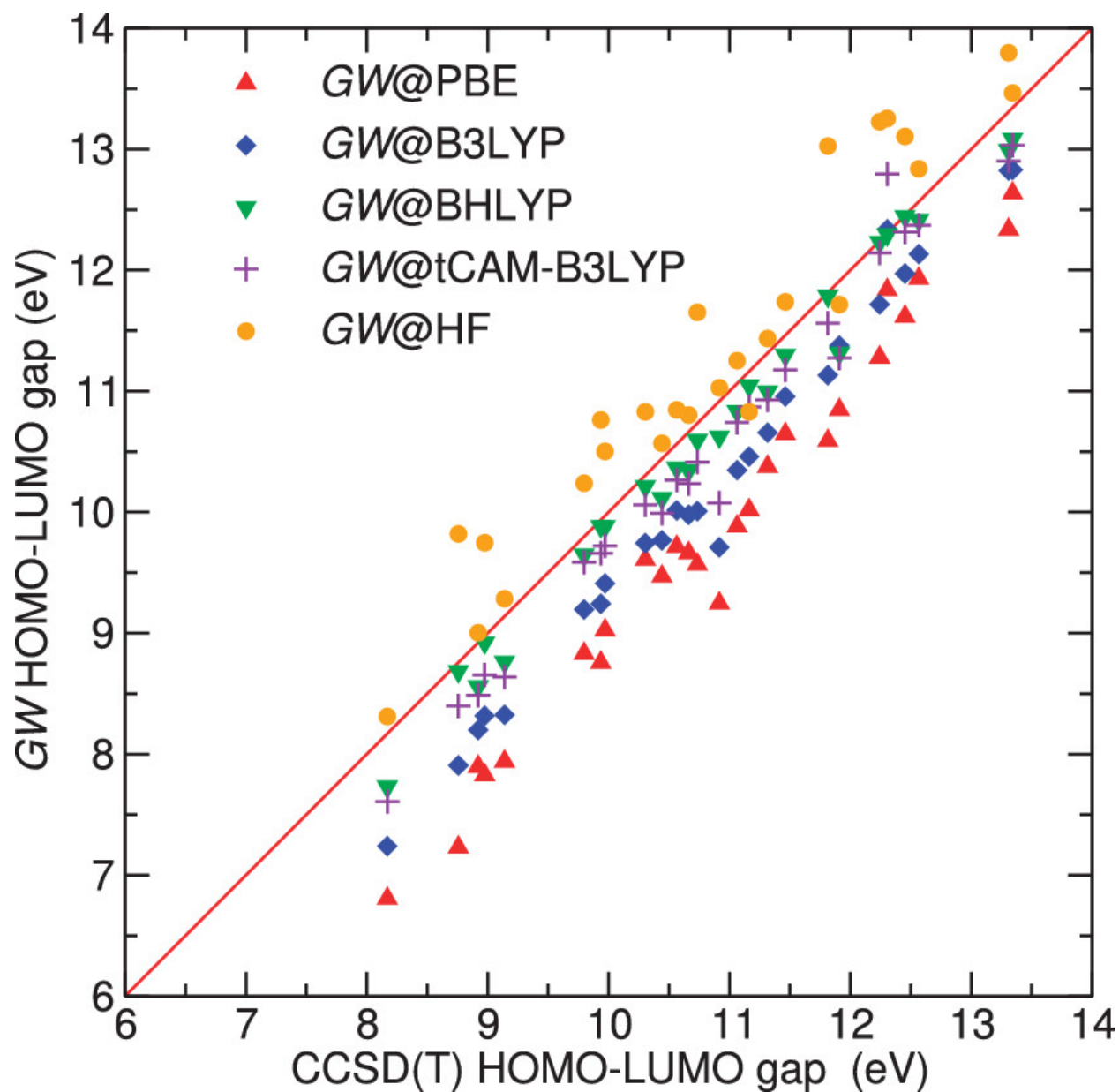


Figure 3.9: Correlation plot for HOMO-LUMO gap from single-shot GW and from CCSD(T)

several factors. If self-consistency in the eigenvalues is not used, then the singlet excitation energies depend critically on (1) the generalized Kohn-Sham (gKS) eigensystem used to construct the GW self-energy and to solve the BSE, and (2) whether or not the TDA is evoked. While we and others have shown that evGW-BSE minimizes starting point dependence and additionally minimizes the difference between the full BSE and TDA results, the requirement of multiple self-consistency steps increases computational demands, which can become prohibitive for larger systems; and for triplets the starting-point dependence survives even in the evGW-BSE case. In fact, no single-shot G_0W_0 approach, without subsequent computationally-demanding GW self-consistency steps, has demonstrated a well-balanced description of both triplets and singlets, of local, extended, charge-transfer, and Rydberg excitations for gas-phase molecules. We will show below that even with eigenvalue self-consistency, triplet energies are still underestimated by roughly 0.5 eV.

In our follow-up benchmark study, we present a detailed analysis of the OTRSH starting point and show that the use of this gKS starting point with G_0W_0 -BSE leads to the lowest mean absolute errors (MAEs) and mean signed errors (MSEs) thus far demonstrated in the literature for the low-lying neutral excitations of Thiel set molecules without the need for self-consistency. In fact, the MSEs (0.02 for singlets and -0.18 for triplets) and MAEs (0.24 for singlets and -0.18 for triplets) are comparable to or lower than those obtained with other functional starting points *after* self-consistency. Additionally, we compare these results with TDDFT using the OTRSH starting point, and find GW-BSE to be superior to TDDFT with the same exchange-correlation functional. This work indicates tuned range-separated hybrids used in combination with GW-BSE can greatly suppress starting point dependence for molecules, leading to accuracy similar to higher-order wavefunction-based theories at reduced computational cost for neutral excitations of molecules without the need for several GW-BSE calculations to iterate to self-consistency.

I should note that some solutions other than OTRSH have been proposed to address starting-point dependence. One of these is a consistent starting point (CSP) scheme, in which the best alpha in a global hybrid is chosen so that the GW correction for the quasiparticle spectrum, not just the HOMO[61, 85], is minimized to a rigid shift of all eigenvalues. The CSP method has not yet been benchmarked for G_0W_0 -BSE neutral excitations; but it is a global PBEh hybrid typically having 25-30% exact exchange and we have seen that the best starting point for G_0W_0 -BSE for singlets (but not so much for triplets) is BHLYP, a global hybrid having 50% exact exchange. Furthermore, we have seen that PBE0 and B3LYP, which each have 25% exact exchange (similar to the CSP schemes) are excellent for TDDFT, but poor starting points for G_0W_0 -BSE neutral singlet and triplet excitations. Thus, here we have focused on the utility of IP tuned hybrids which give accurate KS-HOMO energies and have shown good agreement with experiment for the whole excitation spectrum[24, 86, 87, 88]. Two examples of OTRSH functionals are that of Baer-Neuhauser-Lifshitz (BNL)[55, 56] and the Perdew-Burke-Ernzerhof (PBE)-based OTRSHs[25, 57, 24]. The work in chapter 4[89] shows that OTRSH functionals can be effective DFT starting points for GW-BSE calculations yielding accurate singlet and triplet excitation energies for gas-phase organic molecules; here, we expand on the study outlined in section 3.1 and undertake a systematic

assessment of the OTRSH functional as a starting point for GW-BSE excitation energies in Thiel’s set.

Technical aspects: Basis set, xcfs, and BTEs

We evaluate G0W0@OTRSH, against G0W0@B3LYP (one-shot GW on top of B3LYP[45], which has 20% exact-exchange); G0W0@BHLYP (one-shot GW on top of BHLYP[82], which has 50% exact-exchange); G0W0@CAM-B3LYP (one-shot GW on top of CAM-B3LYP[49], a range-separated hybrid with 25% short-range exact-exchange and full asymptotic exact-exchange); and eigenvalue self-consistent GW (evGW), in which the quasiparticle energies are updated (in both G and the polarizability) one or more times prior to calculating the final self-energy corrections[16].

These xc functionals were chosen for the following reasons. B3LYP and PBE0 are among the most popular choices for TDDFT calculations, while BHLYP has demonstrated good performance as a starting point for GW-BSE. CAM-B3LYP is an untuned range separated hybrid that can be compared to OTRSH, and PBE is a representative from the non-hybrids. With these six functionals we go from 0% at all ranges to 100% HF exchange in the long range for OTRSH (see Table 3.1 below).

As before, in our GW-BSE calculations with the molgw package, the frequency dependence of the GW non-local self-energy is treated analytically, and hence is exact for a given basis set. We use standard approximations to solve the BSE: irreducible vertices are set to 1, the polarizability and other matrix elements are constructed using GW eigenvalues and DFT wavefunctions; the screened Coulomb interaction is evaluated in the random phase approximation (RPA); and a static approximation is taken for the electron-hole screening. We utilize the aug-cc-pVTZ basis set[90]. Following prior work[89], we use the resolution-of-the-identity in the Coulomb metric as implemented in molgw[69], with the auxiliary basis sets of Weigend[91] which are consistent with Dunning basis sets.

For OTRSH, we set $\alpha = 0.2$, which fixes the amount of short-range Fock exchange to 20%. Additionally, we set $\alpha + \beta = 1$ to enforce long-range asymptotic exact exchange. The range separation parameter γ is varied to enforce the ionization potential theorem of DFT through minimization of the target function $J^2(\gamma)$:

$$J^2(\gamma) = [\text{IP}^\gamma(N) + E_{\text{HOMO}}^\gamma(N)]^2 + [\text{IP}^\gamma(N + 1) + E_{\text{HOMO}}^\gamma(N + 1)]^2, \quad (3.1)$$

where the ionization potential of the neutral species with N electrons, $\text{IP}^\gamma(N)$, is determined via a δ SCF approach from total energy differences as $\text{IP}^\gamma(N) = \epsilon_{\text{tot}}^\gamma(N - 1) - \epsilon_{\text{tot}}^\gamma(N)$. Here $\epsilon_{\text{tot}}^\gamma(N)$ and $\epsilon_{\text{tot}}^\gamma(N - 1)$ are total energies of the neutral and cation species respectively. This procedure enforces the DFT ionization potential theorem[92], namely that the energy of the Kohn-Sham highest occupied molecular orbital (HOMO) is equal to the negative of the first ionization potential. For molecules with an unbound $N + 1$ anionic state, only the first of



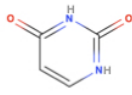
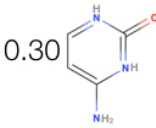


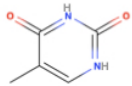
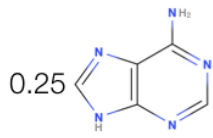



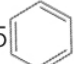
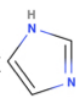
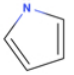

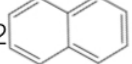
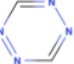
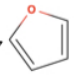
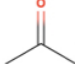
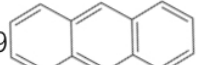
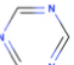
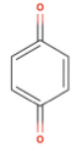
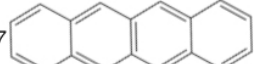
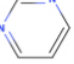

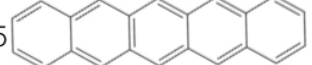
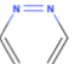

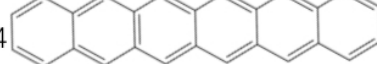
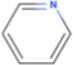

Unsaturated Aliphatic Hydrocarbons		Nucleobases	
0.31 	0.32 	0.35 	0.30 
0.26 	0.25 	0.30 	0.25 
0.23 	0.25 		
0.20 			
Aromatic Hydrocarbons and Heterocycles		Aldehydes, Ketones, Amides	
0.25 	0.32 	0.26 	0.36 
0.22 	0.34 	0.27 	0.27 
0.19 	0.30 	0.32 	
0.17 	0.30 	0.30 	
0.15 	0.25 	0.27 	
0.14 	0.30 	0.25 	

Figure 3.10: Gammas for Thiel's set.

these two terms is minimized. The optimal parameters obtained within this framework for the molecules studied are shown in Fig. 3.10.

In what follows, we compare GW-BSE results for OTRSH starting points for 81 of the Thiel's set singlets comparing with evGW and TDDFT and utilizing different starting points. Importantly, we benchmark GW-BSE against wavefunction theory-based best theoretical estimates (BTEs) of excitation energies, extending our initial study to include a comprehensive analysis of the OTRSH starting point. These BTEs were obtained with multi-state multiconfigurational second-order perturbation theory such as (MS-CASPT2) and various coupled-cluster theories, such as coupled cluster with singles, doubles, and perturbative triples (CCSD(T)) [77].

Table 3.1: xc functionals and %HF

Functional	% HF	TDDFT		G0W0-BSE	
		MSD(eV)	MAE(eV)	MSD(eV)	MAE(eV)
PBE	X=0	-0.45	0.53	-1.08	1.18
PBE0	X=25	0.05	0.24	-0.54	0.62
B3LYP	X=25	-0.07	0.27	-0.62	0.72
BHLYP	X=50	0.43	0.50	-0.19	0.32
CAM-B3LYP	X=19-65; $\gamma = 0.33$	0.22	0.31	-0.24	0.36
OTRSH	X=20-100; $\gamma = 0.19 - 0.36$	0.34	0.38	0.02	0.24

Singlets

In Figure 3.11, we report the mean absolute error (MAE) and the mean signed error (MSE) with respect to BTEs for G0W0-BSE@OTRSH, comparing with other starting points and with TDDFT@OTRSH. For one-shot G0W0 approaches, the MSEs and MAEs reflect a strong starting point dependence, as we have already discussed. As the proportion of exact exchange increases, the MSE evolves from more than negative 1 eV for a PBE starting point to nearly zero for G0W0-BSE@OTRSH. Use of the TDA reduces the MAE and MSE somewhat in the one-shot case for all starting points, although only by about 0.1 eV. Notably, eigenvalue self-consistency greatly suppresses both the MAE and MSE, largely eliminating the starting point dependence and leading to similar results for all functionals.

Among all starting points considered, OTRSH leads to the lowest MSEs and MAEs and is the superior starting point. This is because OTRSH satisfies the ionization potential theorem by construction, and thus eigenvalue self-consistency leads to minimal or negligible improvement. The strong performance of the OTRSH starting point is also evident in Figure 3.12, where we plot the distribution of errors for G0W0-BSE for different starting points.

For all starting points for both G0W0 and evGW, the TDA increases the MSE by 0.1-0.2 eV, essentially shifting the entire distribution of errors up. For all starting points except OTRSH, G0W0-TDA MAEs are smaller than those from G0W0-BSE.

In Table 3.1, we compare the starting point dependence of TDDFT with that of G0W0-BSE. In general, G0W0-BSE has a larger starting point dependence than TDDFT. In Figure 3.13, we see that OTRSH is a better starting point for G0W0-BSE than for TDDFT.

Triples

Whereas evGW and TDA can work in combination with any hybrid DFT functional to produce excellent singlet excitation energies, OTRSH is required for triplet calculations. In figure 3.14 we see that only OTRSH in combination with TDA gives MAEs near 0.2 eV for the Thiel’s set triplets. In figure 3.15, we see that remarkably, when OTRSH is used a starting point, the basis set has a relatively small effect on MAEs.

In summary, we find that OTRSH is an exceptional starting point for one-shot GW-BSE,

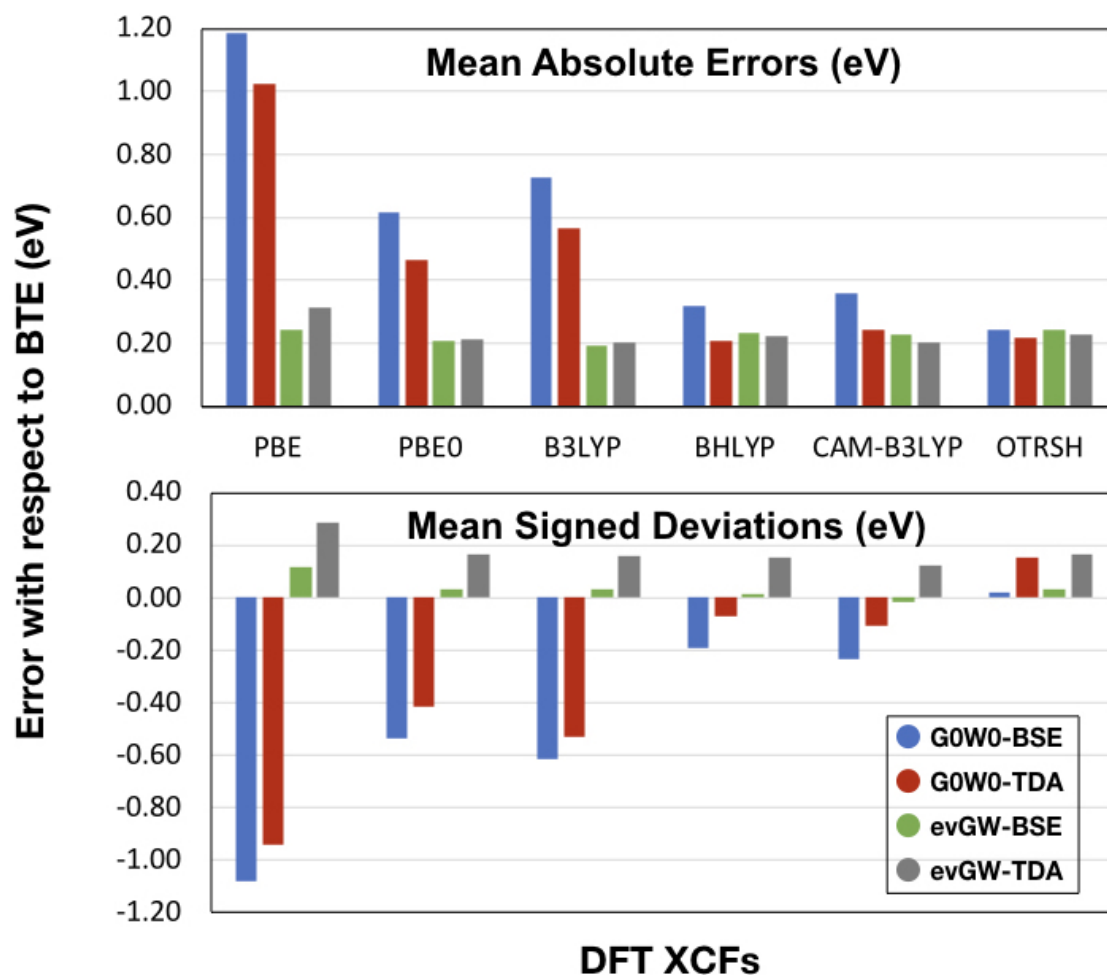


Figure 3.11: The top and bottom graphs summarize respectively the MAEs and MSDs when compared to best theoretical estimates (BTEs) from high-level quantum chemistry wavefunction based methods, including the multireference CASPT2 technique, and coupled cluster theories. The XCfs are listed in order of increasing HF exact exchange percentage. All methods shown here utilize the aug-cc-pVTZ basis set.

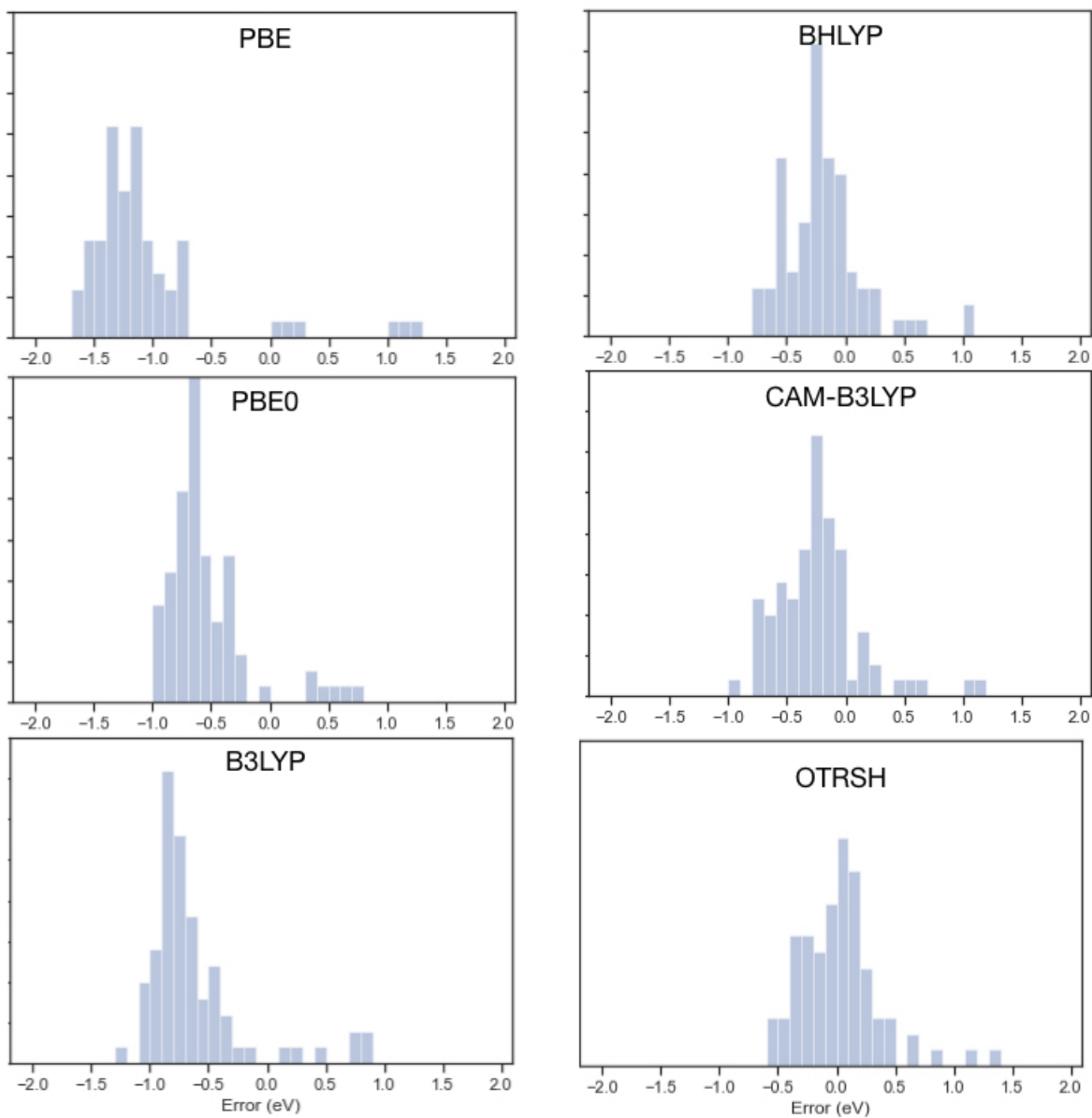


Figure 3.12: Distributions of errors for lowest lying singlets of Thiel set molecules computed from different G0W0-BSE starting points

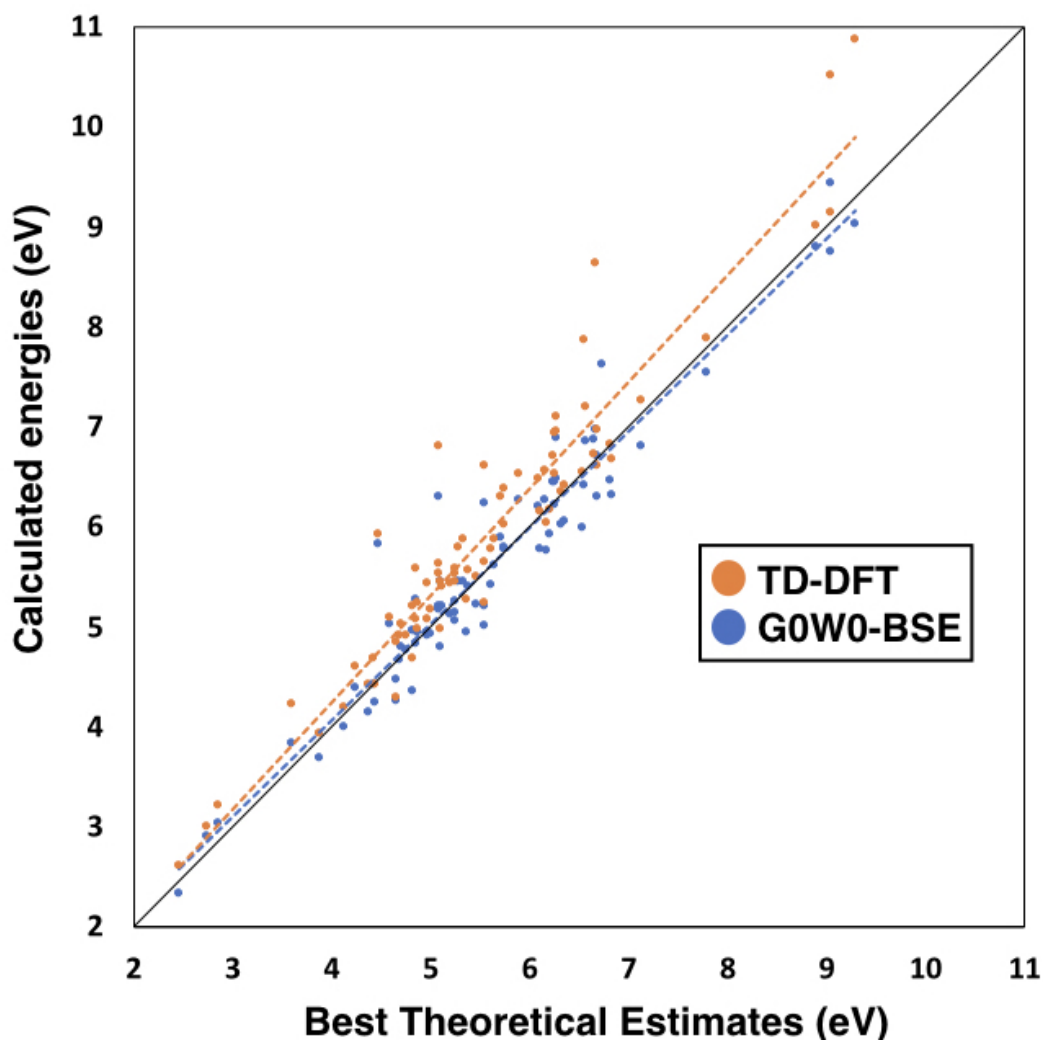


Figure 3.13: Correlation plots for singlets

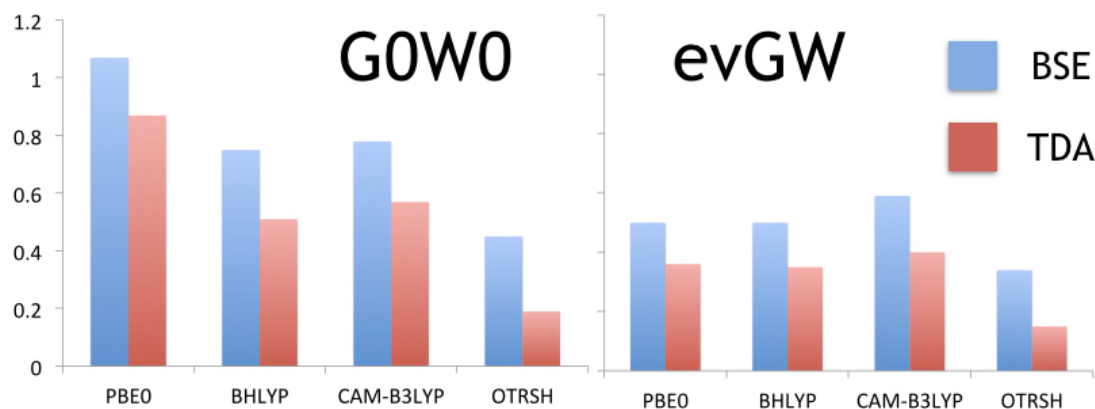


Figure 3.14: Triplet MAEs

proving to be a balanced and economical approach for both singlet and triplet excitations on organic molecules. Furthermore, the use of OTRSH can greatly suppress starting point dependence for molecules, leading to accuracy similar to higher-order wavefunction-based theories at reduced computational cost without the need for several GW-BSE calculations to iterate to self-consistency.

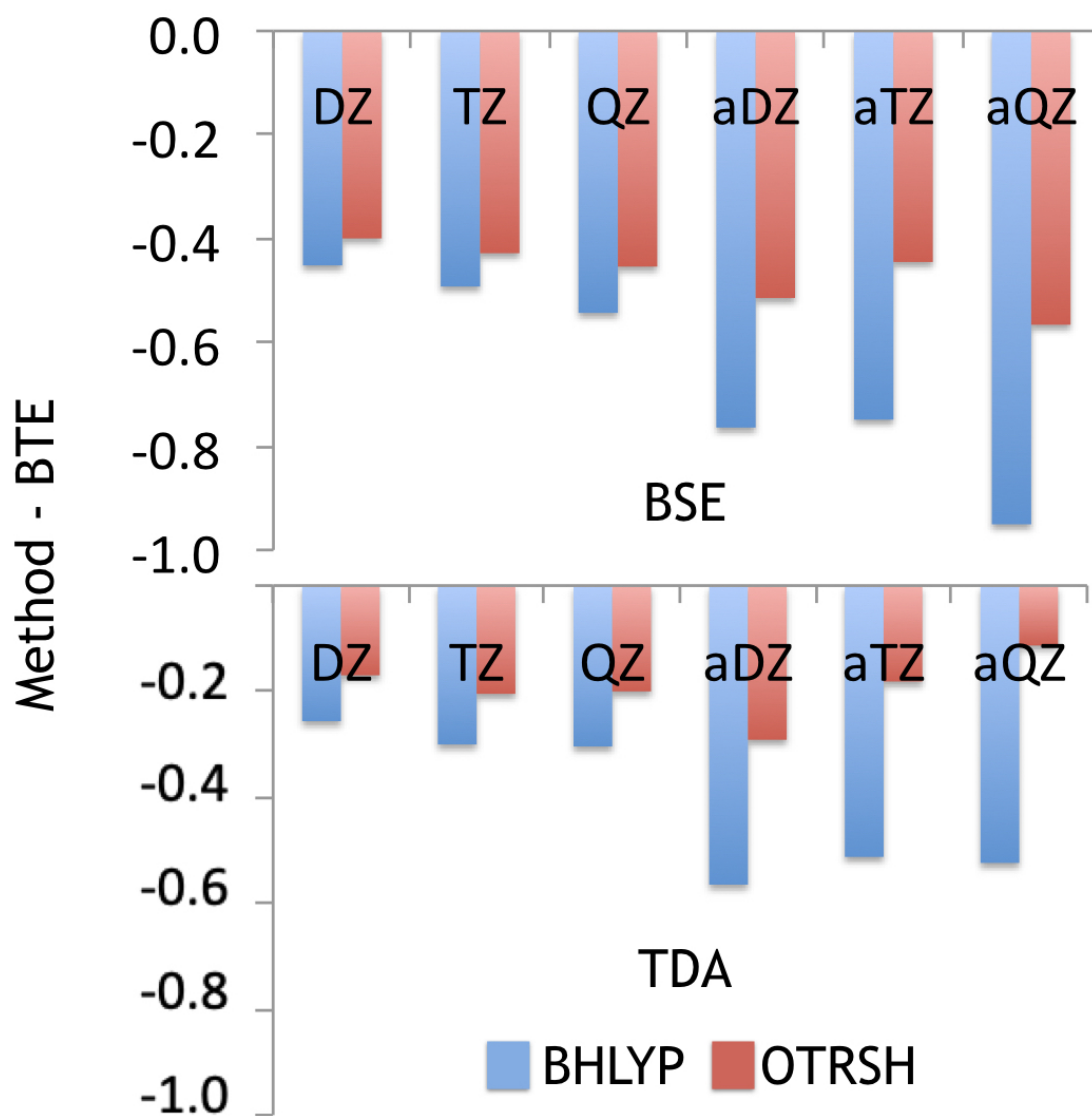


Figure 3.15: Basis set dependence of triplet MAEs

Chapter 4

Assessment of the Bethe-Salpeter equation approach for triplets and triplet instabilities of organic molecules

4.1 Introduction

As we have already discussed, the quantitative prediction and understanding of low-lying excitations in organic molecules is of significant fundamental interest and technological relevance. For example, a better understanding of multiexciton phenomena in organic molecular systems – such as singlet fission (SF) [93, 94, 95], a process by which a singlet exciton decays into two low-energy triplet excitations – can lead to external quantum device efficiencies above 100% [94, 95] and is therefore desirable for next-generation solar cells and other optoelectronic applications. Such multiexciton energy conversion phenomena are dependent on a subtle balance between singlet and triplet excitation energies, the prediction of which call for accurate *ab initio* methods.

For gas-phase acene molecules, the performance of TDDFT for a number of exchange-correlation functionals is well-documented: overall, TDDFT with standard functionals fails to predict triplet excitations [36, 96] by 0.7–1.2 eV, as well as the ordering and absolute energies of the two lowest-lying singlets [97, 98], one of which has charge-transfer-like character [98] (as detailed in Section 4.3). These failures have been ascribed to i) the so-called “low orbital overlap problem” in global hybrid functionals, in which the spatial overlap between relatively far-apart molecular orbitals is usually overestimated; and to ii) triplet instabilities associated with standard TDDFT approximations [98, 99, 100, 101, 96].

Beyond conventional TDDFT approaches, range-separated hybrid functionals (RSH) have been shown to mitigate the above mentioned low orbital overlap problem [102, 103, 98, 96]. As described in the theory chapter, in this class of functionals the Coulomb poten-

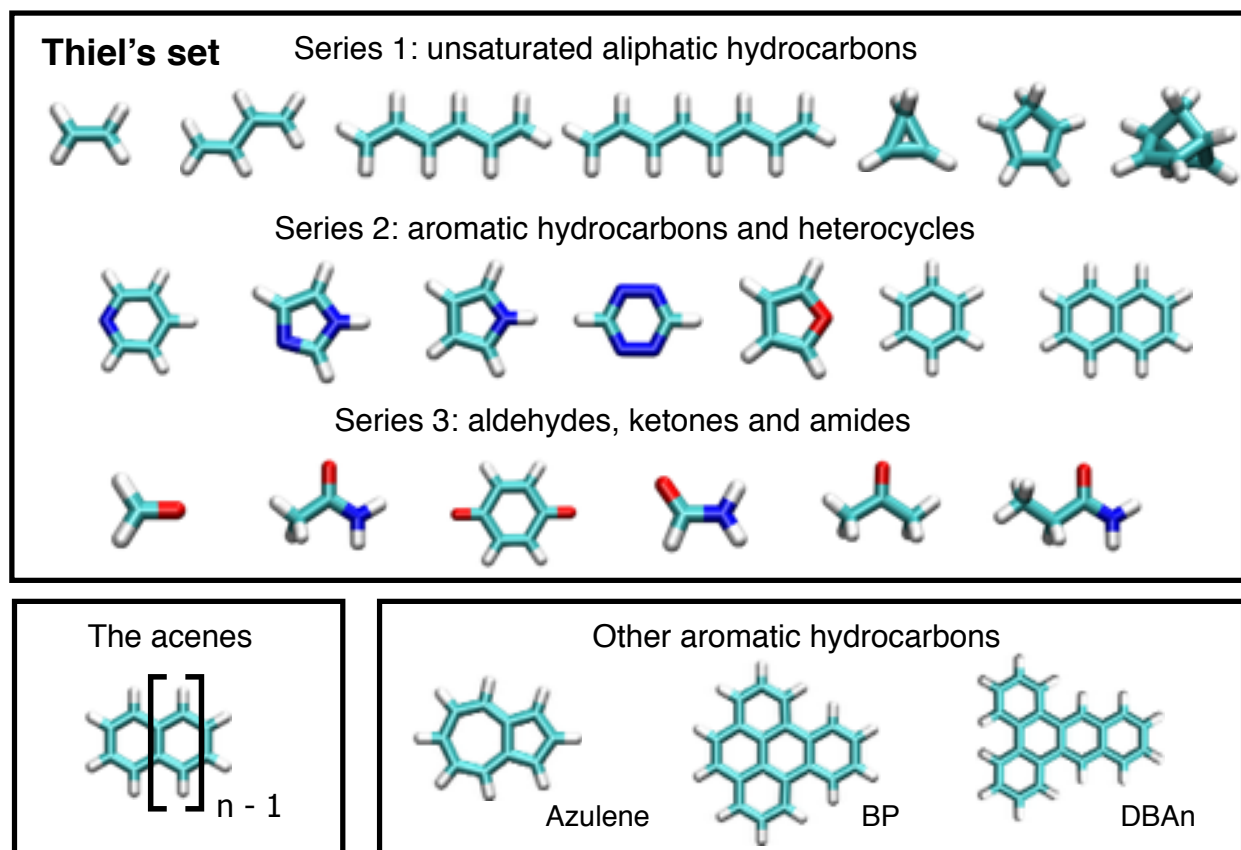


Figure 4.1: Top: Subset of 20 organic molecules from Thiel's set for which triplets are studied here utilizing the OTRSH functional. Bottom: The general formula for an acene molecule, and the three other aromatic hydrocarbons studied here: azulene, benzo[*e*]pyrene (BP) and dibenzo[*a, c*]anthracene (DBAn). H is white, C is light blue, N is dark blue and O is red.

tial is partitioned into short- and long-range contributions, with the important consequence that different fractions of exact exchange can be used in the short and long range [48, 49]. The parameters are either fixed as in, e.g., CAM-B3LYP [49], or tuned to fulfill DFT theorems as in optimally-tuned range-separated hybrid (OTRSH) functionals [25]. Two examples of OTRSH functionals are that of Baer-Neuhauser-Lifshitz (BNL) [55, 56] and the Perdew-Burke-Ernzerhof (PBE)-based OTRSHs [25, 24, 104]. Importantly, CAM-B3LYP, OTRSH-BNL and other RSH functionals have proven quite successful in predicting the low-lying excitations of aromatic hydrocarbons [102, 103, 98, 99, 96] and charge-transfer (CT) excitations [105, 106, 107].

As we and others have shown, GW-BSE has also been successfully applied to gas-phase

molecules [108, 59], and quantitative and extensive benchmark studies are beginning to appear [109, 84, 14, 110, 111]. Yet much remains unknown about the performance of ab initio GW-BSE calculations, particularly their ability to predict acene excitations, charge-transfer-like excitations of aromatic molecules, and more generally, the triplet excitations of organic compounds. The aim of work presented in this chapter has been to address these issues.

Motivated by the success of GW-BSE in general, and its low cost relative to wavefunction methods, in Ref. [89] we assess the performance of different approximations to GW-BSE and determine successful approaches within this framework for the quantitative prediction of low-lying excitations of organic compounds. We evaluate GW-BSE against multireference and coupled cluster references for representative singlet and triplet excitations of 27 organic molecules, including hydrocarbons, heterocycles, aldehydes, ketones and amides (see Figure 4.1). We focus particularly on approximations to GW, including hybrid functional-starting points on one-shot schemes and the effect of partially self-consistent schemes, as described in Section 4.2; and we also focus on the role of the TDA within the BSE, providing a detailed assessment of its performance.

4.2 Computational details

Our calculations start with a self-consistent time-independent DFT calculation, using an approximate exchange-correlation functional (see below). For the molecules considered here, we minimize the total energy with respect to the density using fixed atomic coordinates for all molecules obtained from Ref. [77] (see SI for more details). Starting from the output of our DFT calculations, and using the molgw package [69, 112], we then compute one- and two-particle excitation energies with the GW and GW-BSE approaches, respectively. As is standard, our GW-BSE calculations build on single-particle states, which are coupled in the two-particle BSE equation via the electron-hole interaction kernel. With GW input, BSE is recast into an eigenvalue problem [113], the solution of which yields the energies and eigenstates of the neutral excitations. As detailed in prior work by us and others [114, 63, 87, 115, 86], GW calculations are sensitive to the generalized Kohn-Sham starting point and to whether self-consistency is used. In this work, we build on previous work and use three accurate GW schemes: G_0W_0 @BHLYP (one-shot GW on top of BHLYP [116], which has 50% exact-exchange), G_0W_0 @OTRSH-PBE [42] and eigenvalue self-consistent GW (evGW) in which the quasiparticle energies are updated (in both G and the polarizability) one or more times prior to calculating the final self-energy corrections [114].

In all of the work contained in this thesis the GW-BSE calculations are performed with the molgw package [69, 112], in which the frequency dependence of the GW non-local self-energy $\Sigma(\mathbf{r}, \mathbf{r}', \omega)$ is treated analytically, and hence is exact for a given basis set, without the need for plasmon-pole approximations. For this study, we adopt the aug-cc-pVTZ basis set [90] which ensures convergence better than 0.1 eV for the excitation energies shown here (see SI for details). In order to reduce the computational load, and for the purpose of parallelization,

we use the resolution-of-the-identity in the Coulomb metric [117, 91], as implemented in MOLGW [115, 69], with the well-established auxiliary basis set of Weigend [91] that is consistent with the Dunning basis sets. The resolution-of-the-identity is expected to have a small affect on the GW energies, on the order of 1 meV, as we have demonstrated in the case of benzene [115].

For OTRSH-PBE, as a standard procedure for the acenes [24, 104, 115], we set $\alpha = 0.0 - 0.2$ (see SI) which fixes the amount of short-range Fock exchange to $0 - 20\%$. Additionally, we set $\alpha + \beta = 1$ to enforce long-range asymptotic exact exchange. Then, the range-separation parameter γ is varied to achieve a minimization of the target function

$$J^2(\gamma) = [\text{IP}^\gamma(N) + E_{\text{HOMO}}^\gamma(N)]^2 + [\text{IP}^\gamma(N + 1) + E_{\text{HOMO}}^\gamma(N + 1)]^2 \quad (4.1)$$

where $\text{IP}^\gamma(N)$ is determined via a ΔSCF approach from total energy differences as $\text{IP}^\gamma(N) = \epsilon_{\text{tot}}^\gamma(N - 1) - \epsilon_{\text{tot}}^\gamma(N)$. Here $\epsilon_{\text{tot}}^\gamma(N)$ and $\epsilon_{\text{tot}}^\gamma(N - 1)$ are total energies of the neutral and cation species respectively. This procedure enforces the ionization potential theorem of DFT [50, 51, 52, 53, 54], namely that the energy of the Kohn-Sham highest occupied molecular orbital (HOMO) is equal to the negative of the first ionization potential energy. For molecules with unbound $N + 1$ anionic state, only the first of these two terms is minimized, as in our previous work [115]. The optimal parameters obtained within this framework for the molecules studied are listed in the SI. OTRSH-BNL parameters are taken from Ref. [98].

Our TDDFT calculations are performed with QChem 4.2 [43] with standard settings, excluding core electrons in the correlation computation and neglecting relativistic effects as usual. We use the cc-pVTZ basis set which, relative to aug-cc-pVTZ, converges the neutral-excitation energies satisfactorily: we considered TD-CAM-B3LYP, with and without the TDA, for the singlet L_a and L_b states for all acenes considered herein, and the lowest lying triplet state for benzene, naphthalene and anthracene. For all test cases, the difference between the augmented and unaugmented bases was between 0.001 and 0.087 eV, with an unsigned average difference of 0.028 eV.

4.3 Low-lying $\pi \rightarrow \pi^*$ excitations of aromatic hydrocarbons

In aromatic hydrocarbons, like the acenes, azulene, benzo[*e*]pyrene (BP) and dibenzo[*a, c*]anthracene (DBAn) (see Figure 4.1), the two low-lying singlet excitations are labeled 1L_a and 1L_b [118]. These excitations are well-known to differ significantly in character, and these differences are widely discussed in the literature. The bright (or large oscillator strength) longitudinal ionic 1L_a state involves principally a transition between the highest-occupied molecular orbital (HOMO) and the lowest unoccupied molecular orbital (LUMO), and is often described as having charge-transfer (CT)-like character; while the dark (near-zero

oscillator strength) covalent 1L_b excitation, which arises from a destructive interference [119] of transitions that typically couple the HOMO to the LUMO+1 and the HOMO-1 to the LUMO [120, 121, 98].

The description of these excitations as ionic or covalent comes from valence bond theory, and refers to the distribution of charge in the excited state’s spatial 1-electron orbital. If in the resonance structures describing this orbital the density oscillates from negative to positive with respect to the carbon-atom centers, the excitation is termed “ionic”. If there is no such oscillation and the resonance structures comprise Kekule structures, with alternating double and single bonds, the excitation is termed “covalent”.

The corresponding low-lying triplet excitations are labeled, following the same conventions as above, as 3L_a and 3L_b , respectively. Notice that labeling of unbound molecular orbitals (e.g. the LUMO and LUMO+1 of some acenes) is somewhat arbitrary, since their ordering may change depending on the choice of DFT exchange-correlation (XC) functional and basis set. Nevertheless, the energetics and orbital wavefunctions of the LUMOs of benzene and naphthalene are well characterized with CCSD(T) in Ref. [122].

Predicting both 1L_a and 1L_b presents a challenge for TDDFT approaches due to their different natures. In fact, 1L_a excitations, with their CT-like character [98], are usually poorly predicted by standard TDDFT [121, 98, 123], due to the known shortcoming of many standard functions to describe such excitations, a shortcoming that has the potential to be ameliorated with RSHs having asymptotic exact exchange [98]. While the CT nature of 1L_a excitations and the ability of RSHs to overcome these shortcomings has been questioned, [123] this is not the subject of the matter presented here.

4.4 Results and discussion

We begin with a benchmark of GW-BSE and TDDFT against CCSD(T) for the low-lying singlet excitations of the acenes. We end with an examination of the role of the TDA within both the TDDFT and GW-BSE frameworks.

Predicting the low-lying excitations of the acenes with TDDFT

In Figure 4.2a, we show the mean signed deviation ($\text{MSD} = 1/N_i \sum_i^{N_i} E_i - E_i^{\text{ref}}$) from the CCSD(T) references [99, 122] of representative TDDFT-RSHs explored in this study. Our results within TD-OTRSH-BNL are in excellent agreement with those reported in Refs. [98] and [99]. In addition, we find that TD-OTRSH-PBE low-lying singlets are within 0.05 eV of the corresponding TD-OTRSH-BNL excitations. In fact, as previously discussed [99, 123], the performance of TD-OTRSH based on BNL or PBE for 1L_a and 1L_b relative to CCSD(T) is very consistent: for both approaches, 1L_a is within 0.1–0.2 eV of the reference, but 1L_b presents larger discrepancies (~ 0.4 eV), as does the 1L_b - 1L_a gap, which is within 0.6 eV.

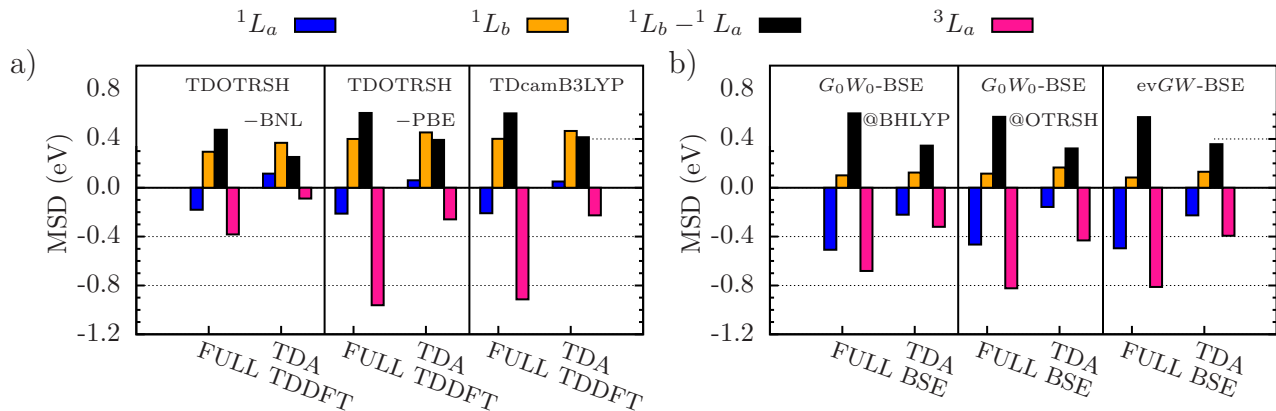


Figure 4.2: MSD (see text for details) with respect to CCSD(T) [122, 99] of calculated neutral excitations of the acene molecules ($n = 1$ to 6). The calculated 1L_a (blue bars), 1L_b (orange bars), and 3L_a (pink bars) excitations, and ${}^1L_b - {}^1L_a$ (black bars) energy difference are shown for a few representative TDDFT and GW-BSE approaches: TD-OTRSH and TD-CAM-B3LYP in panel a, and G_0W_0 -BSE@BHLYP, G_0W_0 -BSE@OTRSH-PBE and evGW-BSE@PBE0 in panel b.

Predicting the low-lying excitations of the acenes with GW-BSE

Having reviewed the accuracy of TDDFT-RSH for the 1L_a and 1L_b excitations relative to CCSD(T), we now discuss the GW-BSE results, focusing on the accuracy of approximations to the underlying GW starting point. In Figure 4.2b, we show the calculated MSD, as defined in the previous section, of representative GW-BSE approaches studied here. Consistent with previously-reported GW results on the charged excitations of the acenes (see for instance Refs. [63], [86] and [115]) hybrid starting points for G_0W_0 or self-consistent GW approaches are required to predict accurate excitations within GW-BSE; relatively low MSDs are found within G_0W_0 -BSE@BHLYP and evGW-BSE, in agreement with recent works [84, 14, 110]. In particular, we highlight that while the OTRSH-PBE starting point yields neutral excitation energies with accuracies similar to other starting-points for aromatic hydrocarbons, OTRSH-PBE leads to markedly improved triplet energetics for the molecules studied here, as discussed later. As shown in Figure 4.2b, for the GW-BSE schemes considered here, the 1L_b state is predicted within 0.1–0.2 eV, whereas 1L_a is underestimated by at least 0.4 eV; additionally, the ${}^1L_b - {}^1L_a$ gap is underestimated by ~ 0.6 eV independent of GW-BSE scheme. The rather poor performance of both GW-BSE and TDDFT approaches, in the context of neutral low-lying singlet and triplet excitations of acene molecules, can be remedied by the Tamm-Dancoff approximation, as discussed next.

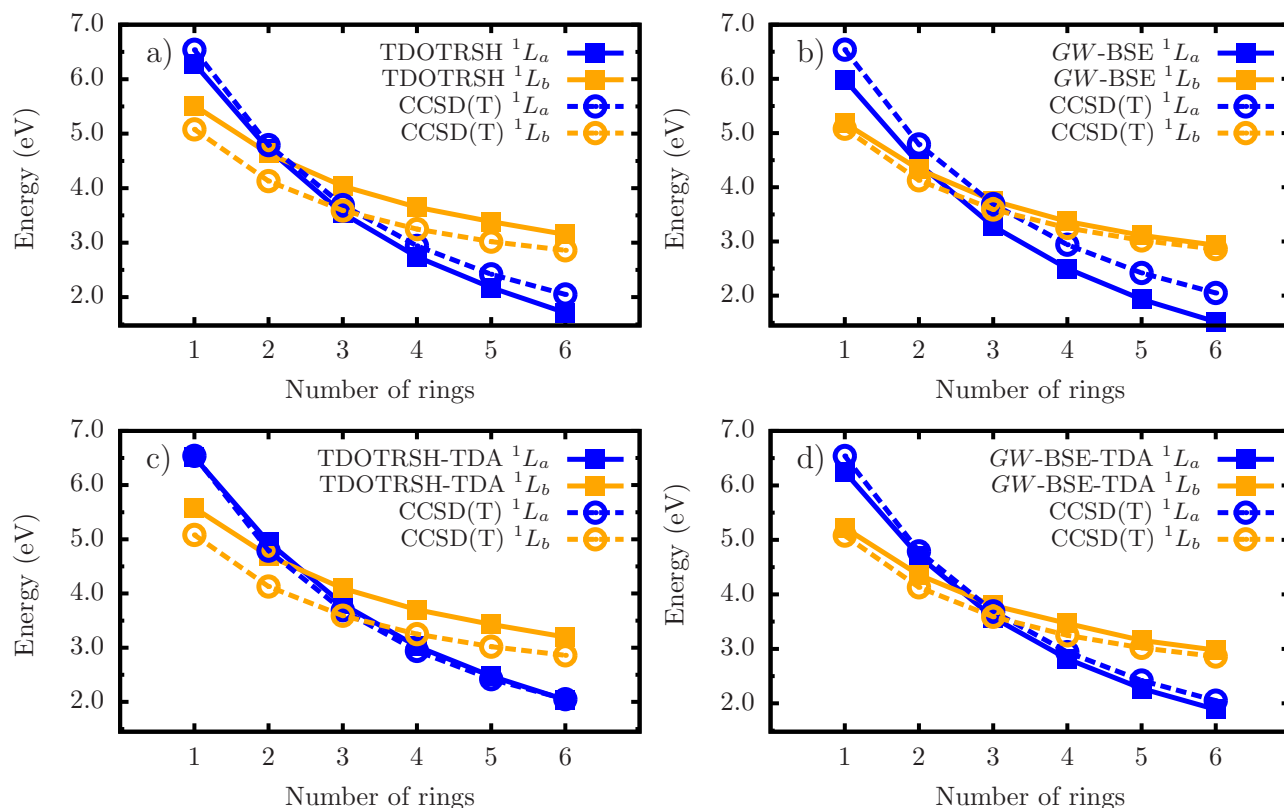


Figure 4.3: Low-lying singlet excitations of acenes calculated with TD-OTRSH-PBE and G_0W_0 -BSE@OTRSH-PBE in panels a and b; 1L_a and 1L_b excitation energies, with blue and orange lines respectively, are compared to CCSD(T) references from Refs. [99] and [77] (dashed lines). The corresponding excitations with the TDA at the TDDFT and GW-BSE theories are shown in panels c and d.

The role of the Tamm-Dancoff Approximation within TDDFT and GW-BSE

The fact that the TDA can improve the description of low-lying neutral excitations of the acenes has been discussed thoroughly in the TDDFT community [100, 124, 12, 96, 36], and here we find that similar arguments apply to GW-BSE. In Figure 4.2, we also show the MSD of the calculated low-lying excited states with TDDFT and GW-BSE within the TDA with respect to the CCSD(T) reference. The calculated 1L_a and 1L_b energies within representative GW-BSE and TDDFT schemes of the acene molecules are shown in Figure 4.3.

Link between TDDFT and triplet instability.

Within Hartree-Fock [125] and within DFT [126], the stability of the spin-restricted solution against that of the more flexible spin-unrestricted solution requires the positive-definiteness of two matrices (one for singlet final states and one for triplet final states) that are precisely the sum of the blocks A and B [See Eq.2.21] used in time-dependent Hartree-Fock (TDHF) or in TDDFT. In other words, if either one of the $A + B$ matrices has a negative eigenvalue, then the ground-state singlet solution is unstable against a spin-unrestricted triplet solution. This is the so-called triplet instability. Consequently, an unstable or close to unstable spin-restricted ground state implies negative or very low eigenvalues in $A + B$, which in turn produce non-physical or too-low neutral excitations in TDHF or in TDDFT [127, 100]. This is why prior work often resorts to the TDA to circumvent the spin-restricted instability situation [127, 124, 36, 100, 96, 101]. The TDA is thus a practical way to prevent the electronic system from sampling the triplet ground state, which is spuriously too low in energy.

Link between the BSE and triplet instability.

In the GW-BSE framework, the connection between triplet instability and the BSE matrix is precisely analogous. However, due to the technicalities of BSE, the connection cannot be demonstrated rigorously. The BSE, evaluated in the standard fashion [7], is indeed a combination of (1) eigenvalues obtained from the dynamical GW self-energy and (2) a kernel, which is an approximate functional derivative of the static GW self-energy, namely the static screened exchange approximation (SEX) [18]. Additionally, the functional derivative $\delta W/\delta G$ is always neglected in the BSE kernel [7]. Thus, following the same logic for GW-BSE as we have done for TDDFT above, the BSE blocks $A + B$ would then lead to stability problems (if present) in the static screened exchange spin-restricted solution. If one admits that the GW quasiparticle energies are not far from the static screened exchange energies, the connection between triplet instability and BSE can be understood, but again, not proven. In situations where the triplet instability occurs or nearly occurs in static screened exchange, the TDA to the BSE may be a good route to obtain meaningful neutral excitation energies. However, this calls for a direct numerical comparison, which we carry out below.

Performance of the TDA within TDDFT.

As demonstrated in prior work [124, 96], the TDA improves the description of the 1L_a singlet and the first triplet 3L_a states because these share a similar origin; both are covalent in the valence bond sense, and involve mainly HOMO to LUMO transitions, whereas L_b energies are virtually unmodified with the TDA. Hence, within the RSH time-dependent approaches used here, the large discrepancy (0.4 eV) on the calculated 1L_b state is not improved by the TDA (see Figure 4.2). On the other hand, we find that the TDA further corrects the 1L_a excitation in the asymptotic limit of longer acene molecules (see panels a and c of Figure 4.3). For example, for pentacene TD-OTRSH-PBE predicts $^1L_a = 2.18$ eV with

TDDFT and 2.48 eV with the TDA, in outstanding agreement with the CCSD(T) reference value of 2.42 eV. In brief, and in agreement with the literature [99, 123], TDDFT-TDA with RSH functionals yield highly accurate CT-like 1L_a energetics, but tends to overestimate 1L_b transition energies.

Performance of the TDA within GW-BSE.

Having reviewed the ability of the TDA within TDDFT to predict the low-lying excitations of the acenes, we now discuss the accuracy of the TDA within GW-BSE for these transitions. Here we expand our discussion to a larger set of aromatic hydrocarbons, including azulene, BP and DBAn (see Figure 4.1) which have well-characterized L_a and L_b states [123]. In Table 4.1 (which can be found at the end of this chapter) we show the calculated singlet and triplet excitations with G_0W_0 -BSE@BHLYP (with and without the TDA) and mean deviations with respect to CCSD(T), as previously defined.

Similar to TDDFT, in GW-BSE we find that independent of GW self-energy scheme, the 1L_a and 3L_a states are improved within the TDA (by at least 0.2 eV, see Figure 4.2 and Table 4.1). While triplet energies remain underestimated by $\sim 0.3 - 0.4$ eV, singlet energies are accurately calculated with GW-BSE-TDA with remaining discrepancies lower than 0.2 eV. The TDA also corrects the ${}^1L_a - {}^1L_b$ energy ordering; as shown in Figure 4.3 these two states cross at naphthalene when following increasing/decreasing ring number n within the full-BSE (panel b), while the crossing is at anthracene within the TDA (panel d), in agreement to CCSD(T). In summary, GW-BSE within the TDA can predict – with excellent quantitative accuracy, an MSD better than 0.2 eV – both ionic CT-like and covalent singlet excitations (such as 1L_a and 1L_b , respectively) of the acenes and other aromatic hydrocarbons.

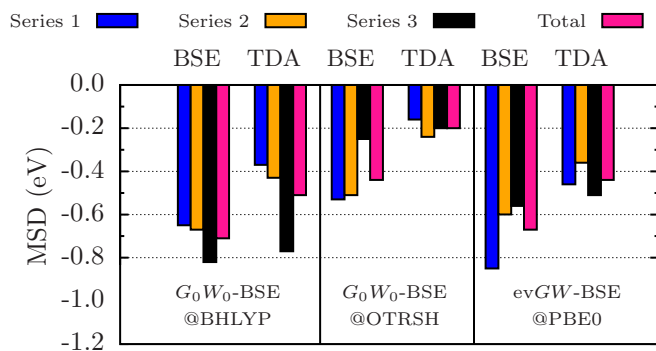


Figure 4.4: First-triplet excitation energies of organic molecules in Thiel’s set (see Figure 4.1) calculated with GW-BSE are benchmarked against reference data [77]. The MSD (read text) corresponding to molecules in Series 1 is shown in blue bars, Series 2 in orange bars, Series 3 in black bars and the total in pink bars. We consider several GW-BSE schemes with the full-BSE and the TDA.

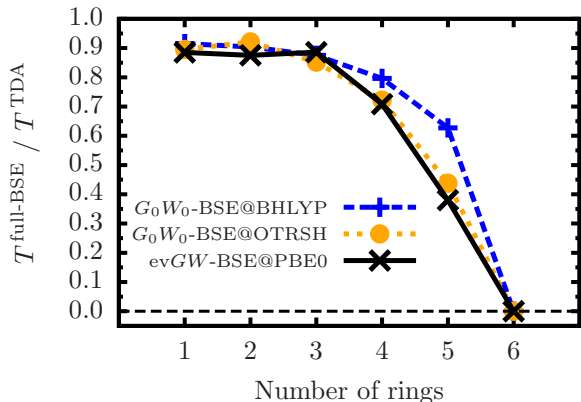


Figure 4.5: Ratio of the first triplet energy (T) calculated within GW-BSE diagonalizing the full BSE Hamiltonian and using the TDA. Several representative GW-BSE schemes are shown: G_0W_0 -BSE@BHLYP in dashed-blue lines and crosses, G_0W_0 -BSE@OTRSH-PBE in dotted-orange lines and circles and evGW-BSE@PBE0 in black lines and crosses. GW-BSE predicts a negative triplet energy (shown at zero) for hexacene for all GW schemes used in this work.

Thiel’s set.

We further analyze the accuracy of GW-BSE and the TDA for a larger set of triplet excitations. We show in Figure 4.4, the MSDs (previously defined) of the calculated first-triplet energies of 20 organic molecules of the Thiel’s set (all energies are tabulated in the SI of our published work ref. [89]). Again, we consider several representative GW-BSE methods; using the BHLYP and OTRSH-PBE starting points for G_0W_0 and evGW. Additionally, we show the MSDs for the molecule categories described in Figure 4.1.

With this larger set of excitations, it becomes clear from our calculations that G_0W_0 @BHLYP and evGW@PBE0, known to perform reasonably well for singlet excitations [14, 84], can present severe errors for triplets, with MSDs of ~ -0.6 to -0.8 eV, as noticed first in Ref. [84] for the BHLYP starting point. The OTRSH starting point for G_0W_0 @BSE has a relatively lower MSD of ~ -0.4 to -0.6 eV, presumably due to the RSH optimal starting point for the underlying GW electronic structure [115, 86], which will be discussed in detail in a separate publication [128]. For all GW-BSE approaches studied here, the TDA improves the first-triplet energy, a fact that we discuss in greater depth below. Further, we note that in agreement with recent work [111], GW-BSE-TDA approaches predict inaccurate triplet energies (with MSD of $-0.4 - 0.5$ eV) when using a global-hybrid starting point. Importantly, within the OTRSH starting-point, GW-BSE-TDA can result in relatively accurate first-triplet energies with a MSD of -0.19 eV.

In order to better understand the good performance of the TDA within GW-BSE for

low-lying triplet energies, we show in Figure 4.5 the ratio of the triplet energy calculated within the full GW-BSE and within the TDA (T/T^{TDA}). When the ratio approaches zero or becomes negative (TDDFT predicts a negative or zero triplet energy), the triplet and its corresponding ground state become unstable, as explained before; hence this ratio acts as a measure of instability [100]. In this work, we find that the full-BSE and the TDA predict similar triplet energies for benzene and naphthalene (ratio close to 0.9), but the triplet ratio drops to less than zero at hexacene independent of the GW approximation; note that for the PBE starting point to GW-BSE, the ratio becomes negative at pentacene (not shown). This implies that GW-BSE, in disagreement with CCSD(T) [122], predicts triplet ground states for acenes larger than pentacene. In analogy to TDDFT, this may be a result of instabilities in the corresponding GW-BSE triplet and ground states; we leave the evaluation of stability conditions in the GW-BSE states to future work.

As mentioned above, triplet instabilities are well-known and documented in Hartree Fock and TDDFT theories [100, 96, 36, 12, 101], and GW-BSE is similarly affected, as shown here and in Ref. [129]. In TDDFT, as in configuration interaction singles (CIS) theory, which mixes only single Slater determinants and is the minimal post-Hartree-Fock method capable of predicting physical excited states, triplet instabilities are overcome with the TDA [101]. Not surprisingly, in GW-BSE the TDA also overcomes triplet instabilities, as we document here, in a manner analogous to TDDFT for molecules.

4.5 Conclusions

In summary, we have benchmarked GW-BSE with CCSD(T) for neutral excitations of aromatic hydrocarbons and heterocycles, including the challenging L_a and L_b excitations heavily documented in prior work with TDDFT. We first explored the accuracy of approximations to GW-BSE and found that G_0W_0 -BSE@OTRSH can yield accurate triplet and singlet excitations, sometimes outperforming other highly-accurate approaches such as evGW-BSE and G_0W_0 -BSE@BHLYP. In particular, for aromatic hydrocarbons, the above mentioned GW-BSE methods can predict accurate 1L_b energetics but generally present significant errors for the 1L_a states. This problem is remedied by using the TDA, which leads, as it does with TDDFT, to a better overall performance, overcoming triplet instabilities, improving triplet energetics, and capturing quantitatively both the charge-transfer-like L_a and covalent L_b singlet excitations of aromatic cyclic compounds.

L_a states						
	Singlets			Triplets		
	BSE	TDA	CCSD(T)*	BSE	TDA	CCSD(T)*
Benz.	5.89	6.13	6.54 ^b	3.60	3.94	4.26 ± 0.11 ^{b,c}
Naph.	4.34	4.59	4.81 ± 0.02 ^{a,b}	2.65	2.93	3.20 ± 0.11 ^{b,c}
Anth.	3.38	3.63	3.68 ± 0.02 ^{a,d}	2.01	2.29	2.41 ± 0.07 ^{c,d}
Tetra.	2.42	2.72	2.94 ^a	1.08	1.36	1.76 ^c
Penta.	1.88	2.21	2.42 ^a	0.57	0.91	1.37 ^c
Hexa.	1.48	1.84	2.05 ^a	< 0 [†]	0.58	1.00 ^c
Azu.	2.00	2.12	1.94 ^d	1.35	1.42	2.18 ^d
BP	3.65	3.82	4.09 ^d	1.95	2.41	2.82 ^d
DBAn	3.48	3.69	3.91 ^d	1.90	2.30	2.73 ^d
MSD	-0.43	-0.18		-0.74	-0.39	
MAD	0.44	0.22		0.74	0.39	

L_b states						
	Singlets			Triplets		
	BSE	TDA	CCSD(T)*	BSE	TDA	CCSD(T)*
Benz.	5.10	5.15	5.08 ^b	4.39	4.42	4.86 ^b
Naph.	4.30	4.32	4.19 ± 0.06 ^{a,b}	3.76	3.79	4.09 ^b
Anth.	3.82	3.79	3.58 ± 0.01 ^{a,d}	3.42	3.43	3.52 ^d
Tetra.	3.33	3.37	3.25 ^a	3.11	3.18	
Penta.	3.10	3.13	3.02 ^a	2.79	2.83	
Hexa.	2.91	2.98	2.86 ^a	†	2.66	
Azu.	3.34	3.49	3.64 ^d	2.09	2.19	2.20 ^d
BP	3.57	3.60	3.50 ^d	2.96	3.11	3.34 ^d
DBAn	3.58	3.61	3.57 ^d	3.34	3.43	3.35 ^d
MSD	0.04	0.08		-0.23	-0.17	
MAD	0.11	0.12		0.23	0.20	

* CCSD(T) data from the literature: ^a Ref. [99], ^b Ref. [77], ^c Ref. [122], and ^d Ref. [123].

† the BSE Hamiltonian contains negative eigenvalues (read text).

Table 4.1: Singlet and triplet energetics of representative aromatic hydrocarbons calculated with GW-BSE@BHLYP with the full-BSE (denoted simply BSE above) and the TDA. We consider benzene (Benz), naphthalene (Naph.), anthracene (Anth.), tetracene, (Tetra.), pentacene (Penta.), hexacene (Hexa.), azulene (Azu.), benzo[*e*]pyrene (BP) and dibenzo[*a, c*]anthracene (DBAn). MSD and MAD with respect to CCSD(T) are also shown (see text). All energies are in units of eV.

Chapter 5

Predicting charged excitations across the oligoacenes

5.1 Introduction

The oligoacene molecules introduced in chapter 4 belong to a class of aromatic hydrocarbons consisting of linearly fused benzene rings (Fig. 5.1). This family of molecules has been studied in the context of a variety of opto-electronic applications, and in particular, the larger acenes and their derivatives are used for field-effect transistors[130] and in solar-cell devices.[131, 132, 133, 95] In addition, acenes and other polycyclic aromatic hydrocarbons are abundant in the universe and their properties are of importance to astrophysics.[134, 135, 136]

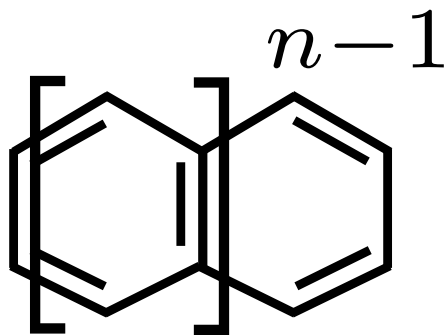


Figure 5.1: The general chemical formula for the acenes.

In the previous chapters I have focused on neutral excitations; here we turn to charged

excitations, namely excited states associated with electron addition and removal. The charged excitations of acene molecules have been well-studied with a variety of computational approaches, including density functional theory (DFT), many-body perturbation theory (MBPT), and wavefunction-based quantum chemistry methods,[137, 138, 139] and hence constitute an excellent benchmark case for the development and refinement of methods. Additionally, aspects of charged excitations for the acenes are still not entirely understood. For example, anion states of benzene and naphthalene are unbound, and hence challenging to measure;[140] further, whether measured excitations are strictly “vertical” or “adiabatic” can be ambiguous. [137, 138, 141]

Numerous theoretical approaches can be used to compute charged excitations, including wavefunction-based methods, such as coupled cluster techniques and quantum Monte Carlo (QMC), as well as DFT and MBPT. While wavefunction-based methods are regarded as highly accurate and the “gold standard”, they exhibit poor scaling and are currently intractable for many complex systems. On the other hand, MBPT within the GW approximation,[18] a Green’s function-based approach built upon Kohn-Sham DFT wavefunctions and eigenvalues, scales more modestly with the number of basis functions and is broadly applicable to a range of molecules, solids, surfaces, and nanostructures. It is therefore useful to quantify the performance of GW approaches relative to high-accuracy wavefunction-based methods for molecular systems, such as the acenes.

Previous studies[142, 114, 79, 61, 143, 87, 144] have benchmarked GW calculations against experiment and couple-cluster techniques for small- to medium-sized molecules, including some acenes. In particular, these works have examined the performance of different DFT starting points and self-consistent GW (see Section. 5.2 for details), and have found that some GW approaches are more predictive for charged excitations in organic molecules than others. However, as valuable as these studies are, they, by design, were not all-inclusive; further, there has yet to be a report of trends for charged excitations across a series of acenes of increasing size.

In this work, we calculate ionization potentials (IPs) and electron affinities (EAs) of acenes, from benzene to hexacene, using MBPT within the GW approximation. We compare our GW results to highly-accurate coupled-cluster calculations, with single, double, and perturbative triple excitations [CCSD(T)]. Since prior CCSD(T) reference calculations relied on extensive extrapolations, especially for the larger acenes, we perform new CCSD(T) calculations and include a comparison to these new results. For completeness, we also benchmark recently-developed exchange-correlation DFT functionals that make use of a system-dependent non-empirically determined amount of exact exchange via the optimally-tuned range-separated hybrid (OTRSH) class of functionals.[25] Special attention is given to the accuracy of approximations within GW: we test convergence issues; the performance of DFT starting points for GW, including global hybrids and OTRSHs; and the performance of eigenvalue self-consistent GW approaches (see Section 5.2 for details).

5.2 Theoretical methods

For small gas-phase molecules, such as the acenes considered here, in principle, IPs and EAs can be determined from DFT via total energy differences between charged and neutral species.[145] However, this Δ SCF approach is limited to frontier orbital energies, ill-defined for states above the vacuum energy (i.e., with negative EA), and can be inaccurate especially for large molecules due to the nature of approximate DFT exchange-correlation functionals.[146, 86, 21] In this work, we produce a quantitative benchmark of ab initio MBPT within the GW approximation, an alternative and more general approach for electron addition and removal energies of acene molecules. Our GW calculations are based on DFT and, as we will show below, they are quantitatively dependent on the solutions to the underlying generalized Kohn-Sham equations (and therefore sensitive to the functional used). Moreover, recent developments in generalized Kohn-Sham DFT suggest that appropriately-constructed exchange-correlation functionals can lead to accurate charged-excitation spectra.[147, 148, 25, 24, 104, 26, 86] In the following sub-sections, we briefly describe our GW approach. after first summarizing a class of range-separated hybrid (RSH) functionals that we use both Here, as in the previous chapters, we use two OTRSH functionals as starting points for our GW calculations and also as an independent reference for comparison with GW: the OTRSH-PBE functional[25, 24, 104] which we have already described in detail and the Baer-Neuhauser-Lifshitz (BNL) functional[55, 56] (see details in Ref.[98]). Within the tuning framework, the optimal γ parameters for benzene through hexacene are found to be 0.25, 0.21, 0.19, 0.17, 0.15, and 0.14 bohr⁻¹ respectively.

In this work, all DFT OTRSH and BNL calculations are performed with the Q-Chem 4.2 software package,[149] and all geometries are relaxed with Q-chem with DFT using the B3LYP[82, 150] functional and a cc-pVTZ basis set.

Many body perturbation theory within the GW approximation

In MBPT, the GW approximation consists of a closed set of equations for the Green’s function G , the screened-exchange W , and the electronic self-energy

$$\Sigma(\mathbf{r}, \mathbf{r}', \omega) = i \int d\omega' e^{i\delta\omega'} G(\mathbf{r}, \mathbf{r}', \omega + \omega') \times W(\mathbf{r}', \mathbf{r}, \omega'), \quad (5.1)$$

which is non-local, non-Hermitian, and frequency dependent.[18, 151, 152, 7, 153] A fully self-consistent solution of the GW equations using large basis sets is currently unfeasible for most systems of interest and further approximations are required. Most frequently, the GW self-energy is applied perturbatively as a first-order correction to generalized Kohn-Sham states obtained from a DFT calculation. This is the so called “one-shot” GW or G_0W_0 , in which for a given i^{th} state, the Kohn-Sham (KS) wavefunction $|i\rangle$ is kept constant and the corresponding eigenvalue E_i is corrected, as follows:[154]

$$E_i^{\text{QP}} = E_i^{\text{KS}} + \langle i | \Sigma(\omega = E_i^{\text{QP}}) - v_{xc} | i \rangle. \quad (5.2)$$

It follows directly from the previous expression that the one-shot GW result may depend much on the quality of the underlying exchange-correlation (XC) functional.

A well-known workaround is to use an XC functional whose generalized Kohn-Sham mean-field spectrum is closer to the actual charged excitation energies, a so-called improved starting point, e.g. hybrid functionals.[63, 61, 155, 64, 143, 156, 87] In this work, we consider the hybrid functionals that have been identified in previous studies,[63, 84] including PBE0[46] and BHLYP,[82] with 25% and 50% exact exchange, respectively. We will also consider the OTRSH functional[56] described above. In the following, we indicate the mean-field starting point with an “@” sign, i.e., G_0W_0 @PBE0, G_0W_0 @BHLYP and G_0W_0 @OTRSH, to refer to one-shot GW on top of PBE0, BHLYP and OTRSH, respectively.

The other approach to mitigate starting-point dependence is to perform a self-consistent calculation.[157, 78, 80] An approximate self-consistent scheme that only updates the eigenvalues entering Σ , while keeping the KS wavefunctions frozen, has been highlighted for molecules recently[114, 14] with promising results. This scheme is known as eigenvalue self-consistent GW, or “evGW”, and involves the iterative updating of the eigenvalues in both the Green’s function G and the screened Coulomb interaction W . A partial eigenvalue self-consistent scheme that only updates eigenvalues in G and not in W has been proposed and used extensively for solids.[158] This approach, “evGW₀”, has been previously reported to be less effective for molecules,[14] but we test it here for completeness. In this work, we perform three to four iterations to converge the partial self-consistent GW results within 0.01 eV; when using a “good” GW starting point (with energies close to the evGW solution, such as BHLYP) only two iterations are needed to reach the same convergence threshold for the molecules considered here.

GW calculations in a Gaussian basis

Our GW calculations, and the computations generating our DFT starting points, are performed with MOLGW[112] code, using Gaussian basis sets. A comprehensive description of this code can be found in Refs.[84],[63] and [68]; but briefly, after a self-consistent DFT calculation, MOLGW evaluates the GW self-energy via a spectral representation of the dynamical polarizability χ , allowing analytical calculation of the self-energy without any loss of information; i.e., χ is calculated exactly in a given basis set. MOLGW makes use of external libraries for the evaluation of electron repulsion integrals, LIBINT, [70] and for exchange-correlation potentials, LIBXC.[71]

The present study uses relatively large basis sets; e.g., hexacene C₂₆H₁₆ in aug-cc-pVTZ requires as many as 1564 basis functions. To deal with these large systems, four-center integrals are evaluated approximately via an approach referred to as the resolution-of-the-identity in the Coulomb metric[117, 91]. This approximation has been used successfully in past GW calculations,[159, 114, 60] and it leads to a drastic reduction in the computational burden: the scaling of the atomic to molecular orbital transforms is reduced to N^4 from N^5 . More specifically, this method involves approximating the 4-center electron repulsion

integrals according to

$$(\alpha\beta|\frac{1}{r}|\gamma\delta) \approx \sum_{PQ} (\alpha\beta|\frac{1}{r}|P)(P|\frac{1}{r}|Q)^{-1}(Q|\frac{1}{r}|\gamma\delta), \quad (5.3)$$

where Mülliken notation is used. The Greek letters represent the basis functions for the wavefunction, whereas the capitals P and Q run over an auxiliary basis set. In practice, we use an approach[69] in which the square root of the matrix $(P|\frac{1}{r}|Q)$ is calculated and thus the evaluation of Eq. (5.3) is further accelerated.

The accuracy of the approximation in Eq. (5.3) relies critically on the ability of the auxiliary basis set to represent the Coulomb interaction properly. In this work, we use the well-established auxiliary basis sets of Weigend,[91] an atom-centered basis consistent with the Dunning basis.[90] We have explicitly determined that approximate use of the resolution-of-the-identity affects the GW energies by at most 1 meV in the case of benzene.

molgw analytically treats the frequency dependence of Σ by calculating the polarizability χ within the random-phase approximation. Then χ is written as a matrix containing all the single excitations available in the basis set, except for the carbon 1s states which are kept frozen. Therefore, the only convergence criteria is the basis set size, which will be carefully checked below.

Basis set convergence

As mentioned above, in this work we use the augmented basis sets of Dunning [90], which are designed to converge smoothly towards the complete basis set limit (CBS). For simplicity, we refer to these basis sets as aDZ, aTZ, and so on, instead of their full-length names aug-cc-pVDZ, aug-cc-VTZ, etc.

In Figure 5.2, we show the convergence of our calculated values for the ionization potential (IP), the electron affinity (EA), and the IP–EA gap with respect to basis set size for benzene to hexacene. All results are obtained with G_0W_0 @PBE0. The basis set is increased in size in the aug–pVnZ series from n=D to 5. To better compare the rate of convergence across the acene series, we have set their aDZ values equal to zero in each case. For anthracene ($n = 3$) and larger acenes, we forgo some calculations with the largest basis sets, aug–pV5Z and aug–pVQZ, due to the significant computational burden.

We find that the calculated IPs and EAs converge monotonically and are well-fit with a simple function, as indicated in Figure 5.2. Remarkably, the IPs and EAs of all acene molecules converge in the same manner, independent of the length of the molecule. In fact, the energy difference between IPs/EAs calculated with the aTZ basis set and the CBS limit is ~ 0.26 eV. Thus, one may evaluate IPs and EAs at the CBS limit for these molecules by first performing GW calculations with the aTZ basis set, and then adding 0.26 eV.

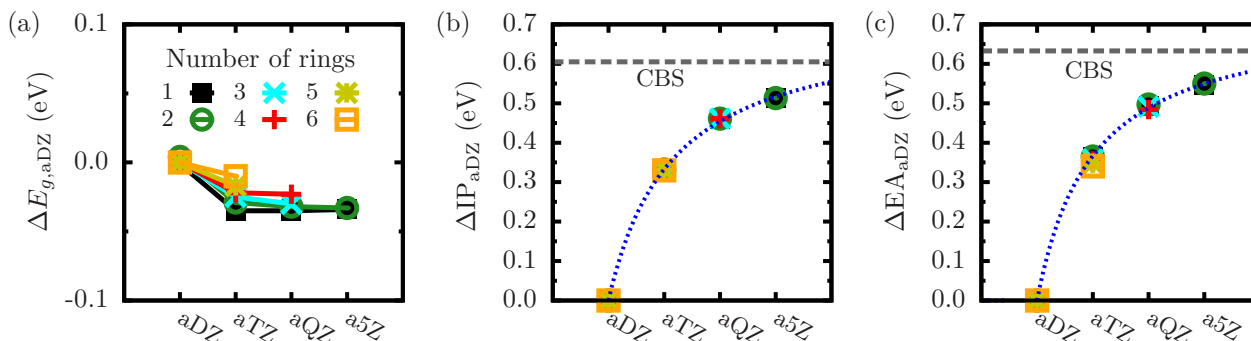


Figure 5.2: Convergence of charged excitations with respect to the basis set size for the oligoacene molecules within GW based on a PBE0 starting point. Calculated IP–EA gap energies (E_g) converge fast with respect to the basis set size, whereas IPs and EAs are extrapolated to the basis set (CBS) limit using a function of the form $f(x) = a + b/(x - x_0)$ (dotted-blue lines). Note that as the molecule size increase, calculations with large basis sets become unfeasible, and hence some points are omitted in the figures. For convenience, we show the energy difference with respect to the results obtained with the aDZ basis, $\Delta E_{aDZ} = E - E_{aDZ}$; In fact, points for different molecules overlap making evident that all quantities converge at similar rates for the different molecules considered here.

5.3 Ionization potentials and electron affinities

Obtaining reference values

Here, we revisit CCSD(T) IP energies in the CBS limit for acene molecules, following the focal point analysis (FPA) approach laid out in Ref.[138]. In the FPA, CCSD(T) best estimates are obtained from single-point calculations at the restricted-HF level and adding incremental improvements to the correlation energy at the second-, third- and partial fourth-order Møller-Plesset levels (MP2, MP3 and MP4SDQ). In turn, these are followed by improvements from coupled-cluster calculations including singles and doubles (CCSD) and a perturbative estimate of the triples (CCSD(T)), and by extrapolating to the CBS limit using Dunning basis sets of increasing size. Interestingly, the data in Ref.[138] exhibit a significant break of ~ 0.1 eV in the trend along the oligoacene series at hexacene. Exploring this further, we find that the MP3 contribution to CCSD(T) is not entirely converged for hexacene, and as indicated in Table S1 of the SI, the MP3 basis set size dependence increases with increasing system size. By repeating the FPA and extrapolating the MP3 corrections from trends observed in smaller acenes and basis sets, we find a difference of -0.1 eV in the resulting IP of hexacene with respect to Ref.[138]. Our resulting CCSD(T) best theoretical estimates (BTEs) for the vertical IPs are shown in Table. 5.1. Our CCSD(T) calculations are performed with the Gaussian 09 E.01 code[74] with standard settings, including core electrons in the correlation computation and neglecting relativistic effects as usual. Details

of our calculations and analysis of the FPA in Ref.[138] are provided in the SI. In addition, we adopt the EA CCSD(T) reference values of Ref.[122].

	Ref.[138]	This work
Benzene	9.45	9.44 ± 0.01
Naphthalene	8.24	8.25 ± 0.01
Anthracene	7.47	7.48 ± 0.03
Tetracene	6.95	6.96 ± 0.03
Pentacene	6.57	6.58 ± 0.03
Hexacene	6.43	6.32 ± 0.03

Table 5.1: Best theoretical estimates based on CCSD(T) calculations following Ref.[138], for the vertical IP of the acenes. Here, we compare our calculations with those of Ref.[138], determined by a focal point analysis[138] at the CCSD(T) level of theory. All energies are in units of eV.

Charged excitations with GW and DFT-OTRSH

In this section, we present and discuss IPs and EAs calculated using DFT-OTRSH and GW, comparing to our CCSD(T) BTEs as defined in the previous section. Experimental values for IPs and EAs of the acenes are given in Refs.[160, 161, 162] and are described as “vertical”; however, recent work[137, 138] with CCSD(T) has suggested that these values are actually “adiabatic” since their best adiabatic estimates match the experimental values within 0.02 eV. Note that the naphthalene EA of -0.190 eV measured by electron transmission spectroscopy,[140] first ascribed as vertical, is now considered adiabatic due to the presence of vibrational features in the spectrum.[163] For these reasons, we choose not to compare explicitly with experiments in this work and instead benchmark against high-level CCSD(T) calculations: we use our own CCSD(T) IPs, as shown in Section 5.3, and take CCSD(T) EAs from Ref.[137]. We note that vertical IP/EAs of anthracene calculated with QMC are in excellent agreement with our CCSD(T) references.[139]

In Figure 5.3, calculated charged-excitations are compared to the CCSD(T) reference data (in black dotted lines and squares). For clarity, only a few representatives of each GW and DFT scheme are shown; G_0W_0 @BHLYP (blue dashed lines and crosses), G_0W_0 @OTRSH (pink dotted lines and filled circles), $evGW$ @BHLYP (green lines and crosses) and OTRSH (yellow dashed lines and circles). Note that quantum Monte Carlo data[139] (dark-grey triangles) agree well with the CCSD(T) BTE values for anthracene. For completeness, the mean signed deviation ($MSD = 1/N_i \sum_i^{N_i} E_i - E_{ref}$) and mean absolute deviation ($MAD = 1/N_i \sum_i^{N_i} |E_i - E_{ref}|$) with respect to the CCSD(T) BTEs for all of the approximations considered in this work are shown in Figure 5.4.

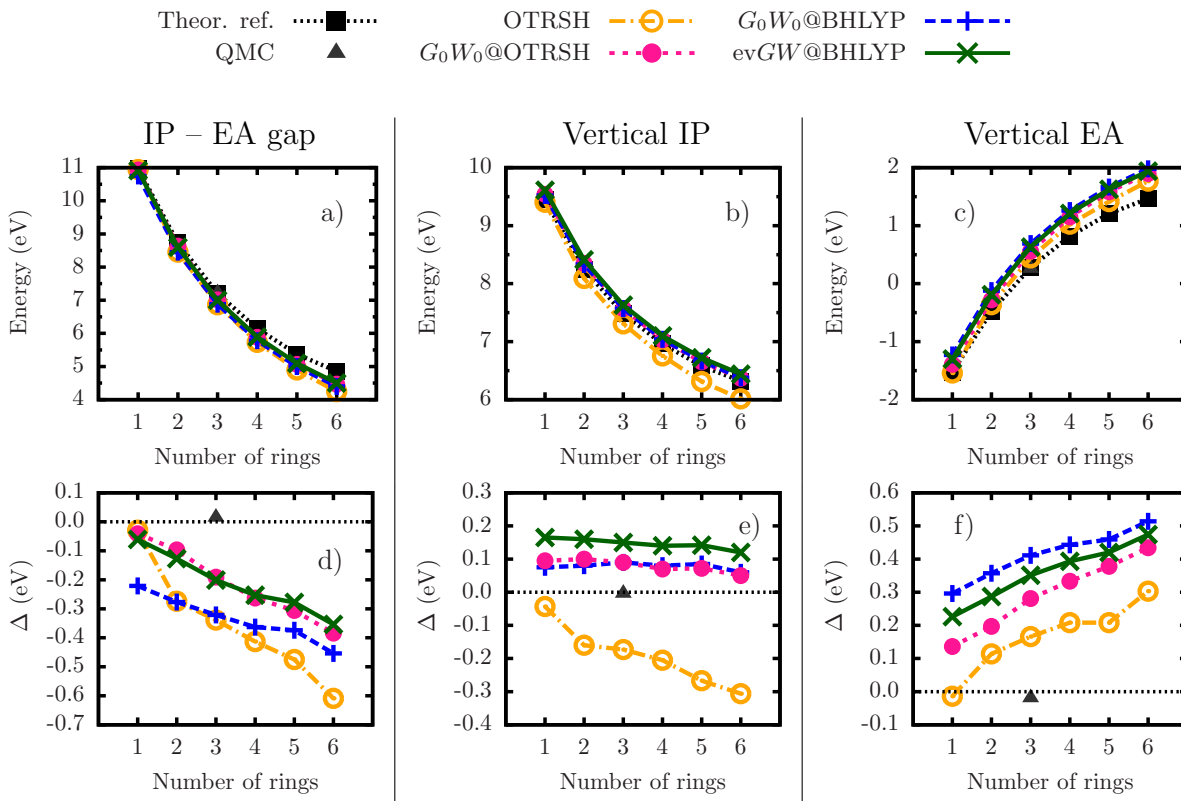


Figure 5.3: Charged excitations of oligoacenes calculated within GW and DFT are compared to CCSD(T); our IPs in Table 5.1 and EAs from Refs.[137]. Calculated IP–EA gaps, vertical ionization potentials (IP), electron affinities (EA) and their corresponding difference with respect to the theoretical reference, Δ , are shown in panels a - f. Several GW approaches are considered (see text). For comparison, quantum Monte Carlo (QMC) data from Ref.[139] for anthracene are also shown.

In Figure 5.3, we plot the IP/EA/gap calculated with OTRSH in yellow circles and dashed-lines; the calculations shown here agree well (within 0.05 eV) with previous works.[104, 148, 24] For benzene, the OTRSH IP and EA are in perfect agreement with the CCSD(T) reference. However, the agreement deteriorates for larger acenes, in agreement with Ref.[148], possibly due to the fact that as OTRSH is tuned to fulfill the DFT ionization potential theorem, its performance is dependent on the reliability of Δ SCF; larger molecules can show larger frontier-orbital delocalization and Δ SCF is known to perform poorly when orbitals are delocalized, e.g. in the asymptotic limit of infinite molecules and in extended systems due to approximate exchange-correlation potentials.[146, 164, 165, 166, 167] Note that BNL gives the best overall agreement to the reference values, with an MAD of only ~ 0.1 eV for the IPs, EAs and gaps, as already found in Ref.[168]. OTRSH exhibits a larger MAD, e.g. ~ 0.3 eV for the IP–EA gap.

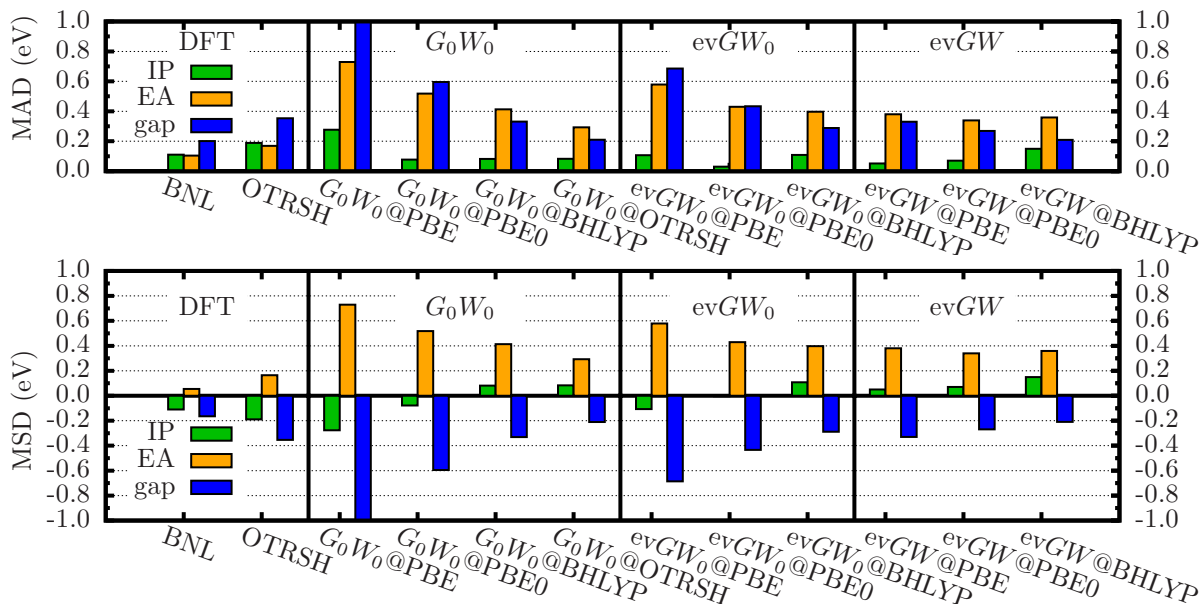


Figure 5.4: Top: Mean absolute deviation (MAD) with respect to the theoretical reference [CCSD(T)] in the calculated IPs (green bars), EAs (orange bars) and IP–EA gaps (blue bars) of the acene family of molecules. Bottom: Mean signed deviation (MSD). Several DFT and GW approximations are considered (see text).

We now turn to our results with G_0W_0 . First, $G_0W_0@PBE$, severely underestimates the QP gaps, with a MSD of -1.0 eV, in agreement with previous findings.[114, 63, 79, 169, 61, 61] The shortcomings of $G_0W_0@PBE$ are well-known and discussed in Refs.[63, 114, 79, 61]. Note that standard G_0W_0 calculations of charged excitations of the acenes have been reported using plane-wave approaches,[62, 104, 170, 169, 144] and the level of convergence and the nature of the frequency-integration schemes can lead to qualitative differences from the work presented here that are well documented.[62, 169]

One known strategy to improve over $G_0W_0@PBE$ is to use an XC functional with a fraction of exact exchange as starting point.[63, 79] We find that the global hybrid providing the best results (lower MAD) is $G_0W_0@BHLYP$, which has an MAD of 0.3 eV in the calculated IP–EA acene gaps (See Figure 5.4), good accuracy at a reasonable computational cost. Notably, the OTRSH starting point leads to highly accurate QP energies, with an MAD for the IP–EA gap of only 0.2 eV, and in close agreement with more expensive evGW schemes (see Figure 5.3).

The excellent performance of $G_0W_0@OTRSH$, as hypothesized in Ref.[24], is consistent with the conclusions of Gallandi and Körzdörfer[143] who explored several GW approaches and found that a tuned long-range separated hybrid (namely the IP-tuned LC- ω PBE[148],

equivalent to OTRSH with $\alpha = 0$ and $\beta = 1$) G_0W_0 starting point yields charged excitation energies within 0.1 eV of experiment and evGW in a set of molecules that includes some (but not all) of the acenes. Their work was extended in Refs.[87] and [86] where a CCSD(T) reference was used, and where it was reported that the LC- ω PBE starting point leads to the smallest MAD (0.2 eV for EAs and 0.1 for IPs) in a set of short- to medium- sized molecules. In agreement with the findings of Ref.[86], the RSH starting point for G_0W_0 with fixed α and γ parameters can lead to the same level of accuracy than G_0W_0 @OTRSH in the IP and EA energy levels of the acene molecules (with a MAD of ≤ 0.3), see Sect. 2 of the SI for details. Prior calculations,[61, 79] including some acene molecules, report that the PBE0 starting point provides the best overall QP energies relative to photoemission experiments along a broad energy range; here, we compare to CCSD(T) and focus only on the frontier molecular levels.

A second approach known to provide accurate QP energies is eigenvalue self-consistency.[114] Here, we test two different levels of eigenvalue self-consistency: partial self-consistency, updating eigenvalues only in G (ev GW_0); and full self-consistency, updating eigenvalues in both G and W (evGW). We find that ev GW_0 leads to unsatisfactory results for these molecules, unless W_0 from BHLYP is used, e.g., ev GW_0 @PBE, ev GW_0 PBE0 and ev GW_0 BHLYP result in a MAD of 0.7, 0.4 and 0.3 eV, respectively, for the IP–EA gap. Moreover, no clear improvement is found with ev GW_0 over G_0W_0 @BHLYP; the two approaches result in nearly equivalent QP energies (within 0.05 eV). On the other hand, evGW results in overall good agreement to the reference values, with an MAD of ~ 0.2 eV for the QP gap (see Figure 5.4). We also highlight that there is not much spread in the evGW QP energies with respect to the DFT starting point; in fact, the evGW gap of benzene is predicted to be 10.9 eV independent of the DFT starting points considered here. For larger molecules, evGW with different starting points can, in some cases, lead to more appreciable differences: for example, a difference of 0.2 eV in QP is observed with PBE or BHLYP starting points for tetracene. In Ref.[79] by considering the extreme starting-points, PBE and HF (with 0% and 100% exact exchange, respectively), a larger difference (~ 0.4 eV) was found in the resulting evGW gaps of organic molecules. Nevertheless, the starting-point dependence of evGW is less than in the case of G_0W_0 , which is typically ~ 1.4 eV for aromatic molecules.[79] Hence, the evGW method is an attractive approach due to its relatively-minimal starting-point dependence and good accuracy, in spite of its higher cost with respect to one-shot G_0W_0 .

The evGW and G_0W_0 approaches and their corresponding self-energy corrections are linearly correlated. In Figure 5.5, we show corrections to the IP–EA gap [$\text{gap}(\text{GW}) - \text{gap}(\text{DFT})$] obtained from both G_0W_0 and evGW. As expected, evGW leads to larger gaps than G_0W_0 @PBE.[114, 148, 87] Interestingly, independent of starting point, we find that our G_0W_0 corrections are consistently 87% of the corresponding evGW corrections (see dashed blue line in Fig. 5.5 with a slope of 0.87 and a standard deviation of < 0.01 eV). Note that six points between 4 and 7 eV lie slightly below this linear trend (dashed blue line); these points use a PBE starting point and are best fit with a slightly smaller slope of 0.85 (not shown). This simple relation, consistent with the tendency of G_0W_0 to underestimate gaps due to over screening[114] and the fact that the screening is similar enough across the acene

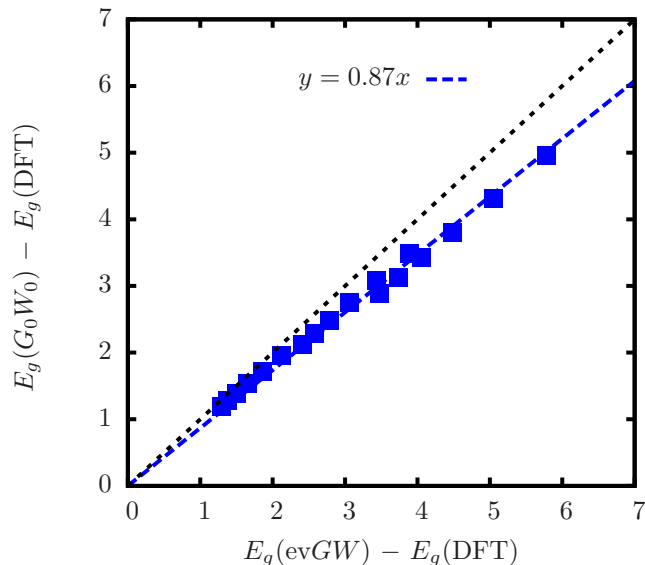


Figure 5.5: Correlation and linear fit between evGW gaps and their corresponding G_0W_0 gaps for the oligoacenes. Results of GW calculations with PBE, PBE0 and BHLYP starting points are used in constructing this plot. All energies are in units of eV.

series, would allow for an accurate estimation of the evGW gap from G_0W_0 corrections for acenes, or even of the G_0W_0 gap from other DFT starting points.

In agreement with recent work, [148, 24, 87, 86] we find that RSH or GW can provide highly accurate frontier orbital energies for small acenes; for benzene, OTRSH and GW@OTRSH gives IPs and EAs within 0.1 eV of the CCSD(T) reference. For medium-sized molecules the accuracy of both RSH and GW decreases; for hexacene OTRSH presents deviations of ~ 0.3 eV in both the IP and the EA, adding to an MAD of ~ 0.6 eV in the gap; the more accurate GW approaches tested in this work (GW@OTRSH, GW@BHLYP and evGW) predict IPs within 0.1 eV but can overestimate EAs by up to 0.4 – 0.5 eV (see Fig. 5.3). Nevertheless, since the deviation grows linearly with the number of rings (N_{ring}), the EAs can be linearly extrapolated from the GW results as:

$$\text{EA} = \text{EA}^{\text{GW@OTRSH}} - (0.087 \text{ eV})N_{\text{ring}} + 0.06 \text{ eV}, \quad (5.4)$$

where we have subtracted a linear function of the number of rings from the GW@OTRSH EA energies, and obtained the EA energies within 0.02 eV of the CCSD(T) reference. This simple relation, though effective here, may not be transferable to other aromatic hydrocarbon families, and in general will not be applicable for any other non-ringed system; GW calculations beyond the approaches used in this work may yield further insight into this trend. It is worth noticing that wavefunctions of larger acenes have some multi-reference character,[171] which might explain the observed limited performance of GW in the large molecule regime.

In this work we fix the fraction of short-range exact exchange in all DFT-RSH calculations; thus one straightforward extension is to tune the α parameter with theorems of DFT, along the lines of Refs.[172], [24] and [173]. Tuning the short-range HF parameter may lead to a better description of systems with localized electrons; nevertheless, for the acenes, with only s and p electrons, it is not evident a priori that such tuning would improve the accuracy of both OTRSH and GW based on an OTRSH starting point. In fact, for benzene and pentacene, setting α to either 0.0 or 0.2 leads to negligible changes (by < 0.1 eV) in the IPs or EAs, as shown in Refs.[24] and [26]. Further, when it comes to the π and π^* orbital energies of representative organic molecules, it has been shown in Ref.[86] that the tuning of the α parameter does not significantly affect the performance of OTRSH or G_0W_0 @OTRSH. Beyond eigenvalue self-consistent GW, total energy differences from GW [bruneval'GW'2009, 174] might also result in more accurate frontier orbital energies. We leave these considerations to be explored in future work.

In summary, our results indicate that going beyond standard G_0W_0 is crucial to achieve CCSD(T) accuracy; including self-consistency, such as in the evGW method, or adding a fraction of exact exchange are both successful strategies for describing charged-excitations. Notably, using OTRSH as a starting point for G_0W_0 provides highly accurate energetics relative to CCSD(T), in agreement with the more expensive evGW results.

5.4 Conclusions

In this work, we have calculated IPs and EAs of acene molecules with DFT, GW, and wavefunction-based approaches. We have built upon and extended the CCSD(T) reference data of Ref.[138] for IPs of the larger acenes. Using this new CCSD(T) reference, we have benchmarked GW under several approximations and DFT with range-separated hybrid methods and found that both G_0W_0 @OTRSH and evGW consistently perform well, yielding quantitative IP energies within 0.1 eV of CCSD(T) across the acene series. Nevertheless, all GW approaches studied here lead to qualitative deviations for the larger acenes, suggesting the need to go beyond eigenvalue-self-consistent GW methods to do better. Moreover, we have found that DFT with OTRSH or BNL functionals can perform as well as the most effective GW approaches for benzene, but their resulting IPs and EAs deteriorate as the molecules get larger in the series, a behavior attributable to the known deficiencies of Δ SCF in the asymptotic limit of large molecules towards extended systems.

Chapter 6

Outlook

Wielding the full power of electronic structure theory to tackle the development and understanding of complex biological, material and energy systems necessarily involves increasingly interdisciplinary efforts and considerations. While the work contained in this dissertation has focused on the low-lying excited states of relatively small to medium gas phase organic molecules, real systems of interest are generally not in the gas phase, are not necessarily small or medium, and involve diverse interactions between molecules in potential energy landscapes formed by, for example: solvation, polymerization, the near-by surfaces of crystalline lattices, confinement in junctions or by segments of protein, temperature and pressure differences, and involvement in metal organic frameworks. Work in the Neaton group (and other groups) is currently underway to determine best practices for the determination of the excited states of large solvated chromophores. How are the OTRSH parameters tuned in such a situation? How much of the solvent should be treated explicitly, and what is the best way to choose which molecules are given explicit treatment? What implicit solvent methods work best in particular situations? How do combinations of solvation techniques interact? In order to answer these questions it will be important to identify each solvent method's contribution in the TDDFT and GW-BSE working equations and then to quantitatively validate the chosen method with small molecule data by for example, performing calculations with and without implicit polarizable continuum models, and in combination with multiple sets of OTRSH parameters, while tracking how observables change as a result of these choices.

Bibliography

- [1] E. Runge and E.K.U. Gross. “Density-Functional Theory for Time-Dependent Systems”. In: *Phys. Rev. Lett.* 52 (1984), pp. 997–1000.
- [2] M.A.L. Marques and E.K.U. Gross. “Time-Dependent Density Functional Theory”. In: *Annu. Rev. Phys. Chem.* 55 (2004), pp. 427–455.
- [3] M.E. Casida. “Time-Dependent Density Functional Theory for Molecules”. In: *Recent Advances in Density Functional Methods 1* (1995), pp. 155–192.
- [4] A.L. Fetter and J.D. Walecka. *Quantum Theory of Many-Particle Systems*. MacGraw-Hill, New York, 1971.
- [5] G.D. Mahan. *Many-Particle Physics*. Kluwer Academic/Plenum Publishers, 2000.
- [6] A. Szabo and N.S. Ostlund. *Modern Quantum Chemistry: Introduction to Advanced Electronic Structure Theory*. Dover Publications, Mineola (N.Y.), 1996.
- [7] Giovanni Onida, Lucia Reining, and Angel Rubio. “Electronic excitations: density-functional versus many-body Green’s-function approaches”. In: *Rev. Mod. Phys.* 74.2 (2002), pp. 601–659.
- [8] B. Le Guennic and D. Jacquemin. “Taking Up the Cyanine Challenge with Quantum Tools”. In: *Acc Chem Res.* 48 (2015), pp. 530–537.
- [9] Andreas Dreuw and Martin Head-Gordon. “Failure of Time-Dependent Density Functional Theory for Long-Range Charge-Transfer Excited States: The Zincbacteriochlorin-Bacteriochlorin and Bacteriochlorophyll-Spheroidene Complexes”. In: *J. Am. Chem. Soc.* 126.12 (2004), pp. 4007–4016. DOI: 10.1021/ja039556n. URL: 10.1021/ja039556n.
- [10] A. Prlj et al. “Qualitatively Incorrect Features in the TDDFT Spectrum of Thiophene-Based Compounds”. In: *J Phys Chem Lett* 6(1) (2015), pp. 13–21.
- [11] Stephan Kümmel. “Charge-Transfer Excitations: A Challenge for Time-Dependent Density Functional Theory That Has Been Met”. In: *Adv. Energy Mater.* 7.16 (2017), p. 1700440. DOI: 10.1002/aenm.201700440. URL: 10.1002/aenm.201700440.
- [12] So Hirata and Martin Head-Gordon. “Time-dependent density functional theory within the Tamm–Dancoff approximation”. In: *Chem. Phys. Lett.* 314.3–4 (1999), pp. 291–299.

- [13] F. Bruneval, S.M. Hamed, and J.B. Neaton. “A systematic benchmark of the ab initio Bethe-Salpeter equation approach for low-lying optical excitations of small organic molecules”. In: *J. Chem. Phys.* 142 (2015), p. 244101.
- [14] Denis Jacquemin, Ivan Duchemin, and Xavier Blase. “Benchmarking the Bethe–Salpeter Formalism on a Standard Organic Molecular Set”. In: *J. Chem. Theory Comput.* 11.7 (2015), p. 3290.
- [15] Dario Rocca, Deyu Lu, and Giulia Galli. “Ab initio calculations of optical absorption spectra: Solution of the Bethe–Salpeter equation within density matrix perturbation theory”. In: *The Journal of Chemical Physics* 133.16 (2010), p. 164109. DOI: 10.1063/1.3494540. URL: 10.1063/1.3494540.
- [16] X. Blase and C. Attaccalite. “Charge-transfer excitations in molecular donor-acceptor complexes within the many-body Bethe-Salpeter approach”. In: *Appl. Phys. Lett.* 99.17 (2011), p. 171909. DOI: 10.1063/1.3655352. URL: 10.1063/1.3655352.
- [17] G. Strinati. “Application of the Green’s functions method to the study of the optical properties of semiconductors”. In: *Riv. Nuovo Cim.* 11.12 (1988), pp. 1–86. DOI: 10.1007/bf02725962. URL: 10.1007/bf02725962.
- [18] Lars Hedin. “New Method for Calculating the One-Particle Green’s Function with Application to the Electron-Gas Problem”. In: *Phys. Rev.* 139.3A (), A796–A823. DOI: 10.1103/physrev.139.a796. URL: 10.1103/physrev.139.a796.
- [19] Wilfried G. Aulbur, Lars Jonsson, and John W. Wilkins. “Quasiparticle Calculations in Solids”. In: (2000), pp. 1–218. DOI: 10.1016/s0081-1947(08)60248-9. URL: 10.1016/s0081-1947(08)60248-9.
- [20] Robert G. Parr and Weitao Yang. *Density-Functional Theory of Atoms and Molecules*. Oxford University Press, May 1994. ISBN: 9780195357738.
- [21] A. J. Cohen, P. Mori-Sanchez, and W. Yang. “Insights into Current Limitations of Density Functional Theory”. In: *Science* 321.5890 (2008), pp. 792–794. DOI: 10.1126/science.1158722. URL: 10.1126/science.1158722.
- [22] Aron J. Cohen, Paula Mori-Sanchez, and Weitao Yang. “Fractional charge perspective on the band gap in density-functional theory”. In: *Phys. Rev. B* 77.11 (). DOI: 10.1103/physrevb.77.115123. URL: 10.1103/physrevb.77.115123.
- [23] Weitao Yang, Aron J. Cohen, and Paula Mori-Sanchez. “Derivative discontinuity, bandgap and lowest unoccupied molecular orbital in density functional theory”. In: *The Journal of Chemical Physics* 136.20 (2012), p. 204111. DOI: 10.1063/1.3702391. URL: 10.1063/1.3702391.
- [24] Sivan Refaely-Abramson et al. “Quasiparticle Spectra from a Nonempirical Optimally Tuned Range-Separated Hybrid Density Functional”. In: *Phys. Rev. Lett.* 109.22 (2012), p. 226405. DOI: 10.1103/PhysRevLett.109.226405.

- [25] Leeor Kronik et al. “Excitation Gaps of Finite-Sized Systems from Optimally Tuned Range-Separated Hybrid Functionals”. In: *J. Chem. Theory Comput.* 8.5 (2012). see references therein., p. 1515. DOI: 10.1021/ct2009363.
- [26] David A. Egger et al. “Outer-valence Electron Spectra of Prototypical Aromatic Heterocycles from an Optimally Tuned Range-Separated Hybrid Functional”. In: *J. Chem. Theory Comput.* 10.5 (2014), pp. 1934–1952. DOI: 10.1021/ct400956h.
- [27] Adèle D. Laurent and Denis Jacquemin. “TD-DFT benchmarks: A review”. In: *Int. J. Quantum Chem.* 113.17 (2013), pp. 2019–2039. DOI: 10.1002/qua.24438. URL: 10.1002/qua.24438.
- [28] Xavier Blase, Ivan Duchemin, and Denis Jacquemin. “The Bethe–Salpeter equation in chemistry: relations with TD-DFT, applications and challenges”. In: *Chem. Soc. Rev.* 47.3 (), pp. 1022–1043. DOI: 10.1039/c7cs00049a. URL: 10.1039/c7cs00049a.
- [29] Milan Delor et al. “Exploiting Chromophore–Protein Interactions through Linker Engineering To Tune Photoinduced Dynamics in a Biomimetic Light-Harvesting Platform”. In: *J. Am. Chem. Soc.* 140.20 (2018), pp. 6278–6287. DOI: 10.1021/jacs.7b13598. URL: 10.1021/jacs.7b13598.
- [30] David J. Garfield et al. “Enrichment of molecular antenna triplets amplifies upconverting nanoparticle emission”. In: *Nature Photon* 12.7 (2018), pp. 402–407. DOI: 10.1038/s41566-018-0156-x. URL: 10.1038/s41566-018-0156-x.
- [31] Michel T. Dedeo, Daniel T. Finley, and Matthew B. Francis. “Viral Capsids as Self-Assembling Templates for New Materials”. In: (2011), pp. 353–392. DOI: 10.1016/b978-0-12-415906-8.00002-9. URL: 10.1016/b978-0-12-415906-8.00002-9.
- [32] Rebekah A. Miller, Andrew D. Presley, and Matthew B. Francis. “Self-Assembling Light-Harvesting Systems from Synthetically Modified Tobacco Mosaic Virus Coat Proteins”. In: *J. Am. Chem. Soc.* 129.11 (2007), pp. 3104–3109. DOI: 10.1021/ja063887t. URL: 10.1021/ja063887t.
- [33] Rodrigo Noriega et al. “Manipulating Excited-State Dynamics of Individual Light-Harvesting Chromophores through Restricted Motions in a Hydrated Nanoscale Protein Cavity”. In: *J. Phys. Chem. B* 119.23 (2015), pp. 6963–6973. DOI: 10.1021/acs.jpcc.5b03784. URL: 10.1021/acs.jpcc.5b03784.
- [34] Benoît Champagne, Maxime Guillaume, and Freddy Zutterman. “TDDFT investigation of the optical properties of cyanine dyes”. In: *Chemical Physics Letters* 425.1–3 (2006), pp. 105–109. DOI: 10.1016/j.cplett.2006.05.009. URL: 10.1016/j.cplett.2006.05.009.
- [35] Jürgen Fabian. “TDDFT-calculations of Vis/NIR absorbing compounds”. In: *Dyes and Pigments* 84.1 (2010), pp. 36–53. DOI: 10.1016/j.dyepig.2009.06.008. URL: 10.1016/j.dyepig.2009.06.008.
- [36] Michael J. G. Peach, Matthew J. Williamson, and David J. Tozer. “Influence of Triplet Instabilities in TDDFT”. In: *J. Chem. Theory Comput.* 7.11 (2011), p. 3578.

- [37] Chr. Møller and M. S. Plesset. “Note on an Approximation Treatment for Many-Electron Systems”. In: *Phys. Rev.* 46.7 (), pp. 618–622. DOI: 10.1103/physrev.46.618. URL: 10.1103/physrev.46.618.
- [38] Dieter Cremer. “Møller-Plesset perturbation theory: from small molecule methods to methods for thousands of atoms”. In: *WIREs Comput Mol Sci* 1.4 (2011), pp. 509–530. DOI: 10.1002/wcms.58. URL: 10.1002/wcms.58.
- [39] P. Hohenberg and W. Kohn. “Inhomogeneous Electron Gas”. In: *Phys. Rev.* 136.3B (), B864–B871. DOI: 10.1103/physrev.136.b864. URL: 10.1103/physrev.136.b864.
- [40] W. Kohn and L. J. Sham. “Self-Consistent Equations Including Exchange and Correlation Effects”. In: *Phys. Rev.* 140.4A (), A1133–A1138. DOI: 10.1103/physrev.140.a1133. URL: 10.1103/physrev.140.a1133.
- [41] John P. Perdew et al. “Prescription for the design and selection of density functional approximations: More constraint satisfaction with fewer fits”. In: *The Journal of Chemical Physics* 123.6 (2005), p. 062201. DOI: 10.1063/1.1904565. URL: 10.1063/1.1904565.
- [42] John P. Perdew, Kieron Burke, and Matthias Ernzerhof. “Generalized Gradient Approximation Made Simple”. In: *Phys. Rev. Lett.* 77.18 (1996), p. 3865.
- [43] Shao, Y. et. al. In: *Phys. Chem. Chem. Phys.* 8.27 (2006), p. 3172. DOI: 10.1039/B517914A.
- [44] Axel D. Becke. “Density-functional thermochemistry. III. The role of exact exchange”. In: *J. Chem. Phys.* 98.7 (1993), pp. 5648–5652. DOI: 10.1063/1.464913.
- [45] P. J. Stephens et al. “Ab Initio Calculation of Vibrational Absorption and Circular Dichroism Spectra Using Density Functional Force Fields”. In: *J. Phys. Chem.* 98.45 (1994), pp. 11623–11627. DOI: 10.1021/j100096a001. URL: 10.1021/j100096a001.
- [46] John P. Perdew, Matthias Ernzerhof, and Kieron Burke. “Rationale for mixing exact exchange with density functional approximations”. In: *J. Chem. Phys.* 105.22 (1996), p. 9982.
- [47] Carlo Adamo and Vincenzo Barone. “Toward reliable density functional methods without adjustable parameters: The PBE0 model”. In: *The Journal of Chemical Physics* 110.13 (1999), pp. 6158–6170. DOI: 10.1063/1.478522. URL: 10.1063/1.478522.
- [48] Thierry Leininger et al. “Combining long-range configuration interaction with short-range density functionals”. In: *Chem. Phys. Lett.* 275.3–4 (1997), pp. 151–160. DOI: 10.1016/S0009-2614(97)00758-6.
- [49] Takeshi Yanai, David P Tew, and Nicholas C Handy. “A new hybrid exchange–correlation functional using the Coulomb b-attenuating method (CAM-B3LYP)”. In: *Chem. Phys. Lett.* 393.1–3 (2004), pp. 51–57.

- [50] John P. Perdew et al. “Density-Functional Theory for Fractional Particle Number: Derivative Discontinuities of the Energy”. In: *Phys. Rev. Lett.* 49.23 (1982), pp. 1691–1694. DOI: 10.1103/PhysRevLett.49.1691.
- [51] Ulrike Salzner and Roi Baer. “Koopmans’ springs to life”. In: *J. Chem. Phys.* 131.23 (2009), p. 231101. DOI: 10.1063/1.3269030.
- [52] Mel Levy, John P. Perdew, and Virahnt Sahni. “Exact differential equation for the density and ionization energy of a many-particle system”. In: *Phys. Rev. A* 30.5 (1984), pp. 2745–2748. DOI: 10.1103/PhysRevA.30.2745.
- [53] John P. Perdew and Mel Levy. “Comment on “Significance of the highest occupied Kohn-Sham eigenvalue””. In: *Phys. Rev. B* 56.24 (1997), pp. 16021–16028. DOI: 10.1103/PhysRevB.56.16021.
- [54] C.-O. Almbladh and U. von Barth. “Exact results for the charge and spin densities, exchange-correlation potentials, and density-functional eigenvalues”. In: *Phys. Rev. B* 31.6 (1985), pp. 3231–3244. DOI: 10.1103/PhysRevB.31.3231.
- [55] Roi Baer and Daniel Neuhauser. “Density functional theory with correct long-range asymptotic behavior”. In: *Phys. Rev. Lett.* 94.4 (2005), p. 043002.
- [56] Ester Livshits and Roi Baer. “A well-tempered density functional theory of electrons in molecules”. In: *Phys. Chem. Chem. Phys.* 9.23 (2007), pp. 2932–2941.
- [57] Sivan Refaely-Abramson et al. “Gap renormalization of molecular crystals from density-functional theory”. In: *Phys. Rev. B* 88.8 (). DOI: 10.1103/physrevb.88.081204. URL: 10.1103/physrevb.88.081204.
- [58] Carsten Ullrich. *Time-dependent density-functional theory*. Oxford University Press, 2012. ISBN: 9780199563029.
- [59] Jeffrey C. Grossman et al. In: *Phys. Rev. Lett.* 86 (2001), pp. 472–475. DOI: 10.1103/PhysRevLett.86.472.
- [60] Xinguo Ren et al. “Resolution-of-identity approach to Hartree–Fock, hybrid density functionals, RPA, MP2 and GW with numeric atom-centered orbital basis functions”. In: *New J. Phys.* 14.5 (2012), p. 053020. URL: <http://stacks.iop.org/1367-2630/14/i=5/a=053020>.
- [61] Thomas Körzdörfer and Noa Marom. “Strategy for finding a reliable starting point for G0W0 demonstrated for molecules”. In: *Phys. Rev. B* 86.4 (July 2012), p. 041110.
- [62] S. Sharifzadeh et al. “Quantitative molecular orbital energies within a G0W0 approximation”. In: *Eur. Phys. J. B* 85.9 (2012), p. 1.
- [63] Fabien Bruneval and Miguel A. L. Marques. In: *J. Chem. Theory Comput.* 9.1 (2013), p. 324.
- [64] Sabine Körbel et al. “Benchmark Many-Body GW and Bethe–Salpeter Calculations for Small Transition Metal Molecules”. In: *J. Chem. Theory Comput.* 10.9 (2014), pp. 3934–3943. ISSN: 1549-9618. DOI: 10.1021/ct5003658.

- [65] P. Koval, D. Foerster, and D. Sanchez-Portal. “Fully self-consistent GW and quasiparticle self-consistent GW for molecules”. In: *Phys. Rev. B* 89.15 (). DOI: 10.1103/physrevb.89.155417. URL: 10.1103/physrevb.89.155417.
- [66] Meiyue Shao et al. “Structure preserving parallel algorithms for solving the Bethe–Salpeter eigenvalue problem”. In: *Linear Algebra Appl.* 488 (2016), p. 148. DOI: 10.1016/j.laa.2015.09.036.
- [67] Marko Schreiber et al. In: *J. Chem. Phys.* 128.13 (2008), p. 134110. DOI: 10.1063/1.2889385.
- [68] Fabien Bruneval. “Ionization energy of atoms obtained from GW self-energy or from random phase approximation total energies”. In: *J. Chem. Phys.* 136.19 (2012), p. 194107.
- [69] Fabien Bruneval et al. “molgw 1: Many-body perturbation theory software for atoms, molecules, and clusters”. In: *Computer Physics Communications* 208 (2016), pp. 149–161. DOI: 10.1016/j.cpc.2016.06.019. URL: 10.1016/j.cpc.2016.06.019.
- [70] E. F. Valeev. *A library for the evaluation of molecular integrals of many-body operators over Gaussian functions*. (Visited on 03/09/2016). 2015. URL: <http://libint.valeyev.net/>.
- [71] Miguel A. L. Marques, Micael J. T. Oliveira, and Tobias Burnus. “Libxc: A library of exchange and correlation functionals for density functional theory”. In: *Comput. Phys. Commun.* 183 (2012), p. 2272.
- [72] Henrik Koch and Poul Jorgensen. “Coupled cluster response functions”. In: *The Journal of Chemical Physics* 93.5 (1990), pp. 3333–3344. DOI: 10.1063/1.458814. URL: 10.1063/1.458814.
- [73] Kerstin Andersson et al. “Second-order perturbation theory with a CASSCF reference function”. In: *J. Phys. Chem.* 94.14 (1990), pp. 5483–5488. DOI: 10.1021/j100377a012. URL: 10.1021/j100377a012.
- [74] M. J. Frisch et al. *Gaussian09 Revision E.01*. Gaussian Inc. Wallingford CT 2009.
- [75] Ansgar Schafer, Hans Horn, and Reinhart Ahlrichs. “Fully optimized contracted Gaussian basis sets for atoms Li to Kr”. In: *The Journal of Chemical Physics* 97.4 (1992), pp. 2571–2577. DOI: 10.1063/1.463096. URL: 10.1063/1.463096.
- [76] Rick A. Kendall, Thom H. Dunning Jr, and Robert J. Harrison. “Electron affinities of the first-row atoms revisited. Systematic basis sets and wave functions”. In: *J. Chem. Phys.* 96.9 (1992), p. 6796.
- [77] Mario R. Silva-Junior et al. In: *J. Chem. Phys.* 133.17 (2010), p. 174318. DOI: 10.1063/1.3499598.
- [78] C. Rostgaard, K. W. Jacobsen, and K. S. Thygesen. “Fully self-consistent GW calculations for molecules”. In: *Phys. Rev. B* 81.8 (2010), p. 085103. DOI: 10.1103/PhysRevB.81.085103.

- [79] Noa Marom et al. “Benchmark of \$GW\$ methods for azabenzenes”. In: *Phys. Rev. B* 86.24 (2012), p. 245127.
- [80] F. Caruso et al. “Unified description of ground and excited states of finite systems: The self-consistent \$GW\$ approach”. In: *Phys. Rev. B* 86.8 (2012), p. 081102. DOI: 10.1103/PhysRevB.86.081102.
- [81] C. Faber et al. “Many-body Green’s function GW and Bethe-Salpeter study of the optical excitations in a paradigmatic model dipeptide”. In: *The Journal of Chemical Physics* 139.19 (2013), p. 194308. DOI: 10.1063/1.4830236. URL: 10.1063/1.4830236.
- [82] Axel D. Becke. “A new mixing of Hartree–Fock and local density-functional theories”. In: *J. Chem. Phys.* 98.2 (1993), p. 1372.
- [83] Katsuki Okuno et al. “Tuned CAM-B3LYP functional in the time-dependent density functional theory scheme for excitation energies and properties of diarylethene derivatives”. In: *Journal of Photochemistry and Photobiology A: Chemistry* 235 (2012), pp. 29–34. DOI: 10.1016/j.jphotochem.2012.03.003. URL: 10.1016/j.jphotochem.2012.03.003.
- [84] Fabien Bruneval, Samia M. Hamed, and Jeffrey B. Neaton. “A systematic benchmark of the ab initio Bethe-Salpeter equation approach for low-lying optical excitations of small organic molecules”. In: *J. Chem. Phys.* 142.24 (2015), p. 244101.
- [85] Noa Marom. “Accurate description of the electronic structure of organic semiconductors by GW methods”. In: *J. Phys.: Condens. Matter* 29.10 (2017), p. 103003. DOI: 10.1088/1361-648x/29/10/103003. URL: 10.1088/1361-648x/29/10/103003.
- [86] Lukas Gallandi et al. “Accurate Ionization Potentials and Electron Affinities of Acceptor Molecules II: Non-Empirically Tuned Long-Range Corrected Hybrid Functionals”. In: *J. Chem. Theory Comput.* 12.2 (2016), pp. 605–614. DOI: 10.1021/acs.jctc.5b00873. URL: 10.1021/acs.jctc.5b00873.
- [87] Joseph W. Knight et al. “Accurate Ionization Potentials and Electron Affinities of Acceptor Molecules III: A Benchmark of GW Methods”. In: *J. Chem. Theory Comput.* 12.2 (2016), pp. 615–626. DOI: 10.1021/acs.jctc.5b00871. URL: 10.1021/acs.jctc.5b00871.
- [88] Juliana Bois and Thomas Korzdorfer. “Size-Dependence of Nonempirically Tuned DFT Starting Points for G0W0 Applied to π -Conjugated Molecular Chains”. In: *J. Chem. Theory Comput.* 13.10 (2017), pp. 4962–4971. DOI: 10.1021/acs.jctc.7b00557. URL: 10.1021/acs.jctc.7b00557.
- [89] Tonatiuh Rangel et al. “An assessment of low-lying excitation energies and triplet instabilities of organic molecules with an ab initio Bethe-Salpeter equation approach and the Tamm-Dancoff approximation”. In: *The Journal of Chemical Physics* 146.19 (2017), p. 194108. DOI: 10.1063/1.4983126. URL: 10.1063/1.4983126.

- [90] Thom H. Dunning. “Gaussian basis sets for use in correlated molecular calculations. I. The atoms boron through neon and hydrogen”. In: *The Journal of Chemical Physics* 90.2 (1989), pp. 1007–1023. DOI: 10.1063/1.456153. URL: 10.1063/1.456153.
- [91] Florian Weigend. “A fully direct RI-HF algorithm: Implementation, optimised auxiliary basis sets, demonstration of accuracy and efficiency”. In: *Phys. Chem. Chem. Phys.* 4 (18 2002), pp. 4285–4291. DOI: 10.1039/B204199P.
- [92] D. P. Chong, O. V. Gritsenko, and E. J. Baerends. “Interpretation of the Kohn–Sham orbital energies as approximate vertical ionization potentials”. In: *The Journal of Chemical Physics* 116.5 (Jan. 2002), pp. 1760–1772. DOI: 10.1063/1.1430255. URL: 10.1063/1.1430255.
- [93] John E. Anthony. “The larger acenes: versatile organic semiconductors”. In: *Angew. Chem. Int. Edit* 47.3 (2008), pp. 452–483.
- [94] Millicent B. Smith and Josef Michl. “Recent Advances in Singlet Fission”. In: *Ann. Rev. Phys. Chem.* 64.1 (2013), pp. 361–386.
- [95] Jiye Lee et al. “Singlet Exciton Fission Photovoltaics”. In: *Acc. Chem. Res.* 46.6 (2013), pp. 1300–1311.
- [96] Michael J. G. Peach and David J. Tozer. “Overcoming Low Orbital Overlap and Triplet Instability Problems in TDDFT”. In: 116.39 (2012), p. 9783.
- [97] Stefan Grimme and Maja Parac. In: *ChemPhysChem* 4.3 (2003), pp. 292–295. DOI: 10.1002/cphc.200390047.
- [98] Natalia Kuritz et al. “Charge-Transfer-Like $\pi \rightarrow \pi^*$ Excitations in Time-Dependent Density Functional Theory: A Conundrum and Its Solution”. In: *J. Chem. Theory Comput.* 7.8 (2011), pp. 2408–2415.
- [99] K. Lopata et al. “Excited-State Studies of Polyacenes: A Comparative Picture Using EOMCCSD, CR-EOMCCSD(T), Range-Separated (LR/RT)-TDDFT, TD-PM3, and TD-ZINDO”. In: *J. Chem. Theory Comput.* 7.11 (2011), p. 3686.
- [100] John S. Sears et al. “Communication: Orbital instabilities and triplet states from time-dependent density functional theory and long-range corrected functionals”. In: *J. Chem. Phys.* 135.15 (2011), p. 151103. DOI: 10.1063/1.3656734.
- [101] M. E. Casida and M. Huix-Rotllant. In: *Annu. Rev. Phys. Chem.* 63.1 (2012), pp. 287–323. DOI: 10.1146/annurev-physchem-032511-143803.
- [102] Bryan M. Wong and Timothy H. Hsieh. In: *J. Chem. Theory Comput.* 6.12 (2010), pp. 3704–3712. DOI: 10.1021/ct100529s. (Visited on 04/06/2016).
- [103] Ryan M. Richard and John M. Herbert. In: *J. Chem. Theory Comput.* 7.5 (2011), pp. 1296–1306. DOI: 10.1021/ct100607w.
- [104] Sivan Refaely-Abramson et al. “Gap renormalization of molecular crystals from density-functional theory”. In: *Phys. Rev. B* 88.8 (2013), p. 081204.

- [105] Tamar Stein, Leeor Kronik, and Roi Baer. In: *J. Chem. Phys.* 131.24 (2009), p. 244119. DOI: 10.1063/1.3269029.
- [106] Jochen Autschbach. “Charge-Transfer Excitations and Time-Dependent Density Functional Theory: Problems and Some Proposed Solutions”. en. In: *ChemPhysChem* 10.11 (Aug. 2009), pp. 1757–1760. ISSN: 1439-7641. DOI: 10.1002/cphc.200900268. URL: <http://onlinelibrary.wiley.com/doi/10.1002/cphc.200900268/abstract> (visited on 01/31/2017).
- [107] Tamar Stein, Leeor Kronik, and Roi Baer. “Reliable Prediction of Charge Transfer Excitations in Molecular Complexes Using Time-Dependent Density Functional Theory”. In: *J. Am. Chem. Soc.* 131.8 (Mar. 2009), pp. 2818–2820. ISSN: 0002-7863. DOI: 10.1021/ja8087482. URL: <http://dx.doi.org/10.1021/ja8087482> (visited on 01/31/2017).
- [108] G Onida et al. “AB-INITIO CALCULATIONS OF THE QUASI-PARTICLE AND ABSORPTION-SPECTRA OF CLUSTERS - THE SODIUM TETRAMER”. In: *Phys. Rev. Lett.* 75 (1995), p. 818.
- [109] Paul Boulanger et al. In: *J. Chem. Theory Comput.* 10.3 (2014), pp. 1212–1218. DOI: 10.1021/ct401101u.
- [110] Denis Jacquemin, Ivan Duchemin, and Xavier Blase. In: *J. Chem. Theory Comput.* 11.11 (2015), pp. 5340–5359. DOI: 10.1021/acs.jctc.5b00619.
- [111] Denis Jacquemin et al. “Benchmark of Bethe-Salpeter for Triplet Excited-States”. In: *J. Chem. Theory Comput.* (2017). <http://dx.doi.org/10.1021/acs.jctc.6b01169>.
- [112] F. Bruneval. *MOLGW: A slow but accurate many-body perturbation theory code*. (Visited on 08/2016). 2015. URL: <http://www.molgw.org>.
- [113] Michael Rohlfing and Steven G. Louie. In: *Phys. Rev. Lett.* 81.11 (1998), p. 2312.
- [114] X. Blase, C. Attaccalite, and V. Olevano. “First-principles GW calculations for fullerenes, porphyrins, phtalocyanine, and other molecules of interest for organic photovoltaic applications”. In: *Phys. Rev. B* 83.11 (2011), p. 115103.
- [115] T. Rangel et al. “Evaluating the GW approximation with CCSD(T) for charged excitations across the oligoacenes”. In: *J. Chem. Theory Comput.* 12 (2016), p. 2834. DOI: 10.1021/acs.jctc.6b00163.
- [116] James B. Foresman and AEleen Frisch. *Exploring Chemistry With Electronic Structure Methods: A Guide to Using Gaussian*. 2 edition. Pittsburgh, PA: Gaussian, 1996.
- [117] O. Vahtras, J. Almlöf, and M.W. Feyereisen. In: *Chem. Phys. Lett.* 213.5–6 (1993), pp. 514–518. DOI: [http://dx.doi.org/10.1016/0009-2614\(93\)89151-7](http://dx.doi.org/10.1016/0009-2614(93)89151-7).
- [118] John R. Platt. “Classification of Spectra of Cata-Condensed Hydrocarbons”. In: *J. Chem. Phys.* 17.5 (1949), pp. 484–495.

- [119] Emilie B. Guidez and Christine M. Aikens. “Origin and TDDFT Benchmarking of the Plasmon Resonance in Acenes”. In: *J. Phys. Chem. C* 117.41 (2013), p. 21466. DOI: 10.1021/jp4059033.
- [120] Kimihiko Hirao, Haruyuki Nakano, and Kenichi Nakayama. “A complete active space valence bond method with nonorthogonal orbitals”. In: *The Journal of Chemical Physics* 107.23 (Jan. 1997), pp. 9966–9974. DOI: 10.1063/1.475300. URL: 10.1063/1.475300.
- [121] Maja Parac and Stefan Grimme. “A TDDFT study of the lowest excitation energies of polycyclic aromatic hydrocarbons”. In: *Chem. Phys.* 292.1 (2003), p. 11. DOI: 10.1016/S0301-0104(03)00250-7.
- [122] B. Hajgató et al. In: *J. Chem. Phys.* 131.22 (2009), p. 224321.
- [123] Barry Moore et al. In: *J. Chem. Theory Comput.* 11.7 (2015), p. 3305. DOI: 10.1021/acs.jctc.5b00335.
- [124] Yi-Lei Wang and Guo-Shi Wu. “Improving the TDDFT calculation of low-lying excited states for polycyclic aromatic hydrocarbons using the Tamm–Dancoff approximation”. In: *Int. J. Quantum Chem.* 108.3 (2008), pp. 430–439. (Visited on 09/25/2015).
- [125] Rolf Seeger and John A. Pople. In: *J. Chem. Phys.* 66.7 (1977), pp. 3045–3050. DOI: 10.1063/1.434318.
- [126] Rüdiger Bauernschmitt and Reinhart Ahlrichs. In: *J. Chem. Phys.* 104.22 (1996), pp. 9047–9052. DOI: 10.1063/1.471637.
- [127] Mark E. Casida et al. In: *J. Chem. Phys.* 113.17 (2000), pp. 7062–7071. DOI: 10.1063/1.1313558.
- [128] Samia Hamed et al. In preparation. 2016.
- [129] R. Zimmermann. In: *Phys. Stat. Sol. (b)* 41.1 (Jan. 1970), p. 23. ISSN: 1521-3951. DOI: 10.1002/pssb.19700410103.
- [130] John E. Anthony. “Functionalized acenes and heteroacenes for organic electronics”. In: *Chem. Rev.* 106.12 (2006), p. 5028.
- [131] Stephen R. Forrest and Mark E. Thompson. “Introduction: organic electronics and optoelectronics”. In: *Chem. Rev.* 107.4 (2007), pp. 923–925.
- [132] Jean-Luc Brédas et al. “Molecular Understanding of Organic Solar Cells: The Challenges”. In: *Acc. Chem. Res.* 42.11 (Nov. 2009), pp. 1691–1699.
- [133] Millicent B. Smith and Josef Michl. “Singlet Fission”. In: *Chem. Rev.* 110.11 (2010), p. 6891.
- [134] Stephen Battersby. *Space molecules point to organic origins*. (Visited on 03/09/2016). 2004. URL: <https://www.newscientist.com/article/dn4552-space-molecules-point-to-organic-origins/> (visited on 03/09/2016).

- [135] G. Mulas et al. “Estimated IR and phosphorescence emission fluxes for specific polycyclic aromatic hydrocarbons in the Red Rectangle”. In: *Astron. Astrophys.* 446.2 (2006), p. 13.
- [136] C. Boersma et al. “The NASA Ames PAH IR Spectroscopic Database Version 2.00: Updated Content, Web Site, and On(Off)line Tools”. In: *Astrophys. J. Suppl. Ser.* 211.1 (2014), p. 8.
- [137] B. Hajgató et al. “A benchmark theoretical study of the electron affinities of benzene and linear acenes”. In: *J. Chem. Phys.* 129.8 (2008), p. 084308. ISSN: 1089-7690. DOI: 10.1063/1.2967182.
- [138] M. S. Deleuze et al. In: *J. Chem. Phys.* 119.6 (2003), p. 3106. DOI: 10.1063/1.1589731.
- [139] Nicolas Dupuy et al. In: *J. Chem. Phys.* 142.21 (2015), p. 214109. DOI: 10.1063/1.4922048.
- [140] P. D. Burrow, J. A. Michejda, and K. D. Jordan. “Electron transmission study of the temporary negative ion states of selected benzenoid and conjugated aromatic hydrocarbons”. In: *J. Chem. Phys.* 86.1 (1987), p. 9.
- [141] Isaac Tamblyn et al. “Simultaneous Determination of Structures, Vibrations, and Frontier Orbital Energies from a Self-Consistent Range-Separated Hybrid Functional”. In: *J. Phys. Chem. Lett.* 5.15 (2014), pp. 2734–2741. DOI: 10.1021/jz5010939.
- [142] Fabien Bruneval. “\$GW\$ Approximation of the Many-Body Problem and Changes in the Particle Number”. In: *Phys. Rev. Lett.* 103.17 (2009), p. 176403. DOI: 10.1103/PhysRevLett.103.176403. URL: <http://link.aps.org/doi/10.1103/PhysRevLett.103.176403>.
- [143] Lukas Gallandi and Thomas Körzdörfer. In: *J. Chem. Theory Comput.* 11.11 (2015), p. 5391. DOI: 10.1021/acs.jctc.5b00820.
- [144] Tonatiuh Rangel et al. “Structural and excited-state properties of oligoacene crystals from first principles”. In: *Phys. Rev. B* 93.11 (2016), p. 115206. DOI: 10.1103/PhysRevB.93.115206.
- [145] Tom. Ziegler. “Approximate density functional theory as a practical tool in molecular energetics and dynamics”. In: *Chem. Rev.* 91.5 (1991), pp. 651–667. DOI: 10.1021/cr00005a001.
- [146] Vojtěch Vlček et al. “Deviations from piecewise linearity in the solid-state limit with approximate density functionals”. In: *J. Chem. Phys.* 142.3 (2015), p. 034107. DOI: 10.1063/1.4905236.
- [147] Sivan Refaely-Abramson, Roi Baer, and Leor Kronik. “Fundamental and excitation gaps in molecules of relevance for organic photovoltaics from an optimally tuned range-separated hybrid functional”. In: *Phys. Rev. B* 84.7 (2011), p. 075144. DOI: 10.1103/PhysRevB.84.075144.

- [148] Thomas Körzdörfer et al. In: *J. Chem. Phys.* 135.20 (2011), p. 204107. DOI: 10.1063/1.3663856.
- [149] Yihan Shao et al. “Advances in molecular quantum chemistry contained in the Q-Chem 4 program package”. In: *Mol. Phys.* 113.2 (2015), p. 184.
- [150] Chengteh Lee, Weitao Yang, and Robert G. Parr. “Development of the Colle-Salvetti correlation-energy formula into a functional of the electron density”. In: *Phys. Rev. B* 37.2 (1988), pp. 785–789. DOI: 10.1103/PhysRevB.37.785.
- [151] James R. Chelikowsky and Steven G. Louie. *Quantum Theory Real Mater.* 1996.
- [152] F. Aryasetiawan and O. Gunnarsson. “The GW method”. In: *Rep. Prog. Phys.* 61.3 (1998), p. 237. ISSN: 0034-4885. URL: <http://stacks.iop.org/0034-4885/61/i=3/a=002>.
- [153] Fabien Bruneval and Matteo Gatti. “Quasiparticle Self-Consistent GW Method for the Spectral Properties of Complex Materials”. In: *First Principles Approaches to Spectroscopic Properties of Complex Materials*. Ed. by Cristiana Di Valentin, Silvana Botti, and Matteo Cococcioni. Topics in Current Chemistry 347. 2014, pp. 99–135.
- [154] Mark S. Hybertsen and Steven G. Louie. “Electron correlation in semiconductors and insulators: Band gaps and quasiparticle energies”. In: *Phys. Rev. B* 34.8 (1986), p. 5390.
- [155] Viktor Atalla et al. “Hybrid density functional theory meets quasiparticle calculations: A consistent electronic structure approach”. In: *Phys. Rev. B* 88.16 (2013), p. 165122. DOI: 10.1103/PhysRevB.88.165122.
- [156] Marco Govoni and Giulia Galli. “Large Scale GW Calculations”. In: *J. Chem. Theory Comput.* 11.6 (2015), pp. 2680–2696. DOI: 10.1021/ct500958p.
- [157] A Stan, N. E Dahlen, and R. van Leeuwen. “Fully self-consistent *GW* calculations for atoms and molecules”. In: *Europhys. Lett.* 76.2 (2006), pp. 298–304. DOI: 10.1209/epl/i2006-10266-6.
- [158] M. Shishkin and G. Kresse. “Self-consistent *GW* calculations for semiconductors and insulators”. In: *Phys. Rev. B* 75 (23 June 2007), p. 235102. DOI: 10.1103/PhysRevB.75.235102. URL: <http://link.aps.org/doi/10.1103/PhysRevB.75.235102>.
- [159] Michael Rohlfing, Peter Krüger, and Johannes Pollmann. “Efficient scheme for *GW* quasiparticle band-structure calculations with applications to bulk Si and to the Si(001)-(21) surface”. In: *Phys. Rev. B* 52 (3 July 1995), pp. 1905–1917. DOI: 10.1103/PhysRevB.52.1905. URL: <http://link.aps.org/doi/10.1103/PhysRevB.52.1905>.
- [160] K. H. Frank et al. In: *J. Chem. Phys.* 89.12 (1988), p. 7569. DOI: 10.1063/1.455720.
- [161] Martin Pope and Charles E. Swenberg. *Electronic Processes in Organic Crystals and Polymer s*. 2 edition. New York: Oxford University Press, 1999.

- [162] *Standard Reference Data. NIST.* (Visited on 03/09/2016). URL: <http://www.nist.gov/>.
- [163] Thomas Heinis, Swapan Chowdhury, and Paul Kebarle. “Electron affinities of naphthalene, anthracene and substituted naphthalenes and anthracenes”. In: *Org. Mass Spectrom.* 28.4 (1993), pp. 358–365. DOI: 10.1002/oms.1210280416. URL: <http://onlinelibrary.wiley.com/doi/10.1002/oms.1210280416/abs%20tract>.
- [164] Sarah R. Whittleton et al. “Density-functional errors in ionization potential with increasing system size”. In: *J. Chem. Phys.* 142.18 (2015), p. 184106. DOI: 10.1063/1.4920947.
- [165] Paula Mori-Sánchez, Aron J. Cohen, and Weitao Yang. “Localization and Delocalization Errors in Density Functional Theory and Implications for Band-Gap Prediction”. In: *Phys. Rev. Lett.* 100.14 (2008), p. 146401. DOI: 10.1103/PhysRevLett.100.146401.
- [166] Margherita Marsili et al. In: *J. Phys. Chem. C* 27 (2013), p. 14229. DOI: 10.1021/jp3121269.
- [167] Jeppe Gavnholt et al. In: *Phys. Rev. B* 78.7 (2008), p. 075441. DOI: 10.1103/PhysRevB.78.075441.
- [168] Tamar Stein et al. “Fundamental Gaps in Finite Systems from Eigenvalues of a Generalized Kohn-Sham Method”. In: *Phys. Rev. Lett.* 105.26 (2010), p. 266802. DOI: 10.1103/PhysRevLett.105.266802.
- [169] Michiel J. van Setten et al. “GW100: Benchmarking G0W0 for Molecular Systems”. In: *J. Chem. Theory Comput.* 11.12 (2015), pp. 5665–5687. DOI: 10.1021/acs.jctc.5b00453.
- [170] Johannes Lischner et al. “Effects of self-consistency and plasmon-pole models on GW calculations for closed-shell molecules”. In: *Phys. Rev. B* 90.11 (2014), p. 115130. DOI: 10.1103/PhysRevB.90.115130.
- [171] Michael Bendikov et al. “Oligoacenes: Theoretical Prediction of Open-Shell Singlet Diradical Ground States”. In: *J. Am. Chem. Soc.* 126.24 (2004), pp. 7416–7417. URL: <http://dx.doi.org/10.1021/ja048919w>.
- [172] Monika Srebro and Jochen Autschbach. In: *J. Phys. Chem. Lett.* 3.5 (2012), pp. 576–581. DOI: 10.1021/jz201685r.
- [173] Daniel Lüftner et al. “Experimental and theoretical electronic structure of quinacridone”. In: *Phys. Rev. B* 90.7 (2014), p. 075204. DOI: 10.1103/PhysRevB.90.075204.
- [174] Fabio Caruso et al. “Bond Breaking and Bond Formation: How Electron Correlation is Captured in Many-Body Perturbation Theory and Density-Functional Theory”. In: *Phys. Rev. Lett.* 110.14 (2013), p. 146403. DOI: 10.1103/PhysRevLett.110.146403.